THE ASSEMBLY OF PATHOGENIC SIGNALING CIRCUITS BY A FAMILY OF BACTERIAL SECRETED EFFECTOR PROTEINS

APPROVED BY SUPERVISORY COMMITTEE

Neal Alto, Ph.D.

David Hendrixson, Ph.D.

Vanessa Sperandio, Ph.D.

Paul Sternweis, Ph.D.

ACKNOWLEDGEMENTS

I am extremely fortunate to have been assisted by numerous individuals during the course of these studies. Collaborators both on the campus of UT Southwestern and away have aided in making my research experiences productive and enjoyable. I would like to begin by thanking my thesis adviser Dr. Neal Alto. His enthusiasm for science is contagious and he has always been willing to provide the guidance I need. I have really enjoyed being one of the first people to have joined the lab and look forward to seeing the wonderful things to come from it in the future.

I would also like to acknowledge the members of the Alto lab. All of you have contributed to this work in some way. I would like to specifically mention the help from Adam Wallenfang, Sarah Sutton, Alyssa Jimenez, and Bethany Weigele, all of whom have collaborated on scientific projects with me in the lab and graciously allowed me to present some of their data. I would also like to thank Andrey Selyunin for providing significant insight into my project and it has been fun working next to him.

I also want to thank other individuals here at UT Southwestern for their collaborations. I want to especially thank Mark Kittisopikul, Dr. Gürol Süel, Dr. Steven Altschuler, and Dr. Lani Wu for their design of the computational model. Without their help, our understanding of the Map signaling network would be incomplete. Drs. Michael Rosen, Michael White, Joel Goodman, Helen Yin, and Ivan D'orso all graciously contributed reagents and advice that were invaluable to our studies. I also am grateful for the Live Cell Imaging Core's assistance. Thank you, Abhijit Bugde and Dr. Katherine Luby-Phelps for your exceptional expertise on capturing dynamic signaling events in real time. I would also like to thank Drs. Kim Orth and Michael Norgard for their guidance during my studies. Additionally, Dr. Orth provided critical insight

into my studies, and for that I am very grateful. I also would like to acknowledge the members of the Orth lab for their helpful insight and comments during our regular joint lab meetings. I also would like to thank them for their willingness to provide tools and reagents to me. Lastly, I would like to thank Dr. Nancy Street, who I consider an excellent friend. She has provided me with plenty of career advice and was a major reason for my choosing UT Southwestern for my graduate studies. I would like to thank members of my thesis committee, Dr. David Hendrixson, Dr. Vanessa Sperandio, and Dr. Paul Sternweis for their guidance and suggestions that have made this work better.

I also would like to thank our collaborators at other institutions. Importantly, I would like to thank Dr. Jijie Chai and his former graduate student Dr. Zhiwei Huang at the School of Life Sciences at Tsinghua University for the elucidation of the structure of Map in complex with Cdc42. Without this insight, the rest of my studies would not be possible. I also would like to thank Dr. Mark Lemmon (University of Pennsylvania), Dr. Scott Emr (Cornell University), Dr. Jack Dixon (University of California at San Diego), and Dr. Pietro De Camilli (Yale School of Medicine) for kindly providing reagents.

Lastly, I would like to thank my family who has always supported me in all of my endeavors. My parents Norah and Bob Orchard have never wavered in supporting my career goals. Their love and support has carried me through many tough times. Also, they have taught me the importance of hard work and perseverance. Thank you, Mom and Dad for all that you have done and will continue to do. I also want to thank my wonderful, loving wife, Megan. I love every day we spend together and cannot imagine living life in any other way. Thank you for putting up with all of the craziness that goes into living with a research scientist. Finally, I

would like to acknowledge anyone who has helped me throughout my graduate school career and due to poor oversight on my part, omitted your name.

THE ASSEMBLY OF PATHOGENIC SIGNALING CIRCUITS BY A FAMILY OF BACTERIAL SECRETED EFFECTOR PROTEINS

by

ROBERT CHARLES ORCHARD II

DISSERTATION

Presented to the Faculty of the Graduate School of Biomedical Sciences

The University of Texas Southwestern Medical Center at Dallas

In Partial Fulfillment of the Requirements

For the Degree of

DOCTOR OF PHILOSOPHY

The University of Texas Southwestern Medical Center at Dallas

Dallas, Texas

May 2013

THE ASSEMBLY OF PATHOGENIC SIGNALING CIRCUITS BY A FAMILY OF BACTERIAL SECRETED EFFECTOR PROTEINS

Robert Charles Orchard II, Ph.D.

The University of Texas Southwestern Medical Center at Dallas, 2013

Supervising Professor: Neal Alto, Ph.D.

Bacterial type III secreted effector proteins facilitate Gram-negative bacterial replication, dissemination, and immune evasion in the infected host organism. While much attention has been focused on the cell inhibitory mechanisms of these virulence factors, there is emerging evidence that bacterial effectors exert direct control over host cellular behavior by assembling new signaling circuits from pre-existing regulatory modules. However, these mechanisms are poorly understood. In this work, we utilize the WxxxE family of effector proteins as a model system to understand how pathogens rewire host signaling cascades. These effectors share a core catalytic domain that functions as a guanine-nucleotide exchange factor (GEF) for Rho family GTPases. Using a structure to function approach, we uncover a GEF-GTPase pairing

mechanism important for signaling fidelity and pathogenic diversity. Guided by these structural insights, we next wanted to know how *E. coli*, an extracellular pathogen, induces the polarization of host actin molecules. By using synthetic derivatives of the enteropathogenic *E. coli* GEF Map, we discover that Cdc42 GTPase activity cycles are controlled in space and time by Map's interaction with F-actin. Mathematical modeling reveals how actin dynamics coupled to a Map-dependent positive feedback loop spontaneously polarizes Cdc42. By reconstituting the system, we further show how cells polarize in response to an extracellular spatial cue. These results demonstrate how pathogens gain systems level control over host signaling networks and suggest a new view of cellular polarity centered on the interaction between GEFs and F-actin. To explore alternative mechanisms that bacteria utilize to assemble circuits, we utilize yeast genetics to identify novel membrane-interactions. We identify for the first time the direct association of the *Shigella* GEF IpgB1 with acidic phospholipids. Surprisingly, we find that these protein-lipid interactions are not required for IpgB1's known role in *Shigella* invasion. However, we do find that IpgB1's interactions with eukaryotic membranes are essential for bacterial replication and persistence within host cells. Furthermore, we identify a pathogenic circuit that connects GTPase activity with phospholipid metabolism. In summation, our findings illustrate the complex evolutionary relationship between pathogen and host, and how investigating these interactions provide insight into endogenous signaling systems.

TABLE OF CONTENTS

PRIOR PUBLICATIONS

Orchard RC, Kittisopikul M, Altschuler SJ, Wu LF, Süel GM, Alto NM. Identification of F-actin as the dynamic hub in a microbial-induced GTPase polarity circuit. *Cell.* 2012. 148(4):803-15.

Orchard RC and Alto NM. Mimicking GEFs: A Common Theme for Bacterial Pathogens. *Cell Microbiol*. 2012. 14(1): 10-8.

Selyunin A, Sutton SE, Weigele BA, Reddick LE, **Orchard RC,** Bresson S, Tomchick D, and Alto NM. The assembly of a GTPase-kinase signaling complex by a bacterial catalytic scaffold. *Nature.* 2011. 469(7328): 107-11.

Summer EJ, Liu M, Gill JJ, Grant M, Bertoli M, Chan-Cortes TN, Ferguson L, Janes C, Lange K, Moore C, **Orchard RC**, Cohen N, and Young R. Genomic and functional analysis of Rhodococcus equi phages ReqiPepy6, ReqiPoco6, ReqiPine5 and ReqiDocB7. *Appl Environ Microbiol*. 2011. 77(2):669-83.

Huang Z, Sutton SE, Wallenfang AJ, **Orchard RC**, Wu X, Feng Y, Chai J, and Alto NM. Structural insights into host GTPase isoform selection by a family of bacterial GEF mimics. *Nat Struct Mol Biol.* 2009. 16(8): 853-60.

LIST OF FIGURES

LIST OF TABLES

LIST OF APPENDICES

LIST OF ABBREVIATIONS

A/E – Attaching and effacing

ABD – Actin-binding domain

Asp – Aspartic acid

BF – Brightfield

BHI – Brain heart infusion

CFTR – Cystic fibrosis transmembrane receptor

DH – Dbl homology

DTT – Dithiothreitol

EDTA – Ethylenediaminetetraacetic acid

Ebp50 – Ezrin binding phosphoprotein 50

EHEC – Enterohemorrhagic *Escherichia coli*

EPEC – Enteropathogenic *Escherichia coli*

F-actin– filamentous actin

Fn – Fibronectin

FPLC – Fast protein liquid chromatography

Gal – Galactose

GAP – GTPase activating protein

GEF – Guanine-nucleotide exchange factor

GFP – Green fluorescent protein

Gln – Glutamine

Glu – Glutamic acid

GST – Glutathione S-transferase

GTPase – Guanosine triphosphatase

IPTG – Isopropyl β-D-1-thiogalactopyranoside

LiAc – Lithium acetate

LatB – Latrunculin B

MBP – Maltose binding protein

Mg^{2+} – Magnesium

Ni-NTA – nickel-nitrilotriacetic acid

PBS – Phosphate buffered saline

PDB – Protein data bank

PEG – Polyethylene glycol

PDZ – PSD-95/Dlg/ZO-1

PH – Pleckstrin homology

Phe – Phenylalanine

PIP – Phosphatidylinositol phosphate

SCV– *Salmonella*-containing vacuole

Gal – Galactose

SD – Synthetic defined

Spp. – Species

TBS – Tris-buffered saline

T3SS – Type III Secretion System

wt – wild-type

CHAPTER ONE
Introduction and Literature Review

Bacterial type III secretion systems hijack host cell signaling pathways

Bacterial pathogens must subvert host cell signaling cascades in order to establish a replicative niche and to avoid immune detection and clearance. A common mechanism for Gram-negative bacterial pathogens to hijack host cellular processes is the secretion of virulence proteins through a type III secretion system (T3SS). The T3SS is a proteinaecious needle-like structure that shares homology with the bacterial flagellum (Cornelis, 2006). Unlike the flagellum apparatus, the T3SS forms a translocon pore in the eukaryotic cell membrane (Figure 1). Secretion of bacterial proteins occurs in an ATP-dependent manner that is thought to unfold the protein and allow it to traverse the needle and enter into the eukaryotic cell (Cornelis, 2006). Therefore, type III secretion transfers proteins directly from the bacterial cytoplasm into the eukaryotic cytoplasm without any extracellular intermediates. After type III secretion, the translocated bacterial proteins affect host cell signaling networks and thus have been coined "effector" proteins.

Numerous animal and plant pathogens harbor T3SSs that are essential for their virulence, including enteropathogenic *Escherichia coli* (EPEC), enterohemorrhagic *Escherichia coli* (EHEC), *Salmonella typhimurium*, *Shigella flexneri*, *Yersinia pestis*, *Burkholderia mallei*, *Pseudomonas aeruginosa*, *Pseudomonas syringae*, and *Ralstonia solanacearum* (Eichelberg et al., 1994; Jarvis et al., 1995; Jarvis and Kaper, 1996; Michiels et al., 1990; Parsot et al., 1995; Preston et al., 1995; Ulrich and DeShazer, 2004; Van Gijsegem et al., 1995; Yahr et al., 1996).

Each of these pathogens harbor a unique repertoire of effector proteins that likely represents their distinct pathogenic niche. Surprisingly, despite variations in life styles (i.e. intracellular vs. extracellular) and tissue tropisms (e.g. lung, gut, plant) these pathogens contain effector proteins that have homologues in a different bacterium. For example, the extracellular pathogen EHEC secretes EspG which shares 21% sequence identity with the *Shigella* effector protein VirA despite the fact that *Shigella* persists within the cytoplasm of infected cells (Elliott et al., 2001). Despite their pathogenic differences, *P. syringae*, *Shigella spp.*, and nontyphoid *Salmonella* strains all encode an effector protein with phosphothreonine lyase activity that potently inactivates the immune response (Li et al., 2007). These examples are only a few of the many observations suggesting that a subset of eukaryotic signaling pathways are preferentially targeted and rewired in a specific manner in order to increase the fitness of the respective bacterial pathogen.

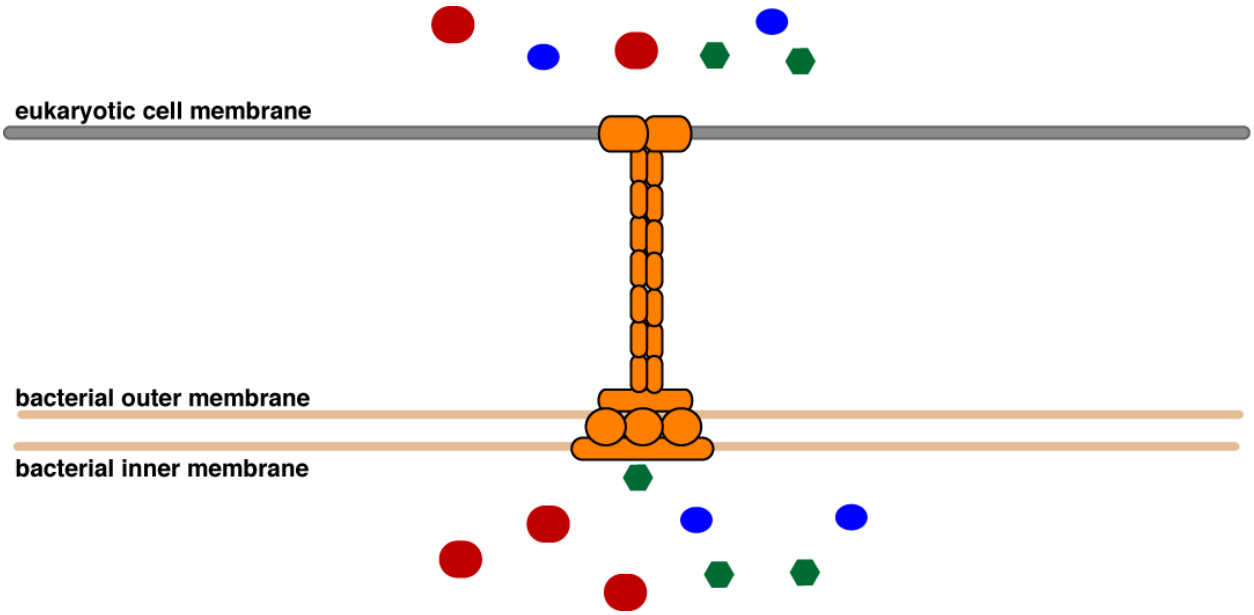

Figure 1. The type III secretion system. A cartoon diagram depicting the type III secretion system (T3SS) in orange. This protein nanomachine can be separated into three parts. First, the basal body spans both the inner and outer membranes of the bacterial cell. Next, an extracellular hollow tube forms at the base of the T3SS and culminates in a translocon pore complex. This structure allows secreted "effector" proteins (colored shapes) to be injected directly into the eukaryotic cell.

Eukaryotic G-proteins as common targets of bacterial pathogens

A common target of bacterial effector proteins are small molecular weight GTPases of the Ras family, also known as G-proteins. These eukaryotic enzymes are responsible for controlling signal transduction pathways, membrane trafficking, cytoskeletal dynamics, nuclear import, and a wide range of other physiological processes (Takai et al., 2001). There are several important features of G-proteins that enable them to carry out their essential functions. First, G-proteins cycle between an inactive GDP-bound state and an active GTP-bound state. Facilitating the interconversion of these states are two groups of proteins: guanine-nucleotide exchange factors (GEFs) and GTPase activating proteins (GAPs). GEFs activate G-proteins by catalyzing the exchange of GDP for GTP. Once bound to GTP, G-proteins adopt an active conformation which enables the protein to interact and activate downstream signaling substrates (Vetter and Wittinghofer, 2001). In contrast to GEFs, GAPs function by binding and accelerating the slow intrinsic hydrolysis rate of the G-proteins, thus inactivating the protein (Bos et al., 2007). An additional level of regulation is the localization of GTPases which are post-translationally modified either on the N-terminus or the C-terminus with lipid moieties. In response to a variety of stimuli, GTPases are recruited from the cytoplasm to specific eukaryotic membranes in which they undergo GTPase conversion and perform their essential functions (Kahn et al., 1988; Zhang and Casey, 1996).

Because of their essential nature and their switch-like activation mechanism, small GTPases are common targets of bacterial virulence factors including type III secreted effector proteins. For example, *Salmonella* directly alters the nucleotide cycling of Rho family GTPases

through the secretion of the bacterial GAP SptP (Fu and Galan, 1999). Another common mechanism to alter G-protein signaling is to block its association with eukaryotic membranes. The cysteine proteases YopT and IpaJ cleave the prenylation and myristoylation regions of Rho and Arf family GTPases, respectively (Burnaevskiy et al., 2013; Shao et al., 2002). In doing so, these effector proteins permanently deactivate the signaling capacity of the GTPases. Additionally, effector proteins can post-translationally modify GTPases in order to block the activation of downstream signaling pathways. The *Vibrio parahaemolyticus* effector VopS AMPylates Rho family GTPases on a conserved threonine residue which sterically hinders substrates from interacting with these modified G-proteins (Yarbrough et al., 2009). These studies and others constitute the large body of work clearly demonstrating that pathogenic bacteria have evolved intricate mechanisms to inhibit G-protein signaling through a range of strategies including proteolysis and post-translational modifications (Flatau et al., 1997; Sekine et al., 1989; Shao et al., 2002; Yarbrough et al., 2009). However, how pathogens induce and orchestrate complex host cellular behaviors through the activation of GTPase signaling cascades by bacterial GEF mimicry is not well understood.

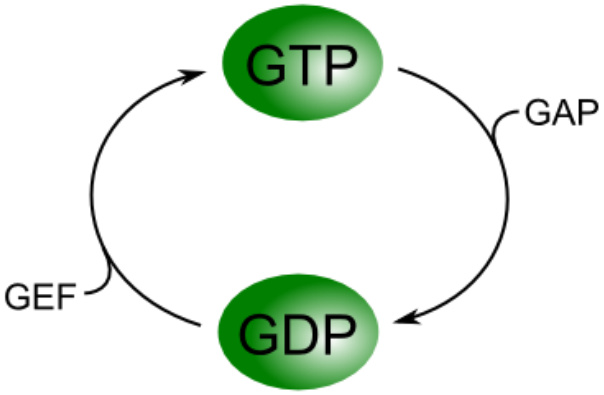

Figure 2. The GTPase cycle. G-proteins cycle between an inactive GDP-bound state and an active GTP-bound state. Two families of enzymes facilitate the interconversion of these states. Guanine-nucleotide exchange factors (GEFs) activate GTPase signaling by facilitating the exchange of GDP for GTP. GTPase activating proteins (GAPs) increase the intrinsic hydrolysis rate of the GTPases and thus turn off the signaling.

A family of bacterial GEF mimics

The identification of the WxxxE/SopE family of effectors

The *Salmonella* type III effector protein SopE was the first reported bacterial GEF. Hardt *et al.* discovered that SopE directly activates Cdc42 and Rac GTPases to induce membrane ruffling at the site of *Salmonella* invasion (Hardt et al., 1998). The discovery lead to the identification of several additional bacterial GEFs that displayed genetic similarity to SopE, including SopE2 (*Salmonella spp.*), BopE (*Burkholderia pseudomallei*), and CopE (*Chromobacterium violaceum*). Until recently, this family of type III effectors was the only Rho-specific GEFs to be identified in bacterial species.

In 2006, Alto *et al.* identified a bacterial effector family that activated GTPase signaling cascades within host cells (Alto et al., 2006). While this family shares very low sequence homology (<15%) they all contain an invariant Trp-X-X-X-Glu signature motif (Alto et al., 2006). The original description of the so called "WxxxE" family (pronounced whi-xee) suggested that these effector proteins directly mimic small GTPases (Alto et al., 2006). However, it was clear from subsequent structural studies that the WxxxE effectors adopt a GEF like fold similar to SopE (Ohlson et al., 2008). This finding was quite surprising since sequence-based alignment of the WxxxE and SopE effector families does not yield any significant homology. Huang *et al.* reported the first GEF activity for three WxxxE family members: Map, IpgB1 and IpgB2 (Huang et al., 2009). Additional reports have confirmed that the WxxxE proteins function as GEFs and not as GTPase mimics (Arbeloa et al., 2010; Klink et al., 2010). Importantly, the structural, pathogenic, and cellular regulation of the SopE/WxxxE family of

bacterial GEFs has greatly increased our understanding of bacterial GEF mimicry at the molecular level.

The catalytic mechanism of GEF mimics

Structural studies investigating the SopE/WxxxE family have been instrumental in understanding the underlying GTPase-activation mechanism utilized by bacterial GEFs. Currently there are solved structures for the GEFs SopE, SopE2, BopE, Map, SifA, and IpgB2 (Buchwald et al., 2002; Huang et al., 2009; Klink et al., 2010; Ohlson et al., 2008; Upadhyay et al., 2004; Williams et al., 2004). A summary of each bacterial GEF's biochemical activity is listed in Table 1. Buchwald *et al.* solved the structure of SopE in complex with Cdc42, providing the first structural insight into bacterial GEF mimics (Buchwald et al., 2002). Surprisingly, SopE does not resemble the Dbl-homology (DH) domain or the Dock Homology Region 2 (DHR-2) domain, the two major classes of eukaryotic Rho GEFs (Figure 3A). Rather, SopE adopts a V-shaped fold consisting of two bundles of alpha helices and an extended catalytic loop that connects the two helical bundles (Figure 3A) (Buchwald et al., 2002). Closer inspection of the interactions between SopE and Cdc42 does reveal general similarities of guanine-nucleotide exchange between bacterial and eukaryotic GEFs. It appears that all GEFs interact extensively with the GTPase switch 1 and switch 2 loops (Buchwald et al., 2002). The GTPase switch loops define the major structural differences between an inactive (GDP-bound) and active (GTP-bound) state (Vetter and Wittinghofer, 2001). More specifically both SopE and the Dbl family of GEFs utilize an acidic residue and an amide side chain to interact with residues

on switch 1 and switch 2, respectively (Buchwald et al., 2002). Recent investigations of the WxxxE family of GEFs illustrate that they too adopt a V-shaped structure similar to SopE (Figure 3A) (Huang et al., 2009; Ohlson et al., 2008). Additionally, the WxxxE proteins utilizes the conserved acidic and amide residues to interact with the GTPase switch loops similar to SopE and Dbl GEFs (Huang et al., 2009). Lastly, both SopE and WxxxE bacterial GEFs induce nearly identical conformational changes around the GTPase nucleotide binding site as the Dbl family of eukaryotic GEFs (Buchwald et al., 2002; Huang et al., 2009). These structural studies have confirmed that both the WxxxE and SopE GEF mimics have converged upon a similar guanine-nucleotide exchange mechanism.

The catalytic loop of these bacterial GEF mimics are important for making contacts with the GTPase switch 1 and switch 2 regions (Buchwald et al., 2002; Huang et al., 2009). Recent studies have demonstrated that the catalytic loop is flexible and that proper orientation is important for GTPase recognition and activation (Klink et al., 2010). For example, in the structures of Map and IpgB2 in complex with Cdc42 and RhoA, respectively, the catalytic loop sits high upon the V fold (Figure 3B). Further examination of IpgB2 shows that the catalytic loop lies much lower on the V structure in the apo-structure compared to when IpgB2 is in complex with RhoA (Figure 3B). Similarly, in the structure of SifA in which there is no GTPase present, the catalytic loop of SifA lies even lower on the structure (Figure 3B). It now appears that reorientation of the catalytic loop may be a mechanism of regulating GEF activity (Klink et al., 2010). Understanding the functional consequences of undergoing such conformational changes remains an outstanding question in the field.

Table 1. Bacterial GEF mimics and their reported biochemical activities

Species	Protein	Family	Substrate(s)	Binding*	GEF Activity*	Structure (PDB)	References
Salmonella	SopE	SopE	Rac1 & Cdc42	Yes	Yes	1GZS	(Hardt *et al.*, 1998)
	SopE2	SopE	Rac1 & Cdc42	Yes	Yes	1R9K	(Friebel *et al.*, 2001)
	SifA	WxxxE	RhoA	Yes	None Detected	3HW2 3CXB	(Ohlson *et al.*, 2008)
	SifB	WxxxE	Unknown	Unknown	Unknown		(Alto *et al.*, 2006)
Burkholderia	BopE	SopE	Rac1 & Cdc42	Yes	Yes	2JOK 2JOL	(Upadhyay *et al.*, 2004)
Shigella	IpgB1	WxxxE	Rac1 & Cdc42	Yes	Yes		(Huang *et al.*, 2009)
	IpgB2	WxxxE	RhoA	Yes	Yes	3LW8 3LWN 3LXR 3LYQ	(Huang *et al.*, 2009; Klink *et al* 2010)
A/E Lesion Pathogens	Map	WxxxE	Cdc42	Yes	Yes	3GCG	(Huang *et al.*, 2009)
	EspM	WxxxE	RhoA	Yes	Yes		(Arbeloa *et al.*, 2010)
	EspT	WxxxE	Rac1 & Cdc42	Unknown	Unknown		(Bulgin *et al.*, 2009b)
Chromobacterium violaceum	CopE	SopE	Rac1 & Cdc42	Unknown	Unknown		(Miki et al., 2011)

***** Binding and GEF Activity refer to whether or not biochemical studies have confirmed binding and nucleotide exchange of GTPase substrates.

Bacterial GEF mimics also provide keen insight into how eukaryotic GEFs function. For example, Klink *et al.* provide new insights into the GTPase-activation mechanism of bacterial GEFs, which has implications for endogenous GEFs as well (Klink et al., 2010). The structure of IpgB2 in complex with RhoA was solved under three different magnesium concentration conditions. With mild treatment of EDTA, excess Mg^{2+} ions were depleted from the complex and the solved structure showed a novel Mg^{2+}-binding site for RhoA (Klink et al., 2010). Typically, Mg^{2+} is found near the β–phosphate of the GDP but at low Mg^{2+} concentrations, the Mg^{2+} relocates to the α–phosphate position of the nucleotide (Klink et al., 2010). This new secondary Mg^{2+}-binding site provides new insight into GTPase-activation through the step-wise transition of GDP for GTP.

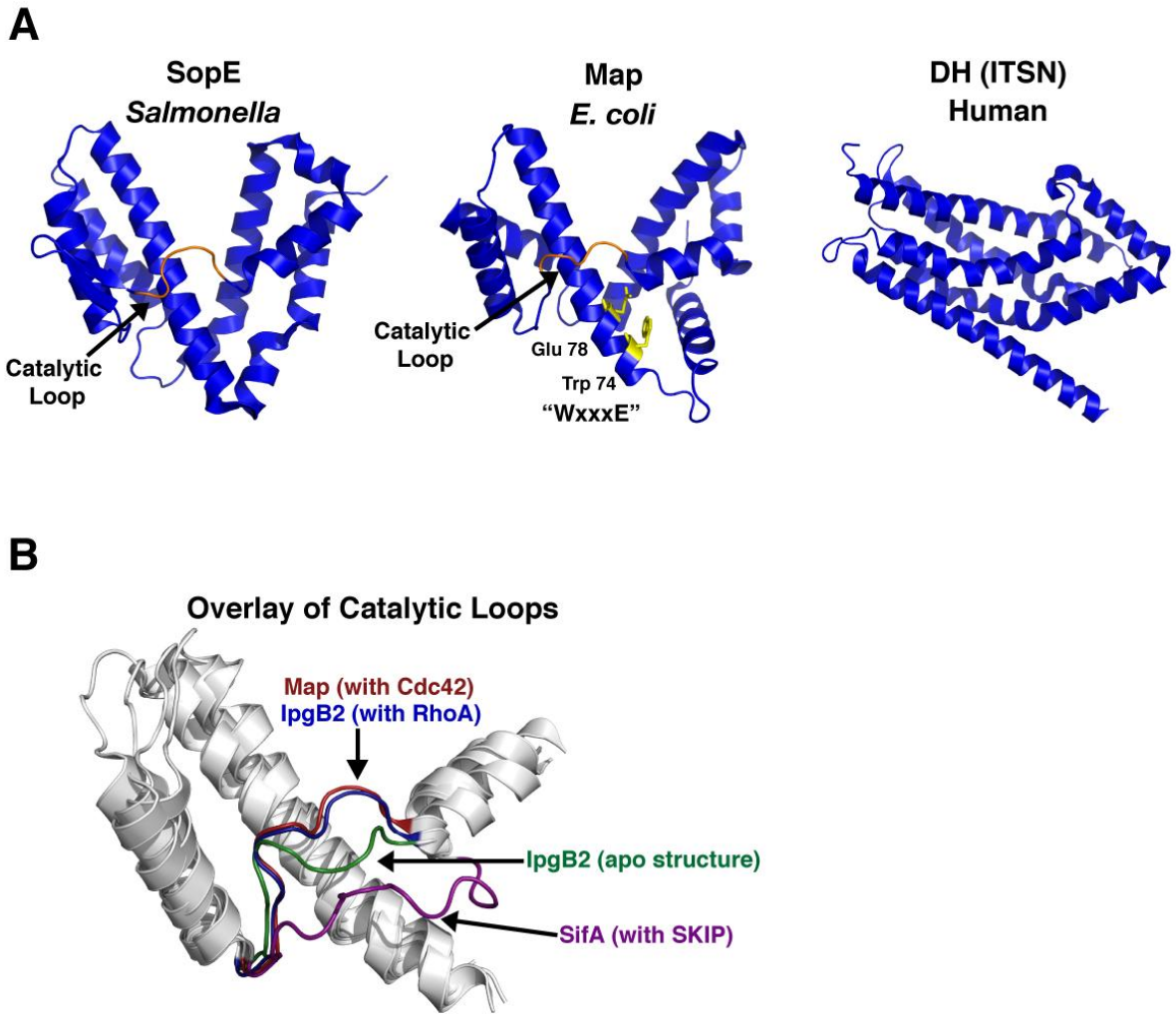

Figure 3. Structural comparison of bacterial GEF mimics. A. Structure of Map from *E. coli* (PDB: 3GCG), SopE from *Salmonella* (PDB: 1ZGS), and the human GEF ITSN (PDB: 1KIL). Highlighted in orange is the catalytic loop of Map and SopE. The side chain of the Tryptophan and Glutamic acid of Map's WxxxE motif are shown as yellow sticks.
B. Comparison of the catalytic loops of the WxxxE GEFs. Structures of indicated GEF constructs were overlayed to illustrate the different position of the loops. Map in complex with Cdc42 (red; PDB: 3GCG) and IpgB2 in complex with RhoA (blue; PDB: 3LXR) lie higher on the V structure compared to the loops of uncomplexed IpgB2 (green; PDB: 3LYQ) and SifA (purple; PDB: 3CXB).

Salmonella GEFs

Salmonella spp. encode four bacterial GEFs, two SopE-type and two WxxxE-type. SopE and its homologue SopE2 are secreted by the SPI-1 T3SS and are required for the entry of *Salmonellae* into non-phagocytic cells (Figure 4A) (Bakshi et al., 2000; Hardt et al., 1998; Stender et al., 2000). These GEFs induce membrane ruffles required for *Salmonella* invasion through the activation of Rac and Cdc42 (Bakshi et al., 2000; Hardt et al., 1998; Stender et al., 2000). While SopE and SopE2 have slightly different substrate preferences with SopE activating both Cdc42 and Rac1 and SopE2 activating Cdc42 (Friebel et al., 2001), Rac1 activation is the primary driving factor for *Salmonella* entry into host cells (Patel and Galan, 2006). However, given that Cdc42 activates Rac1 through GTPase cross talk, either GEF is sufficient to induce host cell invasion.

The cellular invasion mechanism utilized by Salmonella also provides a good example for the complex regulation of bacterial GEFs inside eukaryotic hosts. After SopE induced ruffle formation and invasion, a second type III effector SptP remodels the actin cytoskeleton by inactivating GTPases. SptP functions as a GAP that directly antagonizes the activation of Rac1 and Cdc42 by SopE (Figure 4A) (Fu and Galan, 1999). In order to coordinate the timing of SopE and SptP activity, *Salmonella* utilizes the host proteasome degradation pathway (Figure 4A). The amino terminus of SopE contains an ubiquitination motif that facilitates the rapid degradation of the SopE protein compared to SptP (Kubori and Galan, 2003). By generating chimeric proteins that alter SopE's and SptP's half-life, Kubori *et al.* were able to demonstrate the importance of temporally regulating SopE and SptP activities during *Salmonella* infection

(Kubori and Galan, 2003). Adding to the complexity of the regulation of SopE and SptP is a recent report that the translocation rates of these two proteins are significantly different (Van Engelenburg and Palmer, 2008). Whether other bacteria fine-tune the temporal activity of their GEF mimics through the secretion of antagonizing effectors is an interesting but currently unexplored area of research.

As mentioned above, *Salmonella* also encodes two additional WxxxE type GEF mimics: SifA and SifB. Both SifA and SifB are secreted by the SPI-2 T3SS. While very little is known about SifB, SifA is required for full virulence in macrophages and in mice (Beuzon et al., 2000). SifA is secreted after *Salmonella* internalization and is necessary for the maintenance of the *Salmonella*-containing vacuole (SCV) and generation of *Salmonella*-induced filaments (Sifs; Figure 4A) (Beuzon et al., 2000). Without SifA, *Salmonellae* are no longer able to control the endocytic trafficking to the SCV and bacteria escape out of the SCV (Beuzon et al., 2000; Brumell et al., 2002; Ruiz-Albert et al., 2002). SifA is anchored to the SCV via a C-terminal CaaX box that becomes lipidated (Boucrot et al., 2003; Reinicke et al., 2005). Without this modification on SifA, *Salmonellae* are unable to maintain the SCV (Boucrot et al., 2003).

SifA is a two-domain protein with the N-terminus responsible for interacting with the host protein SKIP and the C-terminus adopts the SopE/WxxxE GEF (Ohlson et al., 2008). The interactions between SifA and SKIP are essential for maintenance of the SCV (Boucrot et al., 2005). SifA's interaction with SKIP is believed to link kinesin-1 activity with the events occurring on the SCV (Boucrot et al., 2005; Dumont et al., 2010). Intriguingly, the small GTPase Rab9 interacts with SKIP, and this interaction is disrupted by SifA (Jackson et al.,

2008). Because Rab9 is involved in late endosomal trafficking, SifA's disruption of the Rab9::SKIP complex may function to antagonize Rab9's native functions (Jackson et al., 2008). Currently, there is not a known function of Rab9 in altering the SCV and the physiological implications of this finding still need to be explored. Future biochemical studies elucidating SifA's and SifB's GTPase target(s) will lend great insight into how *Salmonella* maintain the *Salmonella*-containing vacuole.

Shigella GEFs

Shigella spp. encode two bacterial GEF mimics of the WxxxE family: IpgB1 and IpgB2 (Figure 4B) (Alto et al., 2006; Huang et al., 2009). IpgB1 was initially identified as a type III effector required for efficient invasion of host cells (Ohya et al., 2005). Handa and colleagues presented evidence that IpgB1 recruits the ELMO/DOCK 180 complex to the membrane to activate Rac1 (Handa et al., 2007). Given the recent biochemical data demonstrating IpgB1's GEF activity, this finding needs to be confirmed, and could demonstrate a redundant mechanism to stimulate Rac1 activity. (Huang et al., 2009; Ohya et al., 2005). The N-terminus of IpgB1 associates with the plasma membrane through an unknown mechanism that may be important in regulating GEF catalysis (Handa et al., 2007).

Shigella's other bacterial GEF mimic, IpgB2 is less understood. IpgB2 induces stress fibers in cells through activation of RhoA (Figure 4B) (Huang et al., 2009). *Shigella* strains with the IpgB2 gene deleted are not deficient in cell invasion (Hachani et al., 2008). However, infection of polarized Caco-2 cells with single or double IpgB1/IpgB2 knockout strains produced

some intriguing results. First, while IpgB1 deletion strains were defective for invasion into HeLa cells, the same strains had no defect in polarized cells (Hachani et al., 2008). A double knockout of IpgB1 and IpgB2 revealed a significant decrease in invasion of polarized epithelial cells and attenuation in a murine intranasal model (Hachani et al., 2008). These results, if confirmed, suggest that *Shigella* utilizes a more sophisticated means of invasion than previously appreciated. However, more extensive studies investigating the relationship between IpgB1, IpgB2, and host cell invasion are needed.

Attaching and Effacing (A/E) Lesion Pathogen's GEFs

A/E lesion pathogens include the closely-related bacteria enteropathogenic *E. coli* (EPEC), enterohemorrhagic *E. coli* (EHEC), and *Citrobacter rodentium*. Map, a WxxxE family GEF, is found in all of these pathogens. Map is a Cdc42-specific GEF that induces actin-filopodia protrusions around the infecting bacterium (Figure 4C) (Huang et al., 2009; Kenny et al., 2002). Map was originally identified as a mitochondrial-associated protein that interferes with the maintenance of the organelle's membrane potential (Kenny and Jepson, 2000). However, it is unclear whether the mitochondrial import signal is related to Map's activation of Cdc42. Map also harbors a PDZ-ligand that is important for its cellular regulation (Alto et al., 2006; Simpson et al., 2006). PDZ-ligands are short sequences at the C-termini of proteins that facilitate protein-protein interactions with proteins containing PDZ domains (Harris and Lim, 2001). Map's PDZ-ligand is identical to that of the Cystic Fibrosis Transmembrane Receptor (CFTR) and like the CFTR, Map binds to the PDZ domains of Ezrin Binding Phosphoprotein 50

(Ebp50) (Alto et al., 2006). The generation of filopodia protrusions by Map is dependent upon its ability to interact with Ebp50 (Figure 4C) (Alto et al., 2006; Simpson et al., 2006). Why Map requires Ebp50 for signaling is still unclear. Currently two hypotheses have been presented. First, Ebp50 might serve as a localization motif especially since it is known to associate with transmembrane proteins (Alto et al., 2006). Alternatively, Berger et al. suggest that Ebp50 is required for the stabilization of filopodia through the activation of RhoA (Berger et al., 2009). Future experiments directly testing these hypotheses are necessary.

In addition to Map, A/E lesion pathogens contain two other bacterial GEF mimics: EspM and EspT (both are WxxxE proteins). In a recent survey of clinical EPEC and EHEC isolates, it was discovered that about half of the strains contain *espM* but less than 2% of strains contain *espT* (Arbeloa et al., 2009). EspT activates Rac1 and Cdc42 to generate membrane ruffles that result in the eventual phagocytosis of the bacteria (Figure 4C) (Bulgin et al., 2009a; Bulgin et al., 2009b). This novel finding of an enteroinvasive EPEC (and Citrobacter) may illustrate an evolutionary divergence and eventual emergence of a new class of pathogens (Bulgin et al., 2009a). The more common effector EspM is similar to the *Shigella* protein IpgB2 and activates RhoA to induce stress fibers in infected cells (Figure 4C) (Arbeloa et al., 2008; Arbeloa et al., 2010). During infection, expression of EspM inhibits the formation of the actin pedestals that are characteristic of A/E lesion pathogens (Simovitch et al., 2010). The biochemical and cellular mechanisms attributed to this process have yet to be elucidated, but should provide important insight into A/E lesion pathogenesis. Additional questions remain about EspT and EspM.

Specifically, why do some strains have EspT and EspM while others do not and what is the pathogenic impact of these GEFs?

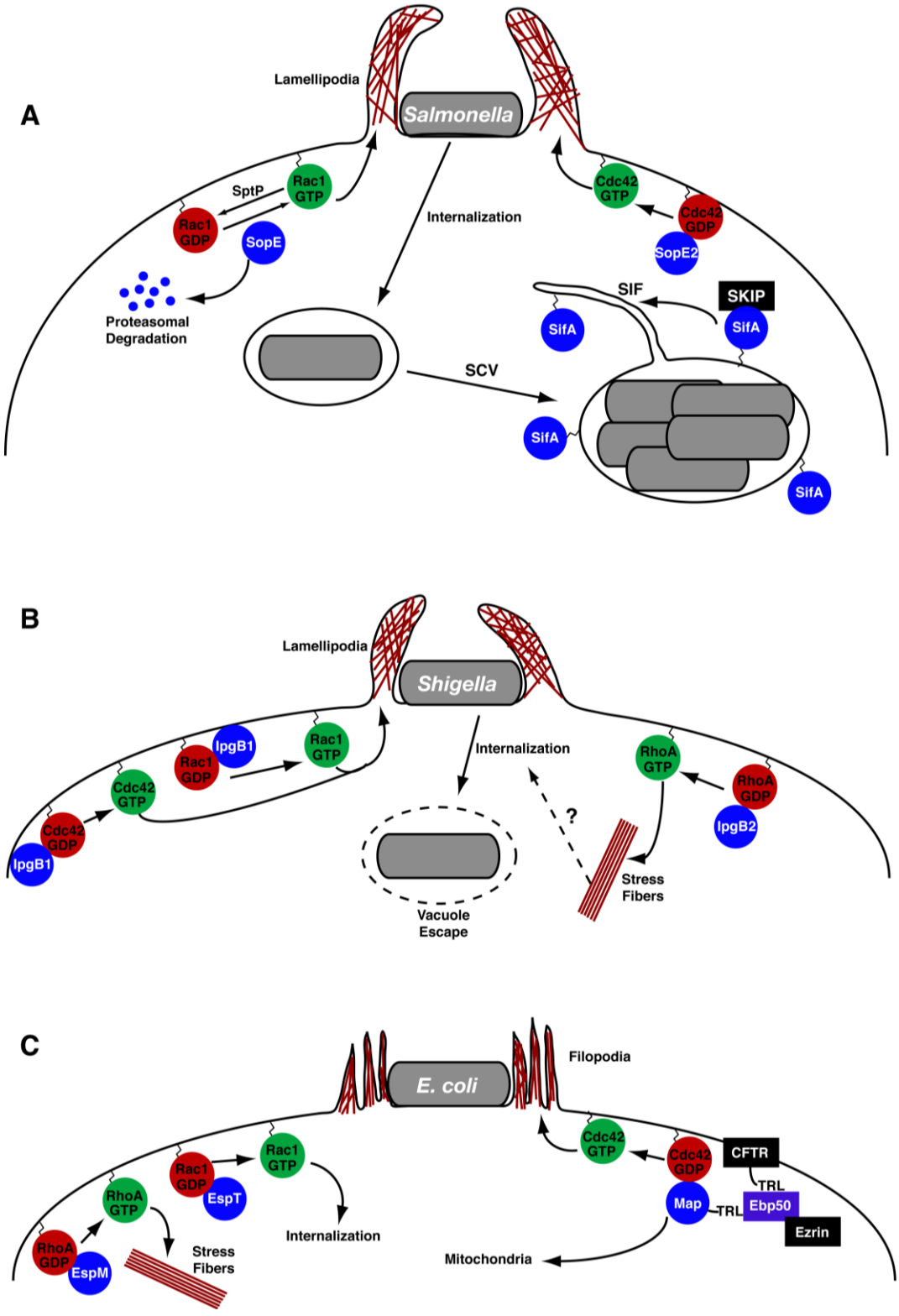
A
Lamellipodia
Salmonella
SptP
Rac1 GTP
Rac1 GDP
SopE
Proteasomal Degradation
Internalization
Cdc42 GTP
Cdc42 GDP
SopE2
SIF
SKIP
SifA
SifA
SCV
SifA
SifA
B
Lamellipodia
Shigella
IpgB1
Rac1 GDP
Rac1 GTP
Cdc42 GTP
Cdc42 GDP
IpgB1
Internalization
RhoA GTP
RhoA GDP
IpgB2
?
Stress Fibers
Vacuole Escape
C
Filopodia
E. coli
Rac1 GTP
Rac1 GDP
EspT
RhoA GTP
RhoA GDP
EspM
Stress Fibers
Internalization
Cdc42 GTP
Cdc42 GDP
CFTR
TRL
Map
TRL
Ebp50
Ezrin
Mitochondria

Figure 4. Bacterial GEFs in pathogenesis. Illustration of the function of bacterial GEFs (blue circles) in *Salmonella* (**A**), *Shigella* (**B**), and *E. coli* (**C**) pathogenesis. The GEFs, SopE, SopE2, IpgB1, IpgB2, and Map are expressed early during infection to generate specific actin structures. SifA is expressed later during *Salmonella* infection and is responsible for maintaining the *Salmonella*-containing vacuole (SCV). Pathways are further described in the text.

Aims of this Study

The overall aim of this study is to understand how the WxxxE/SopE family of bacterial GEFs control GTPase signaling cascades in space and time. While it has been known that bacterial GEFs activate specific GTPases *in vivo* (Alto et al., 2006), the molecular mechanisms underlying this selectivity are unclear. Inappropriate activation of non-cognate GTPases by bacterial GEFs would be detrimental to bacterial fitness as GTPase-isoforms activate distinct signaling pathways. For example, the *E. coli* GEF Map induces filopodia protrusions in a Cdc42-dependent manner, but spurious activation of Rac1 by Map will lead to the internalization of this strict extracellular pathogen (Kenny et al., 2002). In contrast, the *Salmonella* GEF SopE, specifically targets Rac1 signaling to promote bacterial entry into non-phagocytic cells. Uncovering the molecular features that enable bacterial GEFs to recognize specific GTPase-isoforms will further our understanding of the acquisition and evolution of effector proteins.

In addition to catalytic specificity, mammalian GEFs are regulated through extensive protein and lipid contacts or posttranslational modifications (Bos et al., 2007; Yu et al., 2010). However, bacterial GEFs exhibit a compact structural architecture that severely restricts their regulatory interactions (Figure 5). Therefore, how do these simplified GEFs orchestrate complex cellular behaviors with the relative paucity of regulatory modules? Furthermore, are these mechanisms conserved throughout the WxxxE/SopE family or has each individual GEF evolved

a unique method to regulate catalytic activity in space and time? Addressing these questions will provide insight into the means of diversifying a core catalytic domain in order to generate new effector protein functions.

Lastly, pathogens rarely invent new operating principles. Therefore, the bacterial GEFs can serve as tools to probe the complex circuit design of the eukaryotic cell. Because these bacterial GEFs locally activate GTPases at the site of bacterial attachment, the WxxxE/SopE family of GEFs can be used to understand how eukaryotic GEFs spatially amplify signaling cascades while being subjected to rapid diffusion kinetics. In summation, these studies aim to explore how a diverse family of bacterial GEFs has emerged to rewire GTPase signaling circuits and will additionally shed light on the mechanisms that control physiological GTPase signaling events.

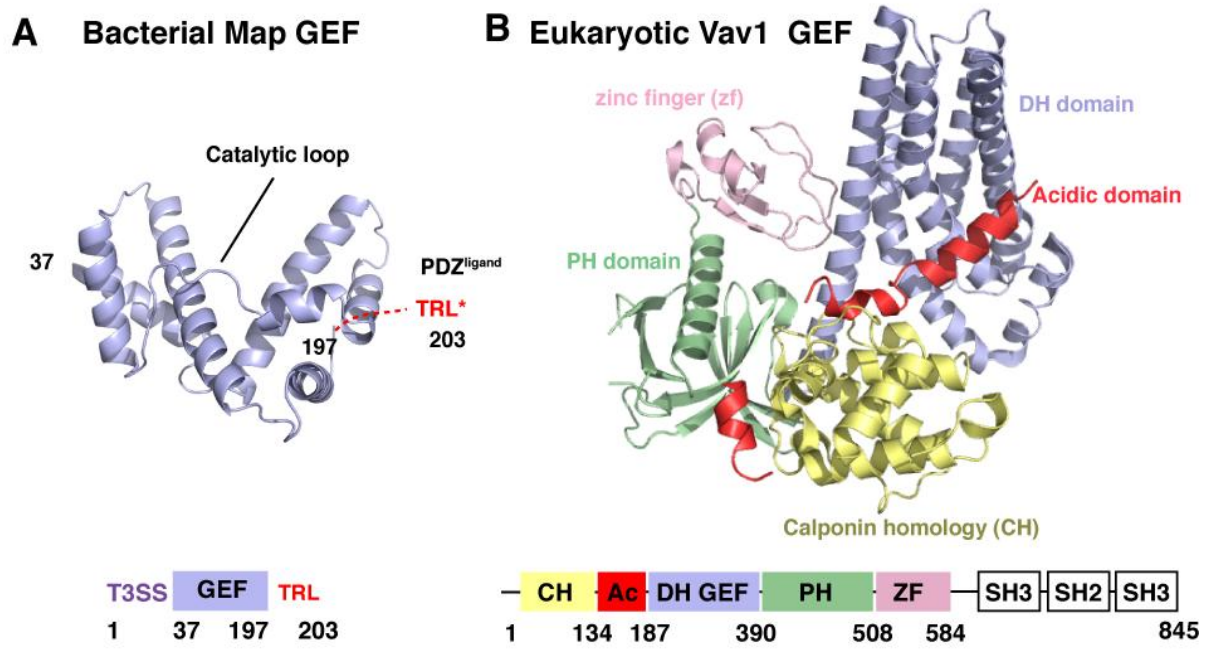

Figure 5. Structural comparison between bacterial and human GEFs. (A and B). Structural comparison (upper) and domain organization (lower) of the *E. coli* GEF Map (PDB: 3GCG) and the human Dbl-family GEF Vav1 (PDB: 3KY9). The domains are color coded as shown in the domain diagrams above. PDZ^{ligand}: PSD-95, Zo-1, DLG domain binding ligands; TRL: residues threonine, arginine, and leucine in single letter amino acid code; DH: Dbl Homology domain; PH: Pleckstrin homology domain. The bacterial GEF Map displays a V-shaped bacterial GEF fold with the only additional functional sequence being a PDZ-ligand (Huang et al., 2009). This minimal architecture is in stark contrast to the sophisticated structural architecture of Vav1, a human Dbl-family GEF (Yu et al., 2010). The Vav1 DH domain (the catalytic region) is regulated through complex multi-domain interactions that respond consecutively to coincident signals in human cells.

CHAPTER TWO
GTPase-Isoform Selection by Bacterial GEF Mimics

Introduction

It has been proposed that the WxxxE family of effector proteins discriminate between different Rho-family GTPase-isoforms based upon the induction of specific cellular phenotypes (Alto et al., 2006). For example, Map induces actin-filopodia protrusions through direct activation of Cdc42, while IpgB1 promotes phagocytic cup formation by activation of Rac1 (Alto et al., 2006; Jepson et al., 2003; Ohya et al., 2005). However, the molecular basis for this selectivity is poorly understood. In contrast, the GTPase-activation and selection mechanism for the Dbl-homology (DH domain) family of eukaryotic GEFs has been elucidated at atomic resolution (Snyder et al., 2002). Snyder *et al*. identified a GTPase "selectivity patch" within the β2-3 interswitch region of the GTPases, which makes extensive interactions with the variable region of the DH domain containing GEFs, forming a "lock and key" pairing mechanisms between Dbl GEFs and their cognate GTPase (Snyder et al., 2002). Closer examination of the interactions between Dbl GEFs and different GTPases reveals a simple model for distinguishing between Cdc42, Rac1, and RhoA isoforms. We were interested in determining if the WxxxE family of bacterial GEFs utilize a similar selection mechanism.

Snyder *et al.* discovered two distinct selection mechanisms that enable Dbl family GEFs to discriminate between GTPase-isoforms (Snyder et al., 2002). A negative selection against Rac1 and RhoA allows Dbl family GEFs to specifically recognize Cdc42. The key GTPase amino acid determinant for this selection is at position 56 which is a phenylalanine in Cdc42,

whereas the equivalent amino acid in Rac1 and RhoA is a tryptophan. To specifically recognize Cdc42, Dbl GEFs make favorable van de Waals interactions with Phe56. However, the larger side chain of tryptophan sterically hinders Cdc42-specific GEFs from interacting with Rac1 and RhoA (Snyder et al., 2002). While Cdc42 specificity is achieved through a negative selection mechanism, RhoA selectivity is determined through positive selection involving ionic interactions between Dbl GEFs and the β2-3 interswitch region of RhoA. The acidic residues at position 45 (Asp) and 54 (Glu) of RhoA repel GEFs that do not have basic amino acids (Lys or Arg) at the corresponding positions (Snyder et al., 2002). Taken together, these two selection mechanisms allow Dbl GEFs to differentiate between closely related GTPase-isoforms.

Ideally, to determine if the WxxxE GEFs utilize a similar selection mechanism to the eukaryotic Dbl family of GEFs, multiple structures containing different GTPases and GEFs in complex should be analyzed. However, at the time of this study only one WxxxE family member's structure (SifA) had been determined and it had been solved in the absence of any GTPase substrate (Ohlson et al., 2008). A major hurdle in the field has been purifying active, recombinant WxxxE proteins as they have a predilection to form insoluble aggregates when expressed in bacteria. In order to gain insight into the GTPase-isoform selection by bacterial GEFs, we undertook a multidisciplinary approach. First, we modeled the sequence of other WxxxE proteins onto the solved SifA structure in order to determine key residues. To test our model predictions, we used a simple life or death screen in yeast to assay GEF activity. Concurrently, we developed a purification protocol to isolate active, recombinant bacterial GEFs

in order to validate our predictions using *in vitro* biochemical assays. Finally, in collaboration with Dr. Jijie Chai we solved the crystal structure of Map in complex with Cdc42.

Combining these approaches, we present compelling evidence that the WxxxE GEFs functionally mimic the catalytic and selectivity mechanisms utilized by the eukaryotic Dbl family of GEFs. These results are surprising because the bacterial GEFs adopt a unique fold and do not share any sequence homology with their eukaryotic counterparts. Importantly, we identify a hypervariable region within the structure of these bacterial GEFs that accurately describes pathogenic diversity at the molecular level. These studies not only contribute insight into the architectural design of bacterial virulence proteins, but provide the tools to dissect these pathogenic signaling networks *in vivo*.

Results

Structural modeling of the interactions between WxxxE proteins and GTPases

A major advancement in the field's understanding of WxxxE effector biology came from the elucidation of the SifA structure. SifA adopts a V-shaped fold that is structurally homologous to the *Salmonella* effector SopE, even though these two effector proteins have no genetic similarities (Ohlson et al., 2008). As described above, SopE is a potent GEF for Cdc42 and Rac1 GTPases (Hardt et al., 1998). Because the structure of SopE in complex with Cdc42 has been solved, we modeled the SopE residues that make contact with Cdc42 onto the structure of SifA (Figure 6). We then took the SifA predicted GTPase contact residues and mapped these residues onto other WxxxE family members based upon secondary structure predictions (Figure

7). These residues will be a major focus of our mutagenesis studies to determine the GTPase-activation and selectivity mechanism of the WxxxE effector proteins.

To evaluate our predictions, we used an *in vivo* yeast viability assay. Previously, our group has demonstrated that inducible expression of the *Shigella* WxxxE effector IpgB2 in yeast activates the Rho1p pathway leading to a severe growth arrest phenotype (Alto et al., 2006). Because it has been historically difficult to purify WxxxE effector proteins and yeast death is an unambiguous assay for IpgB2 functionality, we initially focused our efforts on screening a panel of IpgB2 mutants for activity in yeast.

We introduced mutations in conserved residues of the α2 helix or in the unstructured region between α3 and α4, which is the predicted catalytic loop (Figure 7). Three mutations were individually introduced into the α2 helix: E66A, N76A, D80A (Figure 8A). Position 66 is the conserved glutamic acid in the WxxxE motif that is known to be essential for function in both yeast and mammalian cells (Alto et al., 2006). Based on the structure of SifA, Glu^{66} is important in positioning the catalytic loop. Consistent with previous results, yeast expressing IpgB2 E66A are viable (Figure 8A). The aspargine at position 76 in IpgB2 is conserved, but is not predicted to make GTPase contacts (Figure 6 and 7). Indeed, the IpgB2 N76A mutant had no defect in arresting yeast growth (Figure 8A). The final mutation we made in the α2 helix of IpgB2 is D80A, which we predict to make contacts with the GTPase switch 1 region (Figure 6 and 7). The analogous mutation in SopE D124A abolishes nucleotide exchange activity (Buchwald et al., 2002). Consistent with our predictions, expression of IpgB2 D80A restores

yeast viability (Figure 8A). These data indicate a conserved mechanism of recognizing GTPase substrates by bacterial GEFs through interactions with the α2 helix.

Examination of the putative catalytic loop of the WxxxE proteins reveals a conserved AQSSI motif that is absent in SifA (Figure 7). Therefore, we mutagenized this region in IpgB2 and tested the ability of individual mutants to induce yeast growth arrest (Figure 8B). In support of our model, half of the targeted mutations blocked IpgB2 induced toxicity when expressed in yeast (Figure 8B). Furthermore, deletion of the AQSSI motif (ΔAQSSI) permitted yeast growth under inducing conditions (Figure 8B), validating our structural model. We next turned our attention to identifying residues that are important for distinguishing between different GTPase-isoforms.

While we have identified amino acids that are important for GTPase recognition, these particular residues are unlikely to be involved in dictating substrate specificity for two reasons. First, these residues are conserved amongst all predicted bacterial GEFs despite differences in isoform selection (Figure 7). Additionally, these WxxxE amino acids are predicted to contact the highly conserved switch 1 and switch 2 regions of the Rho family GTPases. Due to the conserved chemistry of these interactions, we believe that the specificity determining region lies in a more variable region of these WxxxE proteins. With only our structure based sequence alignment, we are unable to predict the specificity determinants. Soon after these findings, in collaboration with Dr. Jiji Chai, we were fortunate enough to have solved the X-ray crystal structure of the *E. coli* GEF Map in complex with Cdc42 (Huang et al., 2009). In addition to confirming our findings in yeast, the Map::Cdc42 structure allowed us to identify additional

GTPase interacting residues that could potentially explain the mechanism enabling the pairing of bacterial GEFs with their cognate GTPases.

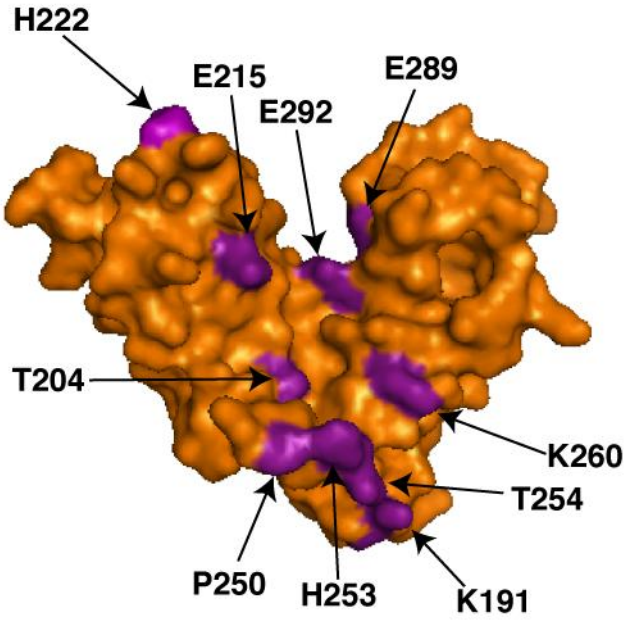

Figure 6. Structural model of SifA's predicted GTPase contacts. Surface projection of the SifA WxxxE fold (PDB: 3CXB). Putative contact regions with GTPases (purple) based on the analogous contact regions previously identified in the SopE::Cdc42 structure (Buchwald et al., 2002).

Figure 7. Structure based alignment of the WxxxE effector family. Alignment of the WxxxE family based upon ClustalW, the structure of SifA, PSIPRED secondary structure predictions, and the SopE::Cdc42 structure. Cartoons depicting the structural elements of SopE (grey) and SifA (gold) are above the sequences. Shaded amino acids denote amino acid similarities.

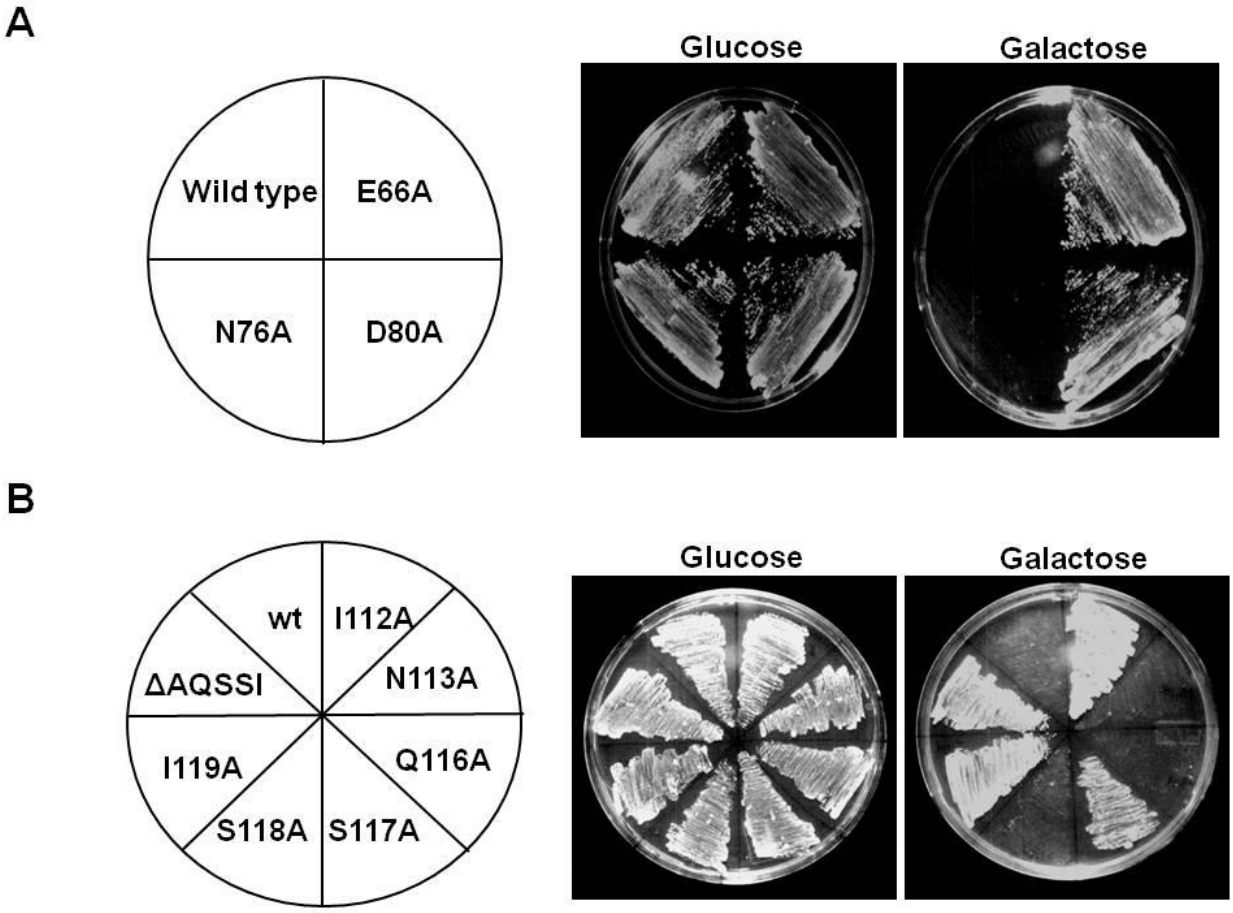

Figure 8. Mutations in the IpgB2 GTPase contact residues rescue yeast toxicity. Wild type (wt) or indicated mutations expressed in yeast under a galactose inducible promoter. Mutations were in either the predicted α2 helix **(A)** or the catalytic loop **(B)**.

The identification of a bacterial GEF hypervariable region that is responsible for GTPase-isoform selection

The Map::Cdc42 structure revealed that Map interacts extensively with the β2-3 interswitch region of Cdc42 (Figure 9). The β2-3 interswitch region is the specificity determinant for the eukaryotic Dbl family of GEFs (Snyder et al., 2002). We hypothesized that the β2-3 interswitch region has a conserved role in isoform recognition by both bacterial and eukaryotic GEFs. Indeed, superimposing the β2-3 region of Rac1 and RhoA onto this region in the Map::Cdc42 structure reveals extensive clashes with Map amino acid side chains (Figure 9). While Map Gln136 makes favorable interactions with Cdc42 Phe56, Gln136 is predicted to cause steric clashes with the bulkier side chain of tryptophan in Rac1 and RhoA in the analogous position (Figure 9). The ability of Map to discriminate Rac1 and RhoA from Cdc42 based upon the smaller side chain of Cdc42-Phe56 is in agreement with the selectivity mechanisms previously proposed for the Dbl-family of GEFs (Snyder et al., 2002). This structured-based model predicts that Map specifically recognizes the Cdc42 β2-3 interswitch region to distinguish between the closely related Rac1 and RhoA isoforms.

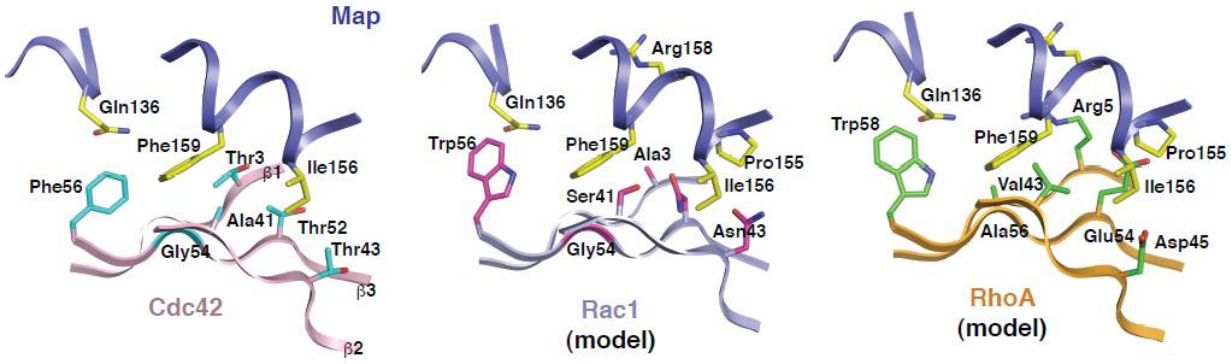

Figure 9. Structural elements of Map that select against Rac1 and RhoA. A comparison of Map–Cdc42 β2-3 structure (left) to two structure-based models obtained by superimposing Rac1 (middle panel) and RhoA (left panel) onto Map. The backbones of Rac1 and RhoA are in light blue and orange, respectively. This figure was generated by Dr. Jijie Chai as part of our structural collaboration.

Consistent with the structural model predictions, Map has GEF activity exclusively for Cdc42 and has no detectable activity towards Rac1 or RhoA (Figure 10A). To directly test the contributions of the β2-3 GTPase residues to the isoform selection of Map, we substituted the Cdc42 β2-3 residues with that of Rac1 and RhoA (Figure 10B). We made combinatorial mutations because no single amino acid change was sufficient to inhibit Map's GEF activity (Data not shown). Compared to wild-type Cdc42, Map had reduced activity against the mutant Cdc42 whose β2-3 residues were switched to those of Rac1 (Figure 10C), and no activity toward the mutant whose β2-3 residues were switched to those of RhoA (Figure 10C). We then reversed the substitutions to convert the β2-3 residues of Rac1 to that of Cdc42 to determine if this region was sufficient for conferring GTPase specificity. Indeed this mutated Rac1 (S41A N43T N52T W56F) can be recognized by Map and had modest nucleotide exchange activity (Figure 10D) compared to the wild-type protein (4.9 ± 0.8 fold). Taken together, these data indicate that the β2-3 interswitch region of Cdc42 is specifically recognized by Map and validates previous *in vivo* findings that Map selectively activates Cdc42 signaling cascades (Alto et al., 2006; Kenny et al., 2002; Simpson et al., 2006).

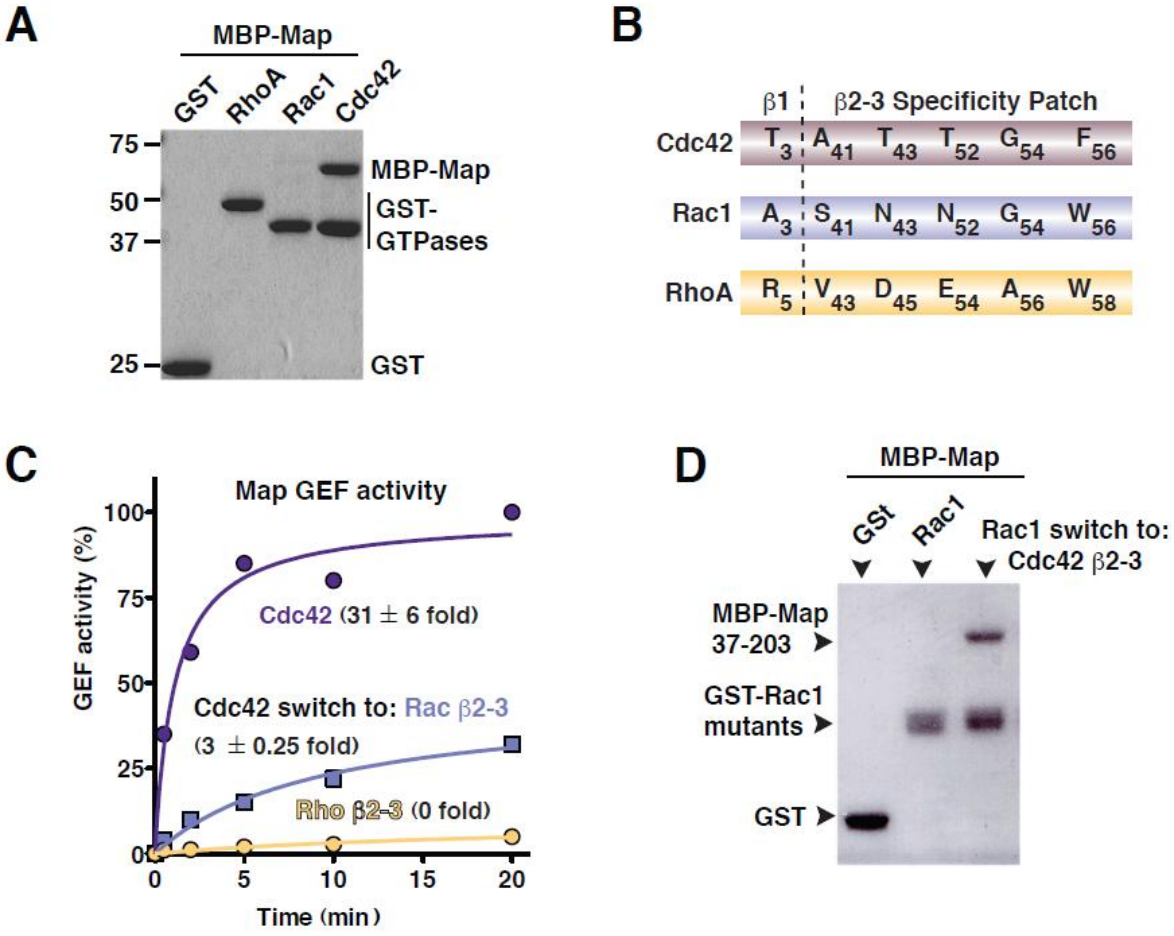

Figure 10. The GTPase β2-3 interswitch region determines Map specificity. (A) Map selectively binds Cdc42. Glutathione-pulldown experiment of GST-tagged RhoA, Rac1, and Cdc42 incubated with MBP-Map. This panel was provided by Adam Wallenfang. **(B)** Alignment of the β1 and β2-3 Cdc42 interface residues that bind Map and their equivalent amino acids in Rac1 and RhoA. **(C)** Time course of GTPγS^{35} nucleotide exchange on Cdc42 (purple), mutant Cdc42 whose β2-3 residues are switched to those of Rac1 (A41S T43N T52N F56W, light blue) mutant Cdc42 whose β2-3 residues are switched to those of RhoA (T43D T52E F56W, orange). Fold induction is presented as the rate of initial velocities (slope from 0 time to 30 s) for the experimental condition over the initial velocity of intrinsic GDP-GTP exchange on native GTPases. The s.e.m. from at least three independent experiments is presented. **(D)** Glutathione pull-down of GST-tagged Rac1 or mutant Rac1 whose β2-3 residues are switched to those of Cdc42 (S41A N43T N52T W56F) with MBP-tagged Map.

We next wanted to determine if other bacterial GEFs distinguish GTPase-isoforms via recognition of the β2-3 interswitch region. Taking our structure based sequence alignment (Figure 7), we examined the conservation of Map's GTPase contact residues with other WxxxE proteins (Figure 11A and 11B). Consistent with our studies conducted with IpgB2 in yeast, we find that the regions of Map that interact with the GTPase switch 1 and switch 2 regions are highly conserved among other bacterial GEFs. In contrast, the α4 and α6 helices of Map that make interactions with the β2-3 region of Cdc42 are highly variable, suggesting that the α4- α6 residues are discriminatory elements for the entire WxxxE family (Figure 11A and 11B).

To experimentally validate this proposal, we performed biochemical assays on the *Shigella* GEFs IpgB1 and IpgB2. Importantly, we were able to isolate recombinant IpgB1 and IpgB2 from *E. coli* using a new purification protocol (see materials and methods for details). Recombinant IpgB1, had robust GEF activity towards Rac1, modest activity for Cdc42, and no detectable activity towards RhoA (Figure 11C). Next, we wanted to determine if the Rac1-specific β2-3 residues are recognized by IpgB1 to discriminate GTPase-isoforms in a similar mechanism as Map. We engineered a Cdc42 mutant that had the β2-3 residues replaced with the Rac1 equivalent amino acids (A41S T43N T25N F56W). IpgB1 stimulated GTP exchange for the Cdc42 to Rac1 β2-3 mutant 4.5 times faster than for wild-type Cdc42 (Figure 11C). Thus the GTPase β2-3 interswitch region is also important for IpgB1 to differentiate between potential substrates.

Based upon the selectivity rules established by Snyder and colleagues, RhoA selectivity is established through interactions with the negatively charged residues Asp45 and Glu54 in the β2-3 region (Snyder et al., 2002). Analysis of the α6 helix of the WxxxE proteins reveals that IpgB2 has two positively charged residues (Arg142 and Lys145) that are predicted to interact favorably with the negatively charged β2-3 region of RhoA (Figure 11A and 11B). Indeed, recombinant IpgB1 displayed prominent nucleotide-exchange activity for RhoA compared to Cdc42 and Rac1 (Figure 11D). The importance of the basic amino acids within the α6 helix in promoting RhoA selectivity is highlighted by the effectors EspM1, EspM2, and EspM3. All three of these effectors activate RhoA signaling cascades within cells and each protein contains two conserved basic amino acids within the α6 helix (Figure 11A) (Arbeloa et al., 2008). Thus we present a model in which bacterial GEFs utilize a hypervariable structural element (α4 and α6 helices) to complementary pair with the β2-3 interswitch strand of distinct GTPase substrates to impart pathogenic diversity (Figure 11E).

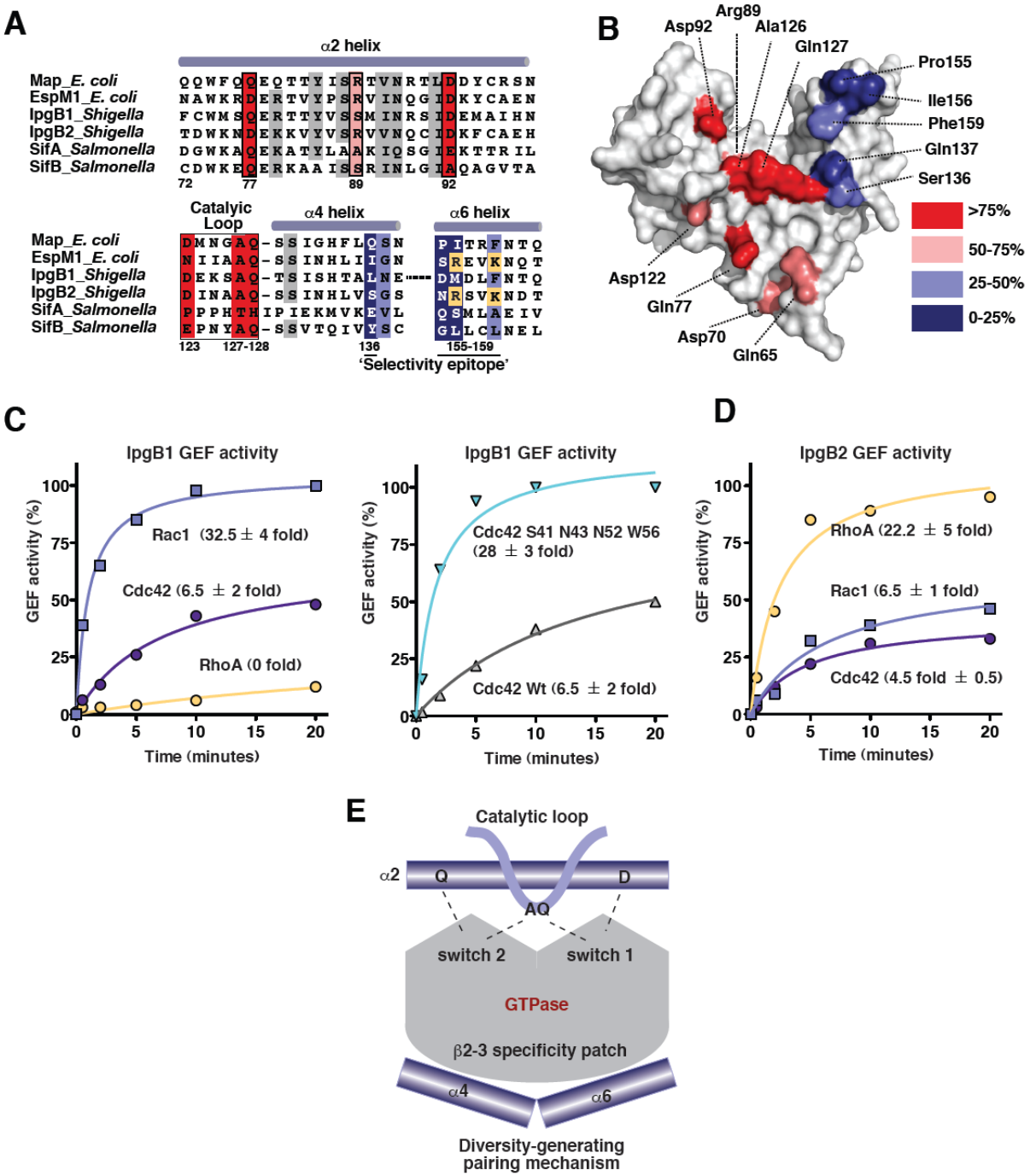
A
α2 helix
Map_E. coli
EspM1_E. coli
IpgB1_Shigella
IpgB2_Shigella
SifA_Salmonella
SifB_Salmonella
72
77
89
92
Catalyic Loop
α4 helix
α6 helix
123
127-128
136
155-159
'Selectivity epitope'
B
Arg89
Asp92
Ala126
Gln127
Pro155
Ile156
Phe159
Gln137
Ser136
Asp122
Gln77
Asp70
Gln65
>75%
50-75%
25-50%
0-25%
C
IpgB1 GEF activity
GEF activity (%)
Time (minutes)
Rac1 (32.5 ± 4 fold)
Cdc42 (6.5 ± 2 fold)
RhoA (0 fold)
IpgB1 GEF activity
Cdc42 S41 N43 N52 W56
(28 ± 3 fold)
Cdc42 Wt (6.5 ± 2 fold)
D
IpgB2 GEF activity
RhoA (22.2 ± 5 fold)
Rac1 (6.5 ± 1 fold)
Cdc42 (4.5 fold ± 0.5)
E
Catalytic loop
α2
Q
D
AQ
switch 2
switch 1
GTPase
β2-3 specificity patch
α4
α6
Diversity-generating
pairing mechanism

Figure 11. A common GTPase selective pairing mechanism of WxxxE GEFs. (A) ClustalW sequence alignment of the WxxxE effectors were manually aligned as in Figure 7. GTPase interacting residues are colored-coded based on their sequence conservation within the family. Dark red residues are most conserved and dark blue the least conserved. The α2 helix, catalytic loop, and α4/α6 helices are shown. The numerical position of important contact residues in Map are indicated. **(B)** The structure of Map is shown in surface representation. The Cdc42-interacting residues of Map are numbered and colored according to their sequence conservation between its family members, as in panel A. **(C)** Left, time course of GTPγS^{35} nucleotide exchange on RhoA (orange), Rac1 (light blue) or Cdc42 (purple) by IpgB1. Right, time course of GTPγS^{35} nucleotide exchange comparing wild-type Cdc42 to mutant forms of Cdc42 in which β2-3 strand residues have been substituted for their Rac1 equivalents (A41S T43N T52N F56W) and induced with IpgB1 **(D)** Time course of GTPγS^{35} nucleotide exchange RhoA (orange), Rac1 (light blue) or Cdc42 (purple) by IpgB2. Experiments are performed as in Figure 7C. **(E)** Cartoon depiction of the full GEF model for bacterial GTPase mimics. Our experiments predict that all bacterial GEF mimics of the SopE/WxxxE family use the conserved catalytic loop– and α2 helix–based guanine-nucleotide exchange mechanism. This is coupled to the α4–α6 diversity-generating pairing mechanism that is used to select for GTPase-isoforms to induce the appropriate signaling events in host cells. Panels C and D contain data conducted by Sarah Sutton.

Discussion

Here we provide mechanistic insight into the GTPase-isoform selectivity by the WxxxE family of GEFs. We find that similar to the eukaryotic Dbl family of GEFs, the WxxxE GEFs discriminate substrates based upon differences in the GTPase β2-3 interswitch region. In support of this model, we demonstrate that Map, IpgB1, and IpgB2 all display different nucleotide exchange activity profiles for Cdc42, Rac1, and RhoA. Importantly, each of these WxxxE proteins has evolved a unique selectivity epitope that pairs specifically with their cognate GTPase β2-3 residues. These findings have been subsequently confirmed through the elucidation of the IpgB2::RhoA structure (Klink et al., 2010). The selectivity residues of IpgB2 that we predicted (Arg142 and Lys145) indeed make electrostatic interactions with the β2-3 residues of RhoA (Klink et al., 2010). Interestingly, the SopE subfamily of GEFs does not

engage the β2-3 region like the WxxxE subfamily, which raises the question of how these GEFs discriminate between various GTPase-isoforms (Buchwald et al., 2002; Huang et al., 2009). Taken together, these data clearly demonstrate the sophistication of bacterial GEF mimics.

Studies by Sasakawa and colleagues have demonstrated that Shigella IpgB1 participates in the invasion of nonphagocytic epithelial cells through the selective activation of Rac1 signaling cascades (Handa et al., 2007; Ohya et al., 2005). In contrast, the attaching and effacing pathogens EPEC and EHEC type III secrete Map GEF molecules that specifically activate Cdc42. Because Rac1, and not Cdc42, facilitates phagocytic cup biogenesis, it is possible that the interconversion between the extracellular life style of EPEC/EHEC and the invasion of host cells by *Shigella,* relies on the simple switch of GTPase diversity by Map and IpgB1, respectively.

In support of this pathogen diversity generating mechanism, *Salmonella,* an intracellular pathogen that resides within a vacuole, encodes two WxxxE effectors (SifA and SifB) that have integral roles in membrane trafficking and positioning of the *Salmonella*-containing vacuole (Beuzon et al., 2000; Boucrot et al., 2005; Brumell et al., 2001; Stein et al., 1996). However, the GTPase targets are unknown for either of these two effectors. Structural and functional studies yield conflicting insight into the substrates of these proteins, especially SifA. Genetic studies indicate that SifA requires another *Salmonella* effector, SseJ, to regulate membrane dynamics (Ruiz-Albert et al., 2002). SseJ is a member of the GDSL family of lipases/esterases and like other members of this family has a broad range of substrates (Ohlson et al., 2005). While genetic abalation of SifA causes *Salmonella* to escape the vacuole and enter the cytoplasm, deletion of

both SifA and SseJ genes from the *Salmonella* genome allows bacteria to remain in a vacuole (Ruiz-Albert et al., 2002). Additionally, SseJ and SifA appear to interact with each other *in vivo* (Ohlson et al., 2008; Ruiz-Albert et al., 2002). Because SseJ becomes more active in the presence of GTP-bound RhoA, it has been hypothesized that SifA functions as a RhoA GEF (Christen et al., 2009; Ohlson et al., 2008). Ohlson *et al.* have reported that SifA can interact with RhoA in the presence of HeLa cell lysate (Ohlson et al., 2008). However, the ability of SifA to catalyze nucleotide exchange on RhoA has not been demonstrated and structural modeling predicts highly unfavorable interactions between SifA and RhoA at the specificity determining region of RhoA (Klink et al., 2010). Because SifA is responsible for altering endomembrane trafficking, it is tempting to speculate that it may activate a small GTPase involved in the general secretory pathway such as an Arf or Rab family member rather than a Rho family GTPase (Beuzon et al., 2000; Ohlson et al., 2008). Future biochemical studies elucidating SifA's GTPase target will lend great insight into how *Salmonella* maintain the *Salmonella*-containing vacuole and the evolution of the WxxxE effector family.

It is intriguing to suggest that Map and its family members have simultaneously maintained a universal guanine-nucleotide-exchange mechanism for GTPase-activation and evolved a pliable GTPase-isoform selection mechanism for the exploitation of new host cell niches. However, it is most likely that properties beyond substrate specificity contribute to pathogenic diversity. For example, in addition to its GEF domain, Map harbors a PDZ (PSD-95/Dlg/ZO-1)-interaction motif at its C terminus. This motif binds directly to the PDZ protein Ebp50, an apically localized scaffold that couples ion channels and transporters to the actin

cytoskeleton. A deletion of the C-terminal PDZ interaction motif, or small interfering RNA knockdown of Ebp50, inhibits actin polymerization induced by Map (Alto et al., 2006). The mechanism underlying the need for this coincident detection is currently unclear. Furthermore, it is unknown whether other bacterial GEFs utilize protein-protein or protein-lipid interactions to regulate their signaling capacity *in vivo*. Future studies exploring these questions are needed to understand the coevolution between bacteria and their host. Nevertheless, these findings demonstrate that the bacterial GEF protein structure is a common, tractable, and genetically inherited module that is exploited by numerous pathogens to generate GTPase signaling diversity in host cells.

Materials and Methods

Yeast Viability Assays

The *ipgB2* gene was cloned into the plasmid pYesDest52 using Gateway technology (Invitrogen). This plasmid has a *Gal1* promoter driving expression of IpgB2. Mutants of IpgB2 were introduced through quick change mutagenesis (Stratagene). All constructs were verified with DNA sequencing. pYesDest52-IpgB2 and derived mutants were transformed into the *InvSc1* yeast strain (Invitrogen) using standard lithium acetate (LiAc) protocol. Briefly, an overnight culture of *InvSc1* was diluted 1:50 in YPAD. After 4 hours of growth at 30°C, yeast were washed once with 50 ml of TE and resuspended in 2 ml of 0.1 M LiAc. The yeast suspension was incubated for 10 minutes at room temperature prior to aliquoting 50 µl into tubes containing 500 ng of the pYesDest52 plasmid and 5 µg of freshly denatured salmon sperm DNA

as a carrier. 350 µl of 100 mM LiAc, 40% PEG 3350 in 1xTE was added to tubes, mixed well, and placed in a 30°C incubator for 30 minutes. After incubation, 44 µl of DMSO was added and the yeast mixture was heat shocked at 42°C for 15 minutes. Cells were washed once with TE and subsequently plated on minimal media lacking uracil. After 2 days of growth at 30°C, yeast were restreaked onto plates containing either glucose as a control or galactose/raffinose to induce protein expression. Viability was scored after 2 days of growth at 30°C.

Protein expression and purification

His6-MBP–tagged Map (residues 37-203), IpgB1 (residues 46-208) and IpgB2 (residues 20-188) were expressed in E. coli BL21 (DE3) cells using 0.4 mM IPTG for 18 hr at 16 °C. Cells were pelleted, resuspended in PBS/DTT buffer (PBS with 2 mM DTT and complete EDTA-free protease inhibitors (Roche), emulsiflexed on ice, and clarified by centrifugation at 15,000 *g* for 15 minutes at 4°C. His6-MBP–tagged proteins were purified on Ni-NTA beads following the manufacturer's instructions (Qiagen). Protein samples were injected into a 24-ml bed volume Sephadex-200 column interfaced to an AKTA FPLC (Amersham), and 0.5-ml elution fractions were collected. Fractions containing monomeric type III effectors were detected by spectrophotometric analysis (at 280 nm) and SDS-PAGE, collected and concentrated to 1 mg ml^{-1}. Samples were frozen and stored at -80° C in a final concentration of 10% glycerol. GST-tagged Rho GTPases were purified on glutathione-Sepharose beads using standard protocols.

GST-pulldown and nucleotide-exchange assays

For GST pull-down assays, Glutathione Sepharose beads (25 µl) were incubated with 50 µg of GST-tagged GTPase and stripped of nucleotide by incubating the beads with TBS/DTT and 10 mM EDTA. Bacterial type III effector proteins (10 µg) were incubated with the GTPases for 1 h at 4°C and washed three times in TBS containing 1 mM EDTA and 1% (v/v) Triton-X 100. Protein interactions were analyzed by SDS-PAGE and Coomassie staining. Guanine-nucleotide exchange assays were conducted as reported previously using concentrations of 0.5 µM for both the bacterial effectors and GTPases (Zheng et al., 1995). Briefly, GTPases were stripped of nucleotide by incubating the protein with high concentrations of EDTA (20 mM Tris pH 8.0, 100 mM NaCl, 2 mM EDTA, 0.2 mM DTT, and 10 µm GDP. After a10 minute room temperature incubation, GTPases were loaded with GDP by adding excess magnesium to the solution (15 mM $MgCl_2$). Assays were initiated through the simultaneous addition of $GTP\gamma S^{35}$ and bacterial GEFs with a final volume of 50 µl. Reactions were stopped through the addition of 950 µl of termination buffer (20 mM Tris pH 8.0, 100 mM NaCl, and 10 mM $MgCl_2$) and applied to nitrocellulose filters attached to a vacuum manifold. After washing three times with termination buffer, radioactivity signal was measured on a scintillation counter. Fold induction is presented as the rate of initial velocities (slope from 0 time to 30 s) for the experimental condition over the initial velocity of intrinsic GDP-GTP exchange on native GTPases. The s.e.m. from at least three experiments is presented.

CHAPTER THREE
Pathogenic E. coli Rewire Host GTPase and Actin Dynamics to Generate a Polarity Circuit

Introduction

The ability of cells to spatially segregate biochemical reactions is an essential feature of all polarity circuits including those found in directional cell migration, asymmetric cell division, and immune function (Drubin and Nelson, 1996; Wedlich-Soldner and Li, 2003). Because of their importance in both single-cell and multi-cellular organisms, the mechanisms underlying cell polarity have been the subject of vigorous investigation for many years. We now recognize that cell polarity is an emergent behavior of a complex biological system. This behavior arises from extensive protein-protein and protein-lipid interaction networks which, when assembled properly, determine the location and dynamics of signal transduction cascades within the cell. Due to the inherent complexity of these systems, the essential molecular connections underlying most polarity circuits are still poorly understood. Thus, identification of simple operating principles that generate cell polarity will greatly expand our understanding of a fundamental biological problem.

Many forms of eukaryotic cell polarity require signaling through Rho family GTPases – the master regulators of the actin cytoskeleton (Jaffe and Hall, 2005). Membrane-bound Rho-proteins shuttle between GDP- and GTP-bound states, but only the GTP-bound state propagates cellular information. The cycling between activity states is tightly regulated by guanine-nucleotide exchange factors (GEFs) that facilitate GTP-binding and Rho activation, and GTPase activating proteins (GAPs) that assist GTP hydrolysis to promote Rho deactivation. While these

conserved regulatory strategies unify Rho GTPase signaling mechanisms across species, they also impose the need for additional protein- and lipid-interactions to control signaling specificity, efficacy, and location within a given cell type. Indeed, microscopy-based studies show that the guanine-nucleotide exchange cycles on Rho, Rac, and Cdc42 are controlled with sub-micron precision along the plasma membrane (Machacek et al., 2009; Nalbant et al., 2004). Due to the complex GTPase activity patterns revealed by these studies, new experimental strategies will be needed to unravel the molecular mechanisms that assemble polarity circuits in space and time.

Because of their essential nature in cell biology, Rho-family GTPases are also common targets of microbial pathogens (Aktories, 2011). Indeed, we have recently identified a large family of bacterial GEFs that potently and specifically activate Rho GTPases (Huang et al., 2009). Upon cell-to-cell contact, bacterial GEFs are injected into the host cell cytoplasm via a Type III Secretion System (T3SS). Once inside the cell, these GEFs rapidly polarize GTPase signal transduction along the bacterial docking interface of host cells. However, unlike mammalian Dbl-family GEFs that are regulated through extensive protein- and lipid-contacts or post-translational modifications, bacterial GEFs exhibit a compact structural architecture that severely limits their regulatory interactions (see Figure 5 for a structural comparison between eukaryotic and prokaryotic GEFs). Therefore, bacterial infection systems offer an alternative strategy to probe the molecular mechanisms of cell polarity since these evolutionarily-simplified GEFs spatially amplify GTPase signaling using minimal networks connections.

In this study, we use the intimate attachment between enteropathogenic *E. coli* (EPEC) and host cells to demonstrate how a network of host/pathogen interactions polarize GTPase

signal transduction in space and time. For this purpose we developed an exogenous, minimal model of GTPase regulation based on our current knowledge of Cdc42 GTPase-activation by Map, a bacterial GEF (Alto et al., 2006; Huang et al., 2009; Kenny et al., 2002). In addition to its compact GEF domain, Map possesses a C-terminal PSD-95/Disc Large/ZO-1 (PDZ)-binding motif that interacts with the PDZ domains of Ezrin binding phosphoprotein 50 (Ebp50) (Alto et al., 2006; Berger et al., 2009; Simpson et al., 2006). Importantly, these protein interactions act as a logical "AND" gate, whereby Map requires both Cdc42 and Ebp50 interactions to regulate F-actin structure and function (see Figure 5). These observations raise the question of whether there are more complex layers of Cdc42 regulation embedded within this bacterial signaling circuit. Do emergent behaviors arise from this specific network design? If so, to what extent will these insights provide a deeper understanding of cell polarity induced by both microbial and mammalian signal transduction systems?

To answer these questions, we combined experimental analyses with mathematical modeling to capture the minimal essential features of the Cdc42 polarity circuit. Unexpectedly, we find that Ebp50 and its binding partner Ezrin function as a molecular scaffold to link Map to the actin cytoskeleton. This interaction network assembles a positive feedback loop that polarizes Cdc42 activity within membrane microdomains. We further show that actin polymerization locally amplifies and temporally sustains Cdc42 signaling in response to external stimulation, thus revealing the molecular and dynamic basis for GTPase polarization during *E. coli* infection. We now propose that bacteria hijack a fundamental circuit architecture that

regulates GTPase signaling activities in a wide range of pathogenic and natural occurring cell polarity systems.

RESULTS

Establishing an experimental model of Cdc42 polarity

Illustrated in Figure 12 is the progression of molecular events that polarize Cdc42 signaling during enteropathogenic *E. coli* (EPEC) infection. The key feature of this system is that EPEC rapidly mobilizes Cdc42 signaling events to the cell surface through a mechanism involving type III secretion of Map, a bacterial GEF (Figure 12). Importantly, Map can only activate Cdc42 when bound to the PDZ domains of Ebp50 through a poorly understood coincidence detection mechanism (Alto et al., 2006; Simpson et al., 2006). Because *E. coli* pathogens secrete up to 40 bacterial effector proteins during infection (Tobe et al., 2006), it has been challenging to dissect the precise role of the Map signaling complex in polarizing Cdc42 at the bacterial-docking interface of host cells.

To overcome this challenge, we performed live-cell imaging on cells ectopically expressing Map protein. To our surprise, Map induced clusters of actin-rich membrane protrusions that emerged stochastically from several discrete regions on the cell surface (Figure 13A). Each cluster was composed of numerous filopodia interconnected by a network of actin lamellipodia (Figure 14). Unexpectedly, F-actin was highly dynamic within the local membrane protrusion, yet these polymerization events did not spread laterally over a 30-minute imaging time-course (Figure 13A). These data indicate that Map polarizes Cdc42 in the absence of

external spatial cues. Indeed, eGFP-Cdc42 was enriched in the actin-rich filopodia clusters induced by Map, whereas Map^{E78A}, a catalytic deficient mutant that does not bind or activate GTPases (Figure 13C), did not polarize Cdc42 in cells (Figure 13A). Using the Cdc42-binding CRIB domain of N-WASP as a probe for the endogenous Cdc42 GTP-activity state (Weiner et al., 2007), we further confirmed that Map locally amplifies and temporally sustains GTPase signal transduction on the plasma membrane (Figure 13A). These stable regions of actin dynamics at the membrane were termed "Cdc42 signaling zones".

We next tested if the induction of Cdc42 signaling zones by Map required its coincident interaction with both Cdc42 and Ebp50 in this model system. As predicted, neither the catalytically inactive mutant of Map (Map^{E78A}, residues 1-203 with E78A mutation) nor a C-terminal PDZ-ligand mutant (MapΔTRL, residues 1-200) produced Cdc42 signaling zones (Figure 13B). The loss of signaling function for MapΔTRL was not due to the lack of GTPase recognition or enzymatic activity since recombinant MapΔTRL bound to the nucleotide-free Cdc42 and induced guanine-nucleotide exchange to a similar extent as wild-type Map *in vitro* (Figure 13C and 13D). These observations establish a robust and tractable experimental model to study the mechanism of spontaneous Cdc42 polarization in the absence of external spatial cues.

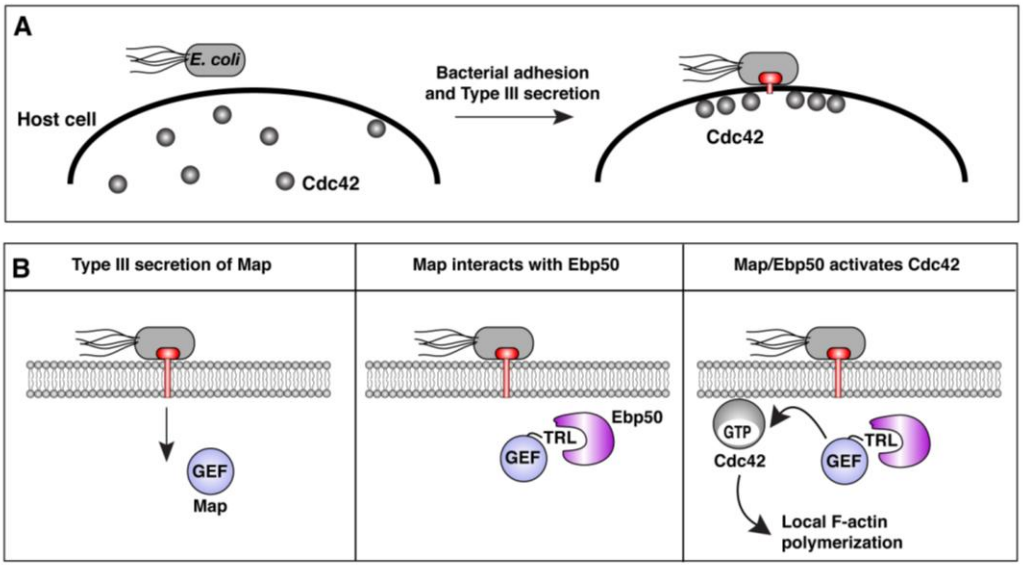

Figure 12. The molecular events that polarize Cdc42 to the EPEC docking interface of host cells. (A and B) Diagram of EPEC-induced Cdc42 polarity in host cells. EPEC adheres to the outer cell surface where it polarizes Cdc42 through type III secretion dependent mechanism (A). Upon type III secretion of Map, its C-terminal PDZ-ligand motif (residues TRL) specifically binds the PDZ domains of Ebp50 and this complex subsequently activates Cdc42 on the membrane.

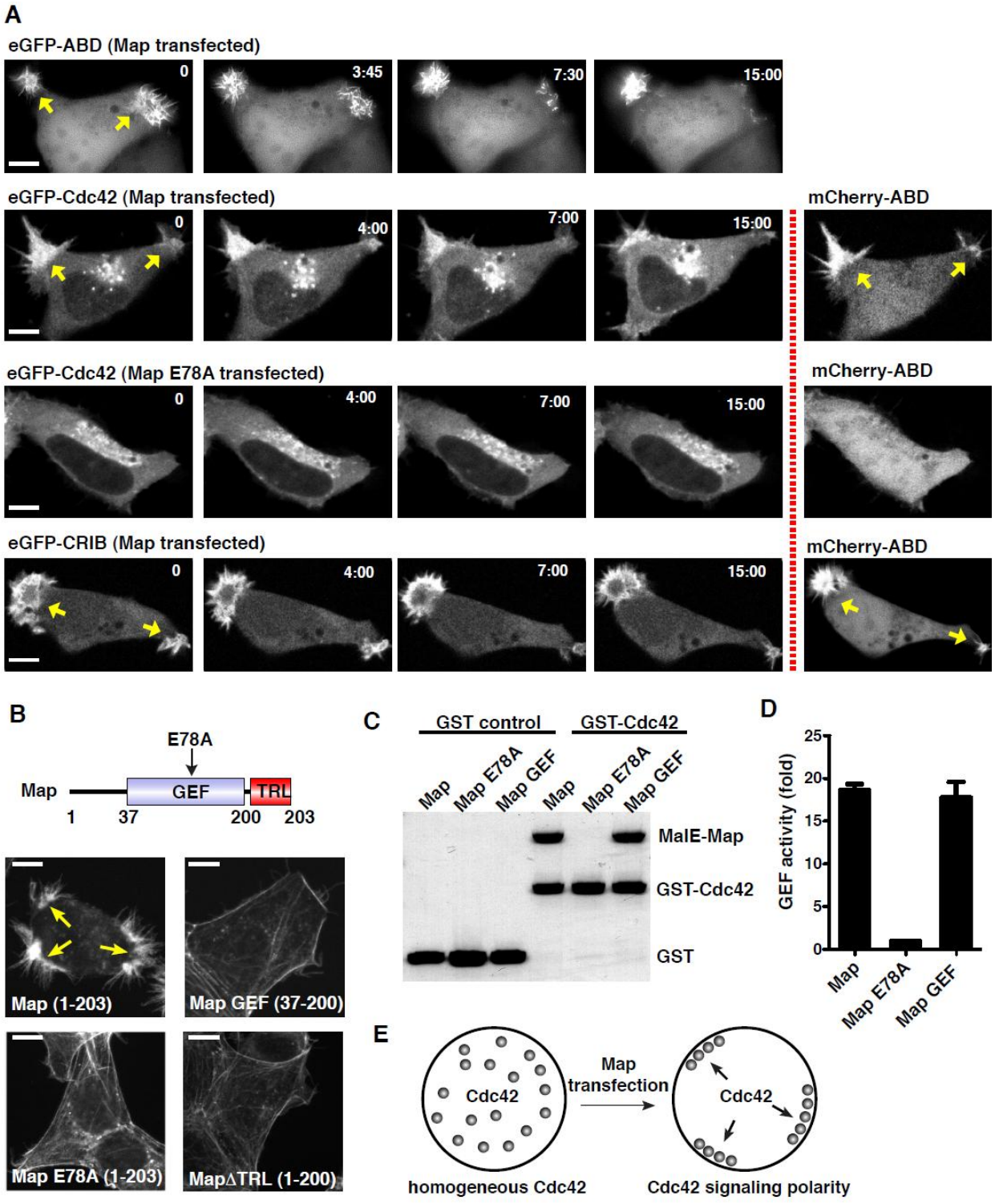
A
eGFP-ABD (Map transfected)
0
3:45
7:30
15:00
eGFP-Cdc42 (Map transfected)
0
4:00
7:00
15:00
mCherry-ABD
eGFP-Cdc42 (Map E78A transfected)
0
4:00
7:00
15:00
mCherry-ABD
eGFP-CRIB (Map transfected)
0
4:00
7:00
15:00
mCherry-ABD
B
E78A
Map
GEF
TRL
1
37
200
203
Map (1-203)
Map GEF (37-200)
Map E78A (1-203)
MapΔTRL (1-200)
C
GST control
GST-Cdc42
Map
Map E78A
Map GEF
Map
Map E78A
Map GEF
MalE-Map
GST-Cdc42
GST
D
GEF activity (fold)
25
20
15
10
5
0
Map
Map E78A
Map GEF
E
Cdc42
Map transfection
Cdc42
homogeneous Cdc42
Cdc42 signaling polarity

Figure 13. Map induces Cdc42 signaling zones in the absence of bacterial cues. (A) Time-lapse fluorescence microscopy of cells co-expressing wild-type Map or the catalytically inactivated GEF mutant Map (MapE78A) with indicated fluorescent probes. F-actin dynamics (mCherry-ABD) were monitored simultaneously with eGFP-Cdc42 or eGFP-$CRIB^{N\text{-}WASP}$. The arrows indicate Cdc42 signaling zones. Scale bar represents 10 μm. **(B)** Fluorescence microscopy of F-actin (rhodamine-phalloidin stain) in HEK293A cells transfected with the indicated Map truncation mutants. The arrows indicate Cdc42 signaling zones. Scale bar represents 10 μm. **(C)** Glutathione sepharose pulldown experiments with nucleotide free GST-Cdc42 in complex with the indicated Map proteins. N-terminal truncations of Map proteins were tagged with MalE: Map (residues 37-203), MapE78A (residues 37-203), and GEF (residues 37-200) as indicated. **(D)** Guanine-nucleotide exchange reactions using GDP-loaded Cdc42 and incubating with Map constructs and $GTP\gamma S^{35}$. GEF activity is presented as the fold over un-stimulated Cdc42 nucleotide exchange rates. **(E)** Cartoon representation of the Cdc42 signaling zones induced by transient transfection of eGFP-Map protein

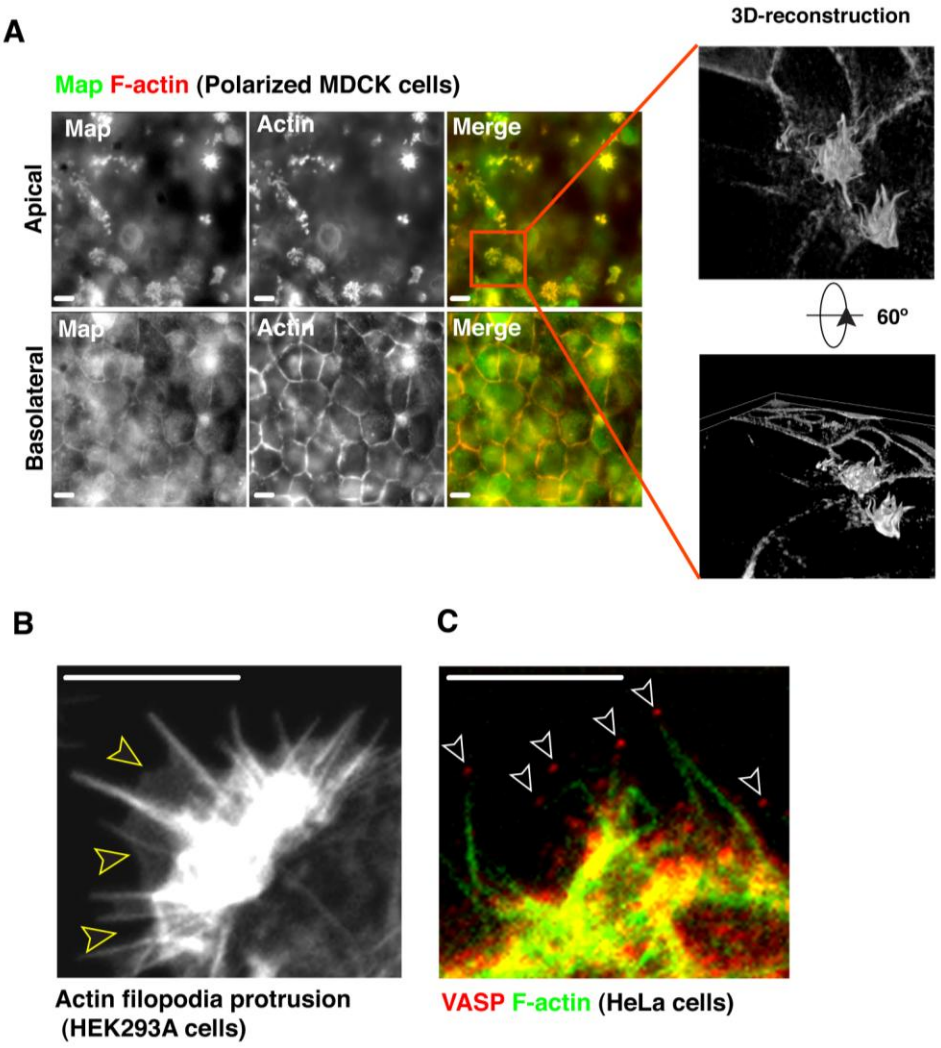

Figure 14. Map induces polarized filopodia bundles in a variety of cell types (A) Confocal microscopy of polarized MDCK cells expressing TAP-Map (FLAG-tag immunoflourescence). F-Actin (red) and Map (green) are shown at the apical and basolateral surface. Confocal sections of the apical or basolateral surface are indicated. Actin filopodia are only detected at the apical surface of Map expressing cells. Scale bar represents 10 µm. Shown to the right is a 3D reconstruction of the nano-comparmentalized actin filopodia morphology induced by Map activation of Cdc42 at the apical cell surface of polarized MDCK cells. Dr. Neal Alto generated the data represented in this panel. **(B)** A fluorescence micrograph of an actin protrusion from a Map expressing HEK293A cell. Filopodia protrusions emanate from a lamellipodia base (marked with open arrow heads). Scale bar represents 10 µm. The emergence of filopodia from a branched network has been extensively studied (Mejillano et al., 2004; Svitkina et al., 2003).

(C) Fluorescence microscopy image of a HeLa cell expressing Map. F-actin (green) protrusions are capped with the protein Vasodilator-stimulated phosphoprotein (VASP; red). VASP is a major regulator of filopodia protrusions and is localized to the tips of filopodia (Rottner et al., 1999). Scale bar represents 10 μm.

A synthetic engineering approach identifies F-actin as an essential signaling platform

Next, we took a synthetic biology approach to test the possibility that Ebp50 targets Map to an essential, yet unknown regulatory network of the host cell. Two pieces of information were critical to this approach. First, the Ebp50 scaffolding complex has been extensively mapped over the past two decades, providing a molecular guide to the essential network connections within the Map signal transduction circuit (Figure 15A) (Bretscher et al., 2000). Second, the isolated GEF domain of Map (residues 37-200) does not polarize Cdc42 activity when expressed in cells, yet is sufficient to activate Cdc42 *in vitro* (Figure 13C). These findings provided the motivation to restore Cdc42 signaling zones by functionally engineering the Map GEF domain with minimal network connections.

Guided by the PDZ-domain interactions between Ebp50 and integral membrane proteins, we individually fused each PDZ-domain of Ebp50 to the GEF domain of Map (Map^{PDZ1} and Map^{PDZ2}). These protein chimeras short-circuited the potential interaction between Map and plasma membrane channels or receptors (Figure 15B). Unexpectedly, neither Map^{PDZ1} nor Map^{PDZ2} induced Cdc42 signaling zones suggesting that Ebp50 does not simply target Map to a trans-membrane receptor complex (Figure 15C). To test whether direct plasma membrane association restored GEF signaling *in vivo*, the dual palmitoylated sequence of Neuromodulin was fused to the N-terminus of Map (^{2xPalm}Map) (Figure 16). ^{2xPalm}Map induced new actin

'microspike' structures that projected laterally over large segments of the plasma membrane and, occasionally, fully encompassed the cell surface (Figure 15C and 15D). Time-lapse microscopy revealed that ^{2xPalm}Map induced a cell spreading phenotype characterized by lamellipodia membrane extensions interlaced with short F-actin microspikes (Figure 15E). Surprisingly however, this gain-of-function phenotype had no resemblance morphologically, quantitatively, or dynamically to the localized filopodia induced by wild-type Map (Figures 15D, 15E, and 16).

Concluding that Ebp50 does not localize Map to the plasma membrane, we next investigated a second key property of the scaffolding complex: F-actin binding (Figure 15A). The 30-residue actin-binding domain (ABD) of Ezrin (Turunen et al., 1994) was fused to the C-terminus of Map (Map^{ABD}), thereby short-circuiting the Ebp50/Ezrin connection to the actin cytoskeleton (Figure 15B). Ectopic expression of Map^{ABD} induced clusters of actin-rich filopodia that projected from several discrete regions of the cell surface (Figure 15C). This actin phenotype had nearly identical geometric boundaries as those observed in Map-expressing cells (Figure 15D). Furthermore, actin filopodia were stably maintained within local regions of the plasma membrane over time, a behavior that recapitulated the Cdc42 signaling zones established by wild-type Map (Figure 15E).

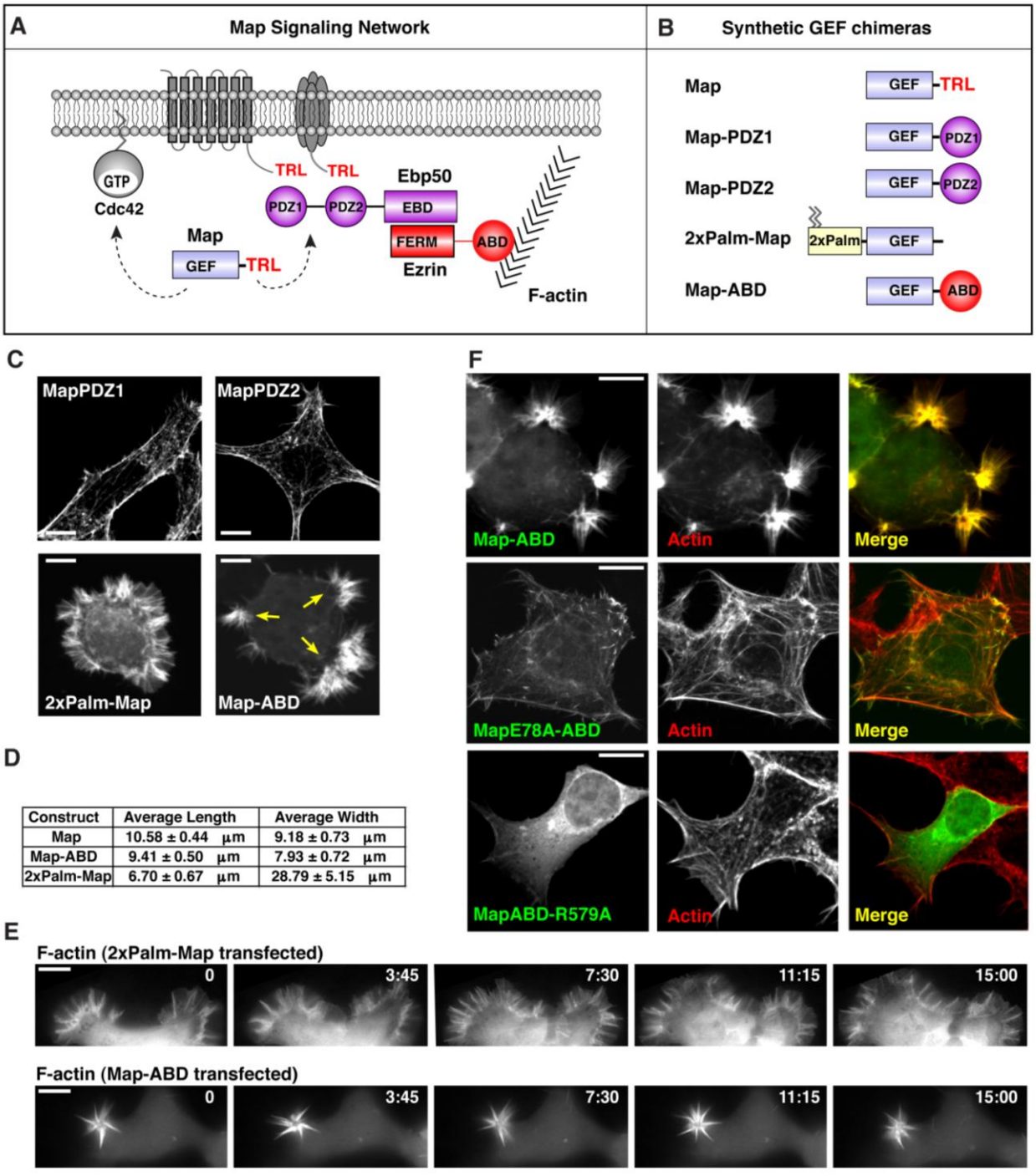

Construct	Average Length	Average Width
Map	10.58 ± 0.44 μm	9.18 ± 0.73 μm
Map-ABD	9.41 ± 0.50 μm	7.93 ± 0.72 μm
2xPalm-Map	6.70 ± 0.67 μm	28.79 ± 5.15 μm

Figure 15. Modular recombination of Map GEF reveals differential Cdc42 signaling behaviors. (A) Schematic of the Map interaction network showing the location of Cdc42, the Ebp50/Ezrin scaffold complex, and its membrane receptor/actin binding topology. T3SS: Type 3 Secretion System signal sequence; TRL: Threonine-Arginine-Lysine PDZ-ligand; PDZ: PSD-95, Discs large, ZO-1 domain; EBD: Ezrin Binding Domain; FERM: Protein 4.1, Ezrin, Radixin, Moesin; ABD: Actin-binding domain. **(B)** Cartoon of the synthetic GEF chimeras used for functional studies. **(C)** Fluorescence microscopy of F-actin (rhodamine-phalloidin) in HEK293A cells transfected with the indicated synthetic GEF chimeras. Scale bar represents 10 μm. **(D)** Geometric measurements of the F-actin phenotypes induced by Map compared to ^{2xPalm}Map or Map^{ABD} as indicated. **(E)** Time-lapse fluorescence microscopy of actin dynamics (eGFP-ABD) in HEK293A cells expressing wild-type ^{2xPalm}Map or Map^{ABD}. Scale bar represents 10 μm. **(F)** Fluorescence microscopy of cells transfected with eGFP-Map^{ABD} (top), GEF inactive mutant (middle) and the actin-binding mutant (bottom). Cells were stained with rhodamine-phalloidin (red) to observe co-localization of synthetic Map proteins with F-actin. Scale bar represents 10 μm.

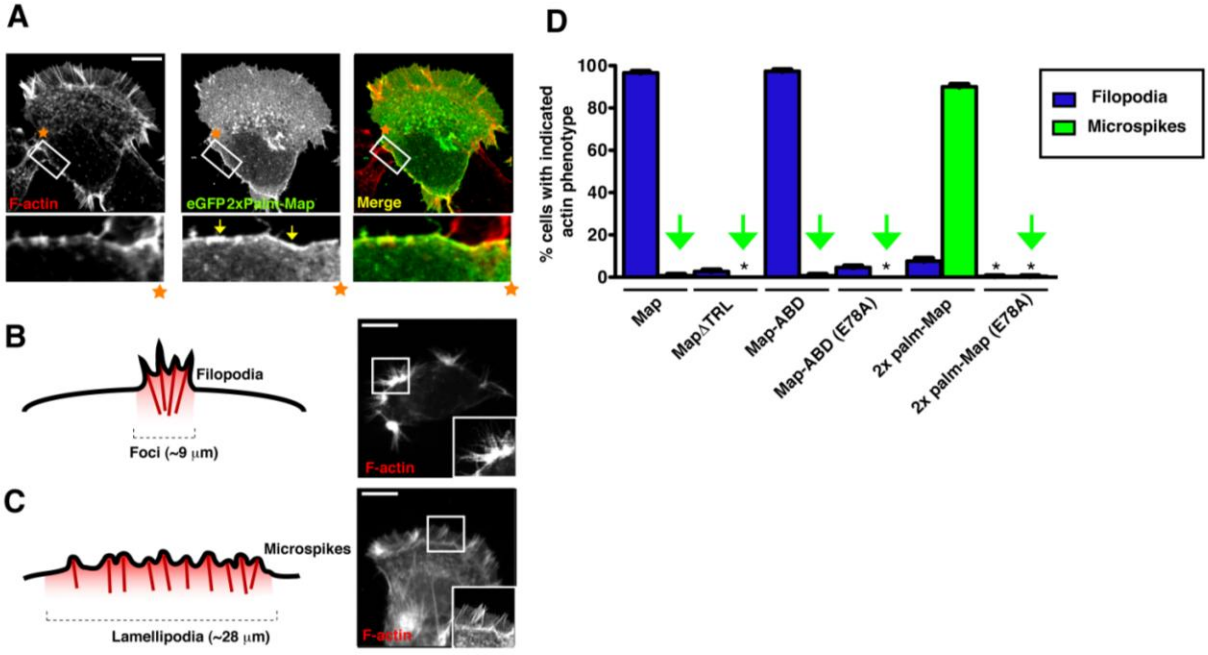

Figure 16. Membrane tethered Map induces microspikes, a distinct actin phenotype from Map induced filopodia. (A) Fluorescent microscopy image of a HEK293A cells transiently transfected with ^{2xPalm}Map and stained with 594-phalloidin. The bottom of the cell outline in the white box shows plasma membrane localization. Shown below each image is an enlarged image (4X) of the boxed region. The orange star marks the orientation of the box and the scale bar represents 10 µm. **(B and C).** Cartoon illustrations depicting the difference between filopodia **(B)** and microspikes **(C)**. Filopodia are classified as protrusions emanating from a small foci (~9 µm), while microspikes are shorter protrusions that cover large membrane distances (~28 µm). Shown to the right of each diagram is a representative fluorescent microscopy image illustrating filopodia in a Map transfected cell and microspikes in a ^{2xPalm}Map transfected cell. The boxed region is a magnified view of the protrusion and the scale bar is represents 10 µm. **(D)** HEK293A cells transfected with indicated Map constructs were classified as containing filopodia or microspikes (n=3). Data are presented as mean ±SEM. The E78A mutation in Map renders the GEF domain inactive. The green arrows point out the quantification for the microspikes for the constructs. This quantification indicates that Map^{ABD} recapitulates the filopodia phenotype that wild-type Map induces, but ^{2xPalm}Map elicits predominantly a microspike phenotype.

The unexpected finding that actin filaments function as a GTPase signaling platform is further supported by the following observations: first, eGFP-tagged Map^{ABD} perfectly co-localized with actin-rich filopodia in transfected cells (Figure 15F). Second, point mutations in either the GEF catalytic domain (Map E78A) or in the Ezrin actin-binding-domain (Ezrin ABD-R579A) (Saleh et al., 2009) inhibited Map^{ABD} from inducing F-actin polymerization (Figure 15F). We therefore conclude that the Ebp50/Ezrin scaffolding complex acts as a molecular bridge to indirectly link Map to the actin cytoskeleton.

Map signals from the tips of actin filaments.

Many mammalian GEFs have been reported to associate with the actin cytoskeleton, yet the functional consequences of these interactions are poorly understood (Figure 17) (Banerjee et al., 2009; Bellanger et al., 2000; Hou et al., 2003). It was therefore of broad significance to explore the functional relationship between F-actin and GTPase signaling in the context of the synthetically engineered Map^{ABD} protein.

A structural model revealed that actin filaments must approach the cell surface to within ~60 Å to form a Map/Cdc42 activation complex on the membrane (Figure 18A). This spatial requirement places strict physical limitations on the Cdc42 activation pathway, as actin-bound Map must be associated with the tips of actin filaments to transduce a signal (Figure 18A, right). To verify this structural model, we examined the actin filament binding properties of Map^{ABD} in the absence of its GEF activity (this allows a direct assessment of Map binding to naturally occurring cytoskeleton structures). As predicted, Map^{ABD} (E78A) was highly enriched at the tips

of actin-microspikes and was conspicuously less abundant on sub-cortical actin stress-fibers (Figure 18B). Moreover, previous studies have shown that the Ezrin-Moesin-Radixin (ERM) family members interact with the barbed-end of actin filaments, a localization that is mediated by the C-terminal ABD (Algrain et al., 1993). These data indicate that Map activates Cdc42 from the tips of actin filaments.

The subcellular location of Map depends on actin polymer dynamics.

Given the dynamic nature of actin-based membrane protrusions, it is likely that actin turnover (polymerization and depolymerization) regulates the location of Map relative to membrane-bound Cdc42. Filopodia-based membrane protrusions are constructed from a highly dynamic polymer network of both bundled and branched actin filaments (Svitkina et al., 2003). To directly visualize Map dynamics at these sites, low levels of mCherry-tagged Map^{ABD} were co-expressed with membrane-targeted eGFP as a positional reference. mCherry-Map^{ABD} formed fluorescent speckles that aligned along actin filaments (Figure 18C). Time-lapse microscopy revealed that Map^{ABD} speckles originated within membrane extensions and moved rapidly toward the cell interior (Figure 18D). This direction and rate of movement of Map^{ABD} was similar to retrograde flow of microinjected rhodamine-labeled actin and transiently expressed protein markers of F-actin dynamics. (Figure 18D and 18E) (Riedl et al., 2008; Theriot et al., 1992; Watanabe and Mitchison, 2002). Although we were unable to discriminate fluorescent speckles of wild-type Map (likely due to the low abundance of the Map/Ebp50/Ezrin trimeric-

complex), its analogy with Map^{ABD} suggests that Map signal transduction is also controlled by actin-filament dynamics.

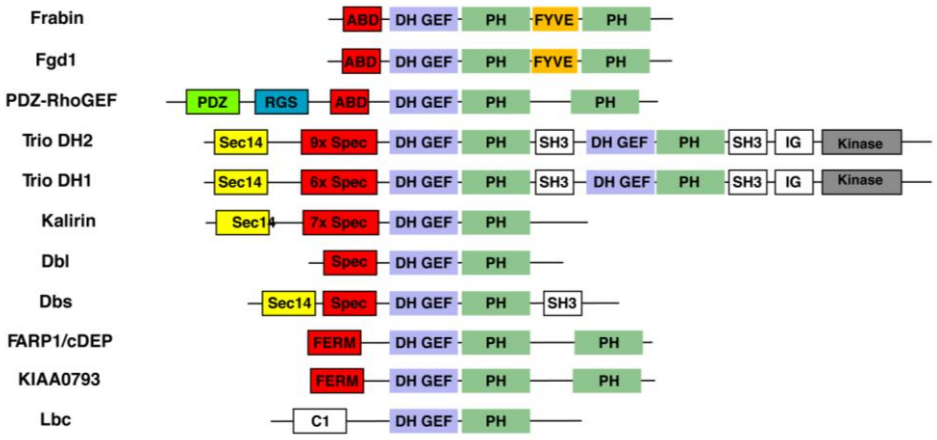

Figure 17. Eukaryotic RhoGEFs can associate with F-actin. Domain organization of eukaryotic GEFs that can interact with F-actin either directly or indirectly. Frabin, Fgd1, and PDZ-RhoGEF, have a conserved F-actin binding domain (Banerjee et al., 2009; Hou et al., 2003; Obaishi et al., 1998). Trio DH2, Trio DH1, Kalirin, Dbl, and Dbs have spectrin repeats which are associated with binding cytoskeletal proteins (Bellanger et al., 2000; Bi et al., 2001; Djinovic-Carugo et al., 2002). cDEP and KIAA0793 have a FERM domain which are often associated with the cytoskeleton motifs (Diakowski et al., 2006). Lastly, the GEF Lbc has been reported to associate stress fibers through an unknown mechanism (Olson et al., 1997). Abbreviations: DH GEF (Dbl homology domain), PH (pleckstrin homology domain), FYVE (Fab1, YOTB, Vac1, and EEA1 domain), PDZ (PSD-95, Dlg, and ZO-1/2 domain), RGS (regulator of G protein signaling domain), C1 (protein kinase C conserved region 1), ABD (actin-binding domain), Sec14 (domain in phosphatidylinositol transfer protein Sec14), Spec (spectrin repeats), SH3 (src homology 3 domain), IG (immunoglobulin domain).

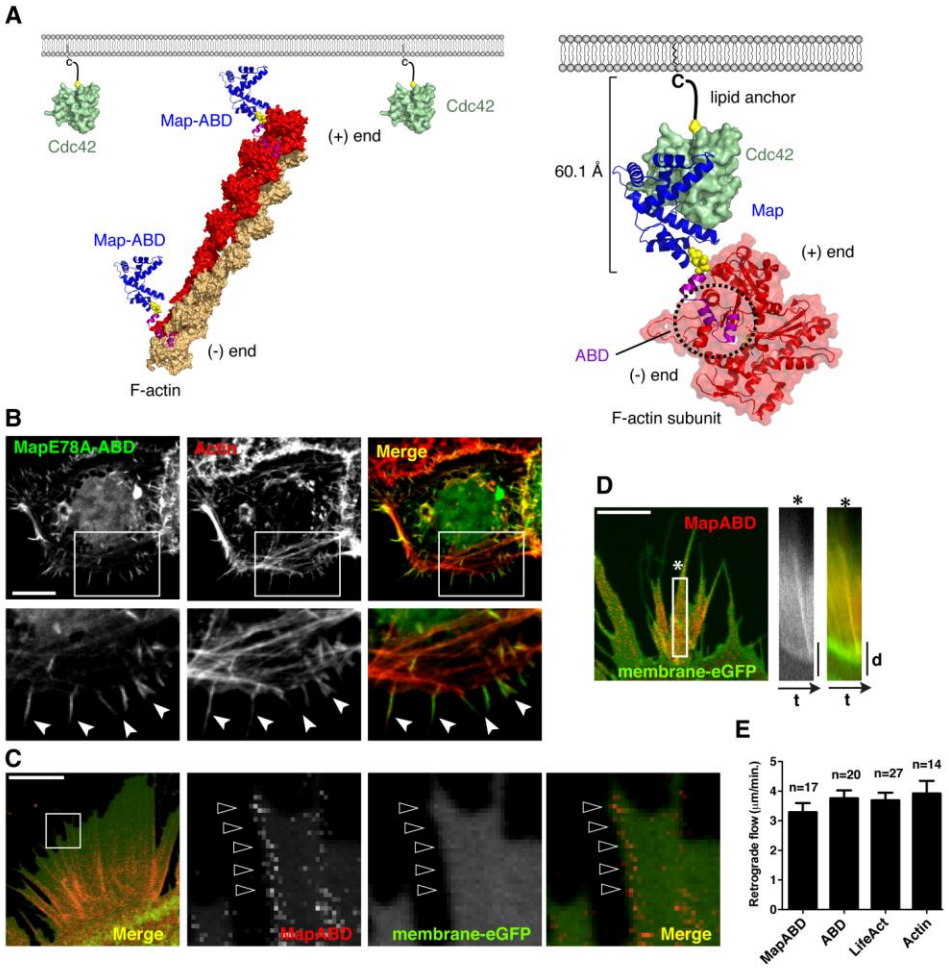

Figure 18. Map signals from the actin cytoskeleton. (A) Structural organization of the Map signaling network. Cdc42 (green) is localized to the membrane through palmitoylation on the C-terminal CaaX box. Map^{ABD} (Map in blue and ABD in fuchsia) is tethered to a single F-actin subunit (red) extracted from an actin filament oriented with the barbed end toward the plasma membrane. Yellow spheres indicate linker regions whose structures are not solved. Known structures of Map/Cdc42 (PDB: 3GCG), Moesin ABD (PDB: 1EF1) and F-actin (PDB: 3MFP) were used in the model and the interaction between Moesin ABD and F-actin is a hypothetical orientation. **(B)** Fluorescence microscopy of a cell transfected with eGFP-Map^{ABD} (E78A) and stained with rhodamine-phalloidin (red) to observe the actin cytoskeleton. The boxed region of each panel is magnified (2x) below. The synthetic protein preferentially binds to the tips of actin filaments (arrows) compared to the sub-cortical actin structures. Scale bar represents 10 μm.

(C) Fluorescence microscopy of cells co-expressing low levels of mCherry Map^{ABD} and membrane-targeted eGFP as a reference. Magnified (5x) view of the boxed region depicts mCherry Map^{ABD} speckles generated near the cell surface and align along actin cables. Scale bar represents 10 µm. **(D)** Time-lapse microscopy of the cell reveals a wave of Map^{ABD} moving away from the cell by actin retrograde flow. The first kymograph depicts mCherry Map^{ABD} moving retrograde while the second kymograph is the merge with eGFP-membrane probe. The star is placed to orient the kymograph and the still framed image. Scale bar represents 10 µm. **(E)** Quantification of retrograde flow of mCherry-tagged constructs indicated. Data was extracted from multiple time-lapse microscopy images using kymograph analysis in ImageJ. Data are presented as mean ±SEM.

Mathematically modeling the Map signaling system reveals an actin-based positive feedback loop

In summary, our data reveals three critical aspects of the bacterial signaling system: First, the binding interaction between Map and the actin cytoskeleton is necessary to polarize Cdc42 on the membrane; second, actin dynamics control the location of Map relative to Cdc42; and third, these molecular interactions induce spontaneous cell polarity in the absence of spatial cues. To determine if these findings can be integrated into a theoretical framework of cell polarity, we developed a mathematical model that describes the minimal set of interactions in a virtual cell. The mathematical model was mainly constructed by Mark Kittisopikul, Dr. Gürol Süel, Dr. Lani Wu, and Dr. Steven Altschuler as part of an extensive collaboration to understand the Map signaling network (Appendix A).

In theory, our model is based on the principle that spontaneous Cdc42 polarity results from the stochastic fluctuations of Map and F-actin between the cytosol and a membrane-proximal "surface compartment" (Figure 19A). We propose that the probability of Cdc42 activation is dependent on the coincidence of two events occurring independently: first, an actin filament

must transition from the cytosol to the surface compartment (Figure 19A, point 1) and second, a Map molecule must bind near the tip of this actin filament (Figure 19A, point 2). Once recruited to the membrane, Map converts GDP-inactive Cdc42 to its GTP-active state (Figure 19A, point 3). Active Cdc42 diffuses laterally along the cell surface (Figure 19A, point 4), which recruits new actin filaments to adjacent membrane sites (for example by stimulating the N-WASP-Arp2/3 complex) (Miki et al., 1998). Together, this progression of molecular events initiates a positive feedback loop by increasing the actin tip density along the membrane, further recruiting new Map molecules to membrane-bound Cdc42 (Figure 19A, point 5).

We first considered the scenario where Map directly interacts with F-actin (Figure 19A). Literature values were used to estimate the rates of actin filament dynamics near the membrane (k_{on} and k_{off}), the affinity of interaction between Map and F-actin (k_{bind} and k_{off}), and the regulatory cycle of Cdc42 (k_{GEF}, k_{GAP}, D) (Table 2). Furthermore, experimental data was used to calibrate the positive feedback term (k_{fb}) (Figure 20A). Computational simulations resulted in the spontaneous polarization of Cdc42-GTP and the accumulation of new actin filaments within discrete regions of the plasma membrane (Figure 19B). Cdc42-GTP signaling zones occupied 9.28 ± 0.74% of the total surface area *in silico*, a value that closely matched the measured width of Cdc42 signaling zones in Map expressing cells (12.1 ± 0.83%) (Figure 20B). In addition, the model gave rise to temporally stable Cdc42 guanine-nucleotide exchange cycles on the plasma membrane as is observed *in vivo* (Figure 20C and Figure 13A). These data indicate that the stochastic assembly of a Cdc42/Map/F-actin complex is required to establish polarity within discreet membrane zones. Consistent with this interpretation, Map was unable to polarize

Cdc42-GTP in the absence of its GEF activity (Figure 19C) or when decoupled from the actin cytoskeleton (Figure 19D). Thus, our stochastic model of polarity agrees with the structural, mutational, and cellular analysis presented in Figures 13-16 and 18.

A scan of model parameter values revealed a direct relationship between the rate of actin filament tip accumulation along the plasma membrane (parameter k_{on}) and the strength of the actin-based positive feedback loop (parameter k_{fb}) in determining the number and width of Cdc42 signaling zones (Figure 20D). We also found that Cdc42 is rapidly depolarized when actin cytoskeleton dynamics are computationally disrupted at a discrete point in time (Figure 19E). To test this model prediction experimentally, Cdc42 localization was monitored in the presence of low concentrations of Latrunculin B (LatB, 50nM), an actin-monomer binding drug that potently inhibits actin filament nucleation. Addition of LatB caused the rapid depolarization of Cdc42 in cells expressing Map^{ABD} (Figure 19F and 19G). Cdc42 polarity was re-established upon drug removal, providing direct evidence that actin polymerization locally amplifies and temporally sustains Cdc42 polarity in response to an actin-bound GEF (Figure 19F and 19G).

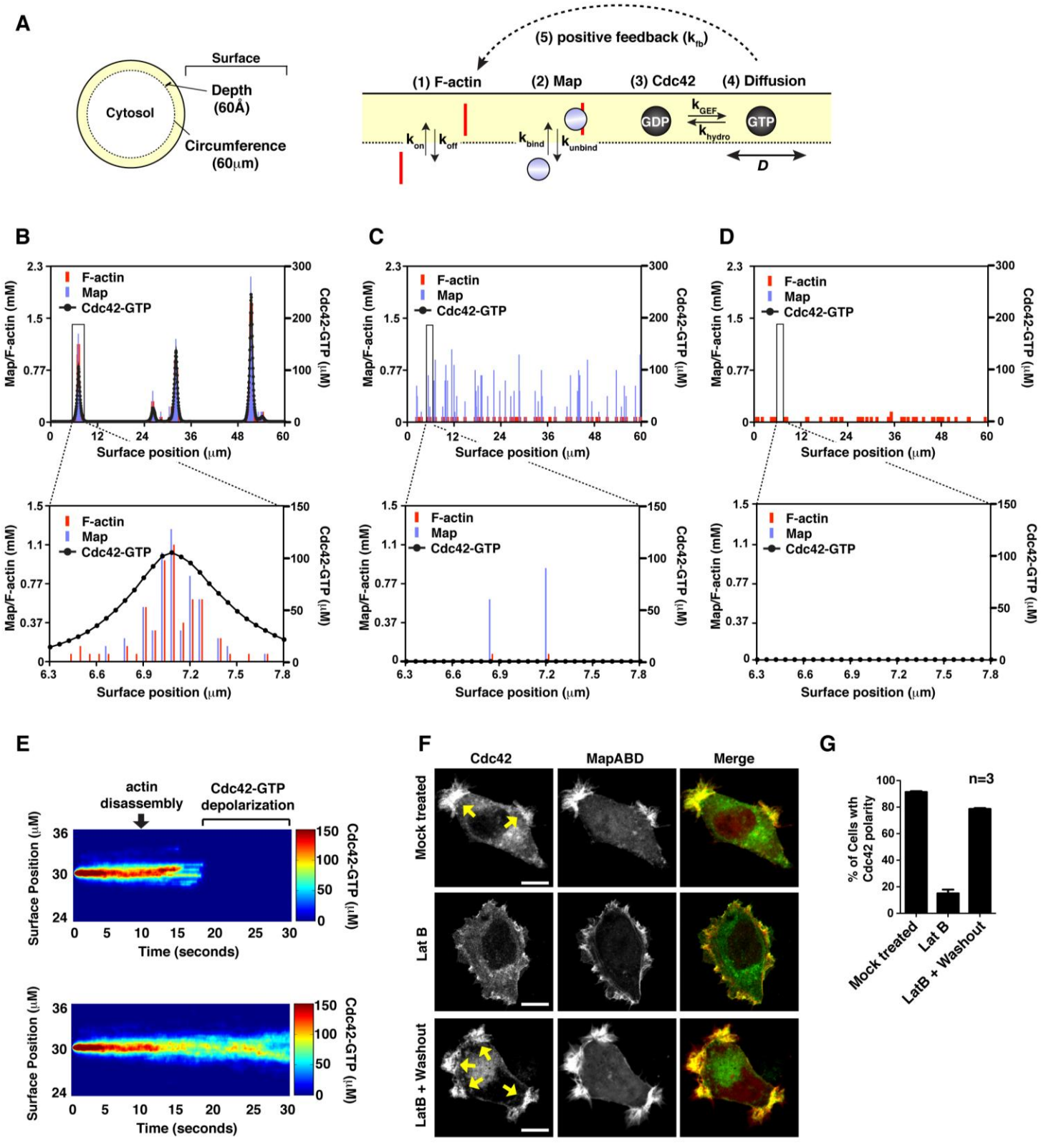
A
Surface
Depth (60Å)
Cytosol
Circumference (60μm)
(5) positive feedback (k_{fb})
(1) F-actin
(2) Map
(3) Cdc42
(4) Diffusion
k_{on}
k_{off}
k_{bind}
k_{unbind}
GDP
GTP
k_{GEF}
k_{hydro}
D
B
C
D
F-actin
Map
Cdc42-GTP
Map/F-actin (mM)
Cdc42-GTP (μM)
Surface position (μm)
E
actin disassembly
Cdc42-GTP depolarization
Surface Position (μM)
Time (seconds)
F
Cdc42
MapABD
Merge
Mock treated
Lat B
LatB + Washout
G
n=3
% of Cells wth Cdc42 polarity
Mock treated
Lat B
LatB + Washout

Figure 19. Mathematical model of the Map signaling circuit. (A) Schematic of the virtual cell (60µm circumference) partitioned into cytoplasm and a surface compartment (6nm depth). The model parameters are shown as: (1) k_{on}, k_{off} the rate of actin filament association and dissociation from the surface compartment; (2) k_{bind}, k_{unbind} the rate of Map association and dissociation from F-actin; (3) k_{GEF}, k_{hydro} the rate of Guanine-nucleotide exchange and GTP hydrolysis; and (4) *D* the rate of Cdc42-GTP diffusion on the membrane; (5) k_{fb} the rate of positive feedback induced by Cdc42-GTP recruiting new actin filaments to the surface compartment. **(B)** Single cell simulation showing the concentrations of F-actin (red bars), Map (blue bars), and Cdc42-GTP (dotted line) per 60nm increments of the cell surface compartment (X-axis). Cdc42-GTP concentrations are plotted as a line graph to clearly resolve the signaling zones from Map and F-actin concentrations. The numerical value bars for Map were manually offset from F-actin by 18nm for visual purposes. The boxed region corresponds to the graph below. **(C-D)** Single cell simulation in which the parameter k_{GEF} is set to 0 **(C)**, or k_{bind} is set to 0 **(D)**. Data is plotted as in **(B)**. **(E)** Kymographs of Cdc42-GTP concentration (color bar) along the cell surface (y-axis) over time (x-axis). Upper panel: computational simulation in which F-actin is disassembled by setting k_{fb}=0 and k_{on}=0 at time 10 seconds (arrow). Lower panel: computational simulation with no actin perturbation (control). Color bar is indicated at right. **(F)** Fluorescence microscopy showing eGFP-Cdc42 polarity in cells expressing mCherry-Map^{ABD}. Cells were either treated with DMSO (mock treated, upper panel) or treated with 50 nM Lat B for 30 minutes (LatB, middle panel). After 30 minutes, the LatB was washed out and cells were allowed to recover for 10 hours (LatB + Washout, lower panel). Scale bar represents 10µm. **(G)** Quantification of the number of Cdc42 signaling zones in the population of cells shown in Figure 19F. Panels **B**-**E** were generated by Mark Kittisopikul as part of our collaboration.

Table 2. Variables used in the mathematical model

Variable	Description	Simulation Unit	Physical Unit
T	Time	Sec	sec
X	Membrane Position	compartment	60 nm
M(t)	MapGEF in the cytosol	molecules / cell	455 fM
$m_x(t) \equiv m(x,t)$	Map near the membrane at position x and time t	molecules / compartment	77 µM
A(t)	Actin filaments not attached to the membrane	filament / cell	455 fM
$a_x(t) \equiv a(x,t)$	Actin filaments near the membrane at position x and time t	filaments / compartment	77 µM
$c_x(t) \equiv c(x,t)$	Cdc42 concentration at position x and time t	µM	1 µM

Table 3. Parameters used in the mathematical model.

Parameter	Value	Units	Description	Reference
k_{on}	2.4	sec^{-1}	Attachment rate of filaments to the membrane	(Marchand et al., 2001)
$k_{off\backslash}$	0.6	sec^{-1}	Detachment rate of filaments to the membrane	(Marchand et al., 2001)
k_{bind}	1	sec^{-1} $filament^{-1}$	Binding rate of MapABD to actin	(Roy et al., 1997)
k_{unbind}	6.5	sec^{-1}	Unbinding rate of MapABD to actin	(Roy et al., 1997)
k_{gef}	77	sec^{-1} $molecule^{-1}$ µM	Catalytic rate of Cdc42 activation through GTP exchange	(Friebel et al., 2001; Huang et al., 2009)
k_{hydro}	3.5	sec^{-1}	GAP mediated hydrolysis rate of Cdc42	(Zhang et al., 1997)
D	0.036	sec^{-1} μm^2	Diffusion rate constant of Cdc42 along the membrane	(Marco et al., 2007; Wedlich-Soldner et al., 2003)
k_{fb}	0.0012	sec^{-1} μM^{-1}	Cdc42 Mediated actin filament attachment	Appendix A
$V_{compartment}$	2.16E-20	L	Volume of a near membrane compartment	(Milo et al., 2010)
A_T	400	Molecules	Total amount of actin	Appendix A
M_T	400	Molecules	Total amount of Map	Appendix A

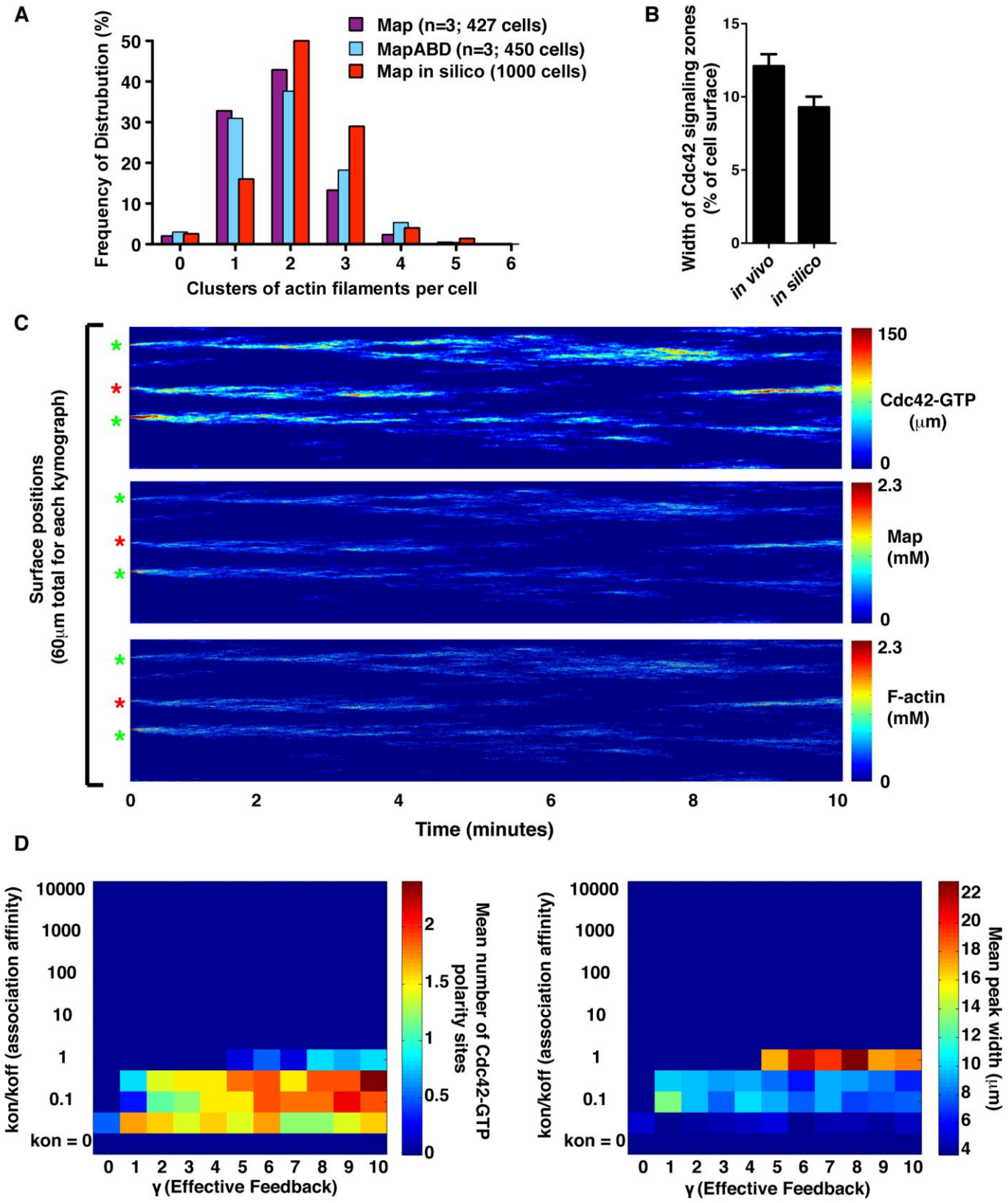
A
Frequency of Distrubution (%)
Map (n=3; 427 cells)
MapABD (n=3; 450 cells)
Map in silico (1000 cells)
Clusters of actin filaments per cell
B
Width of Cdc42 signaling zones (% of cell surface)
in vivo
in silico
C
Surface positions (60μm total for each kymograph)
Cdc42-GTP (μm)
Map (mM)
F-actin (mM)
Time (minutes)
D
kon/koff (association affinity)
γ (Effective Feedback)
Mean number of Cdc42-GTP polarity sites
Mean peak width (μm)

Figure 20: Computational Modeling of Map induced polarity. (A) Frequency histogram displaying the correlation between the number of Cdc42 signaling zones for Map (purple) and Map^{ABD} (cyan) expressing cells (in 3 independent experiments and over 400 cells) and the number of corresponding activity peaks generated computationally from 1000 individual cells (green). For more information on how the peaks were counted please see Appendix A. **(B)** Graph showing the average widths of Cdc42 signaling zones determined *in vivo* and *in silico*. 55 protrusions from 23 cells were used to calculate the mean width of Cdc42 signaling zones induced by Map in vivo. 33 protrusions from 8 simulations were used to calculate the mean width of Cdc42 signaling zones induced by Map *in silico*. **(C)** Kymograph analysis of a simulation in which the distribution of Cdc42-GTP (top), Map (middle), and F-actin (bottom) is monitored over time (x-axis) in the 60 μm virtual cell (Y-axis). The green asterisks mark Cdc42 signaling zones that persist through the entire 10-minute simulation; whereas the red asterisks mark Cdc42 signaling zones that disappear during this time frame. These results are consistent with the longevity and dynamics of Cdc42 signaling zones observed in Map expressing cells (Figure 13A). **(D)** A parameter scan in which k_{on}/k_{off} (y-axis) and γ (effective feedback; x-axis) have been varied as described in Appendix A. The mean number of foci (left) and the average Cdc42 activity peak width (right) were counted (color bars). The computational data in this figure was generated by Mark Kittisopikul.

Reconstitution of Cdc42 polarity in response to external spatial cues

It is important to note that Cdc42 is not polarized randomly during *E. coli* infection, but is precisely recruited to the bacterial docking interface of host cells. How then can our model of stochastic cell polarity described above be reconciled with the deterministic behavior observed during bacterial infection? Our mathematical model provided an essential platform to uncover the molecular nature of these events. Because local Cdc42 activation is initiated by the spontaneous interaction between F-actin and the membrane, it is logical to assume that an external signal that stabilizes F-actin on the membrane would polarize Cdc42 activity at this site. Indeed, nucleating a small number of actin filaments at the membrane prior to running computational simulations resulted Cdc42 activation and a local peak of F-actin accumulation (Figure 21A). Both the actin-based positive feedback loop (Figure 21B) and Map binding to F-actin (data not shown) was essential to polarize Cdc42. These data suggest that Cdc42 polarization can be triggered by local outside-in stimulation of actin polymerization.

To experimentally test this computational prediction, fibronectin-coated beads (Fn-beads) were used to initiate F-actin nucleation at discrete locations on the plasma membrane (Figure 21C). As shown previously, Fn-beads induce clustering of β-integrins and subsequent actin filament attachment to these membrane sites (Figure 22A) (Miyamoto et al., 1995). Remarkably, engagement of Fn-beads to cells ectopically expressing Map induced bursts of actin polymerization that were tightly localized to the sites of surface stimulation (Figure 21D). New actin filopodia were generated at 79 ± 0.7% of Fn-bead binding sites in Map expressing cells (Figure 21E) and these sites were enriched in Cdc42 activity (Figure 22B and 22C). Decoupling Map GEF activity from the Ebp50/Ezrin complex using the MapΔTRL mutant (residues 1-200)

failed to induce actin polymerization and Cdc42 accumulation, suggesting that Map/actin attachment is an essential feature of the polarity circuit (Figure 21E and 22A). Consistent with this notion, over 80 ± 3.4% of Map^{ABD} expressing cells induced local sites of actin polymerization whereas membrane-targeted ^{2xPalm}Map was non-responsive to Fn-Bead stimulation (Figure 21E and 22A). Finally, time-lapse microscopy was used to observe the timing and propagation of actin polymerization in response to outside-in stimulation (Figure 21F). Most importantly, eGFP-tagged Map^{ABD} was recruited to Fn-bead binding site just prior to inducing bursts of F-actin polymerization (Figure 22G). Taken together, these data confirm that a series of stochastic interactions between F-actin, Map, and membrane-bound Cdc42 can generate signal polarity in response to an external spatial cue. They also suggest a concerted mechanism for the excitation of GTPase signal transduction initiated through bacterial infection.

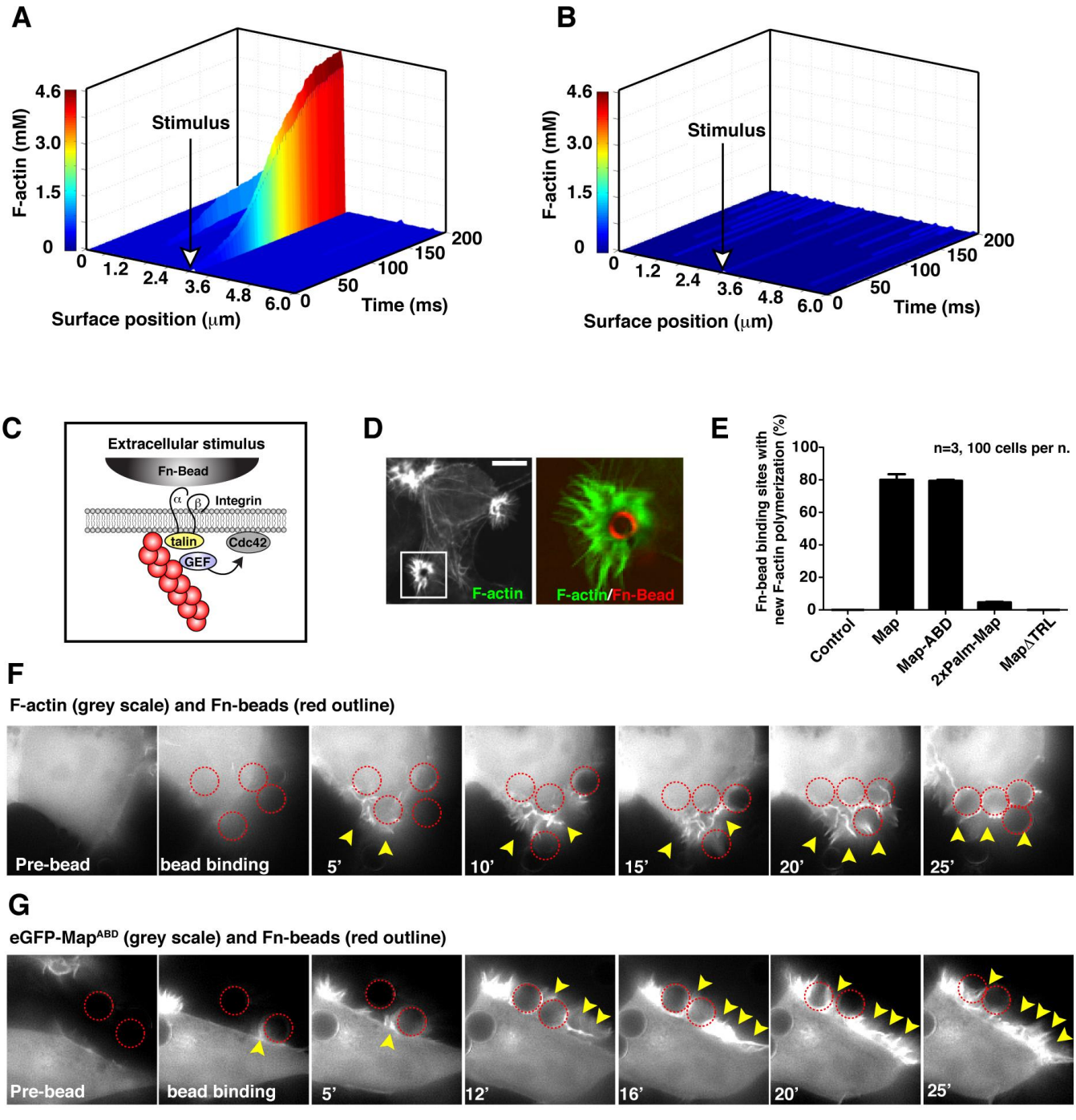
A
F-actin (mM)
4.6
3.0
1.5
0
Stimulus
0
1.2
2.4
3.6
4.8
6.0
Surface position (μm)
0
50
100
150
200
Time (ms)
B
F-actin (mM)
4.6
3.0
1.5
0
Stimulus
0
1.2
2.4
3.6
4.8
6.0
Surface position (μm)
0
50
100
150
200
Time (ms)
C
Extracellular stimulus
Fn-Bead
α
β
Integrin
talin
Cdc42
GEF
D
F-actin
F-actin/Fn-Bead
E
Fn-bead binding sites with new F-actin polymerization (%)
n=3, 100 cells per n.
100
80
60
40
20
0
Control
Map
Map-ABD
2xPalm-Map
MapΔTRL
F
F-actin (grey scale) and Fn-beads (red outline)
Pre-bead
bead binding
5'
10'
15'
20'
25'
G
eGFP-Map^ABD (grey scale) and Fn-beads (red outline)
Pre-bead
bead binding
5'
12'
16'
20'
25'

Figure 21. Reconstitution of cue-dependent polarity in the Map signaling system. (A-B) Computational simulation of a single cell in which an individual membrane compartment was seeded with F-actin attachments prior to running the simulation with (left) or without (right) positive feedback (k_{fb}) in the system. The simulation results are plotted as a 3-D graph showing the surface position (x-axis) and the concentration of F-actin filaments (y-axis) over time (z-axis). The site of seeded F-actin attachments is shown with a white arrow. **(C)** Cartoon depicting the β-integrin signaling connection between Fn-bead binding to the outer cell surface and actin filament attachments to this membrane site. **(D)** Fluorescent micrograph of actin-rich filopodia clusters induced by Fn-bead binding to a Map^{ABD} expressing cell. F-actin is visualized (left) and the boxed region is magnified to illustrate the filopodia protrusions (green) around the Fn-bead (pseudo-colored red). **(E)** Quantification of the number of Fn-beads that induced the F-actin phenotype shown in the presence of cells expressing the indicated synthetic Map construct. Data are presented as mean ±SEM. **(F)** Time-lapse microscopy of HEK293A cells engaging Fn-beads (outlined in red). These cells are co-expressing Map with eGFP-ABD as a visual marker for actin polymerization dynamics in response to Fn-bead binding. Arrowheads indicate new sites of F-actin polymerization. **(G)** Time-lapse microscopy eGFP-Map^{ABD} showing GEF recruitment to the sites of Fn-bead engagement (outlined in red) and its subsequent localization within newly formed membrane protrusions (arrowheads). Panels **A** and **B** were generated by Mark Kittisopikul.

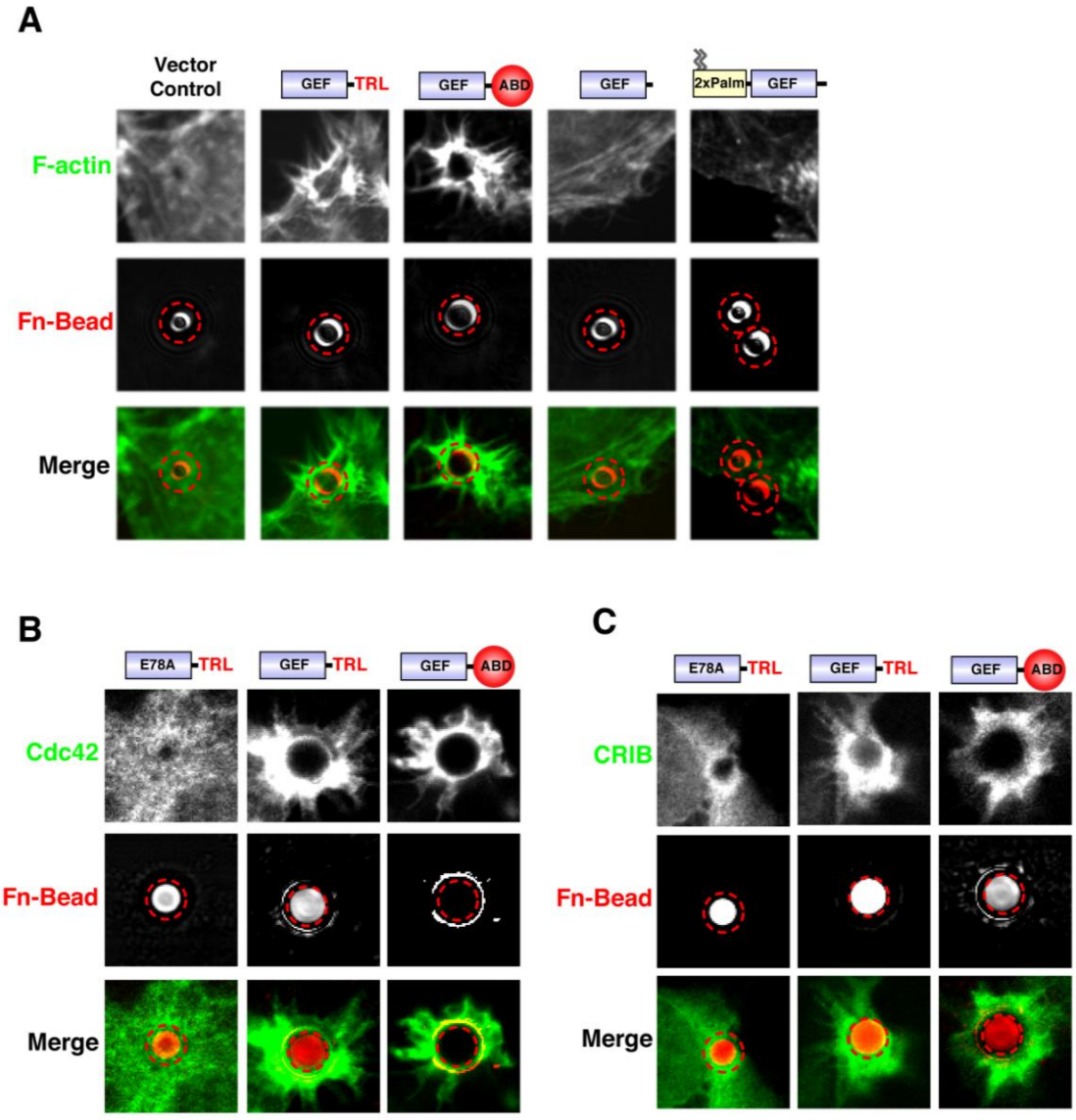

Figure 22. Cue dependent GTPase polarity requires an actin-based positive feedback loop
(A) Fluorescent microscopy images of F-actin (green) in transfected cells that are engaging Fn-beads (pseudo-colored red). The vector control shows a small F-actin ring surrounding the bead revealing a seeding event. Only wild-type Map and Map^{ABD} are able to sense and respond to this seeding event, due to an actin-based feedback loop. The GEF alone or the GEF linked to the membrane (^{2xPalm}Map) are unable to elicit cytoskeletal dynamics around the beads. Because of the reflective nature of the Fn-bead, we found it helpful to outline the 5 µm bead diameter with a red-dashed line.

(B) Fluorescent micrographs depicting Fn-beads recruiting eGFP-Cdc42 in Map and Map-ABD expressing cells, but not in MapE78A cells. **(C)** Fluorescent micrographs depicting Fn-beads recruiting eGFP-CRIB (the Cdc42 interacting domain of N-WASP) in Map and Map-ABD expressing cells, but not in MapE78A cells.

The actin-based positive feedback loop is essential for Cdc42 polarity during EPEC infection.

Given that the Map signaling system is responsive to outside-in signaling cues, it is intriguing to propose that *E. coli* induces an intracellular "landmark" by first creating a small, local perturbation in actin polymerization (Figure 23A, points 1-2). Concomitantly, type III secreted Map protein would monitor the internal cellular state by directly interacting with the Ebp50/Ezrin complex (Figure 23A, points 3). This host/pathogen interaction specifically recognizes the actin landmark established by bacterial adhesion (Figure 23A, points 4). Together, these initiating events trigger an actin-based positive feedback loop, leading to initial Cdc42 polarization and subsequent burst of actin polymerization at the site of bacterial infection (Figure 23A, point 5-7). In agreement with this molecular scheme, type III secretion of Map induced spatially localized actin filopodia at the EPEC infection site of host cells (Figure 23B and 23C) (Alto et al., 2006; Kenny et al., 2002). This spatial regulation requires the Ebp50/Ezrin complex since type III secretion of a MapΔTRL mutant displayed reduced levels of cellular F-actin dynamics (Figure 23C) (Alto et al., 2006; Simpson et al., 2006). Most importantly, complementation of the EPECΔ*map* strain with a plasmid encoded Map^{ABD} chimera rescued local actin filopodia dynamics, indicating that direct attachment of Map to F-actin polarizes Cdc42 to a discrete subcellular location (Figure 23C). Thus, the actin-based positive feedback

circuit is required to locally amplify and temporally sustain Cdc42 activity at the bacterial docking interface of host cells.

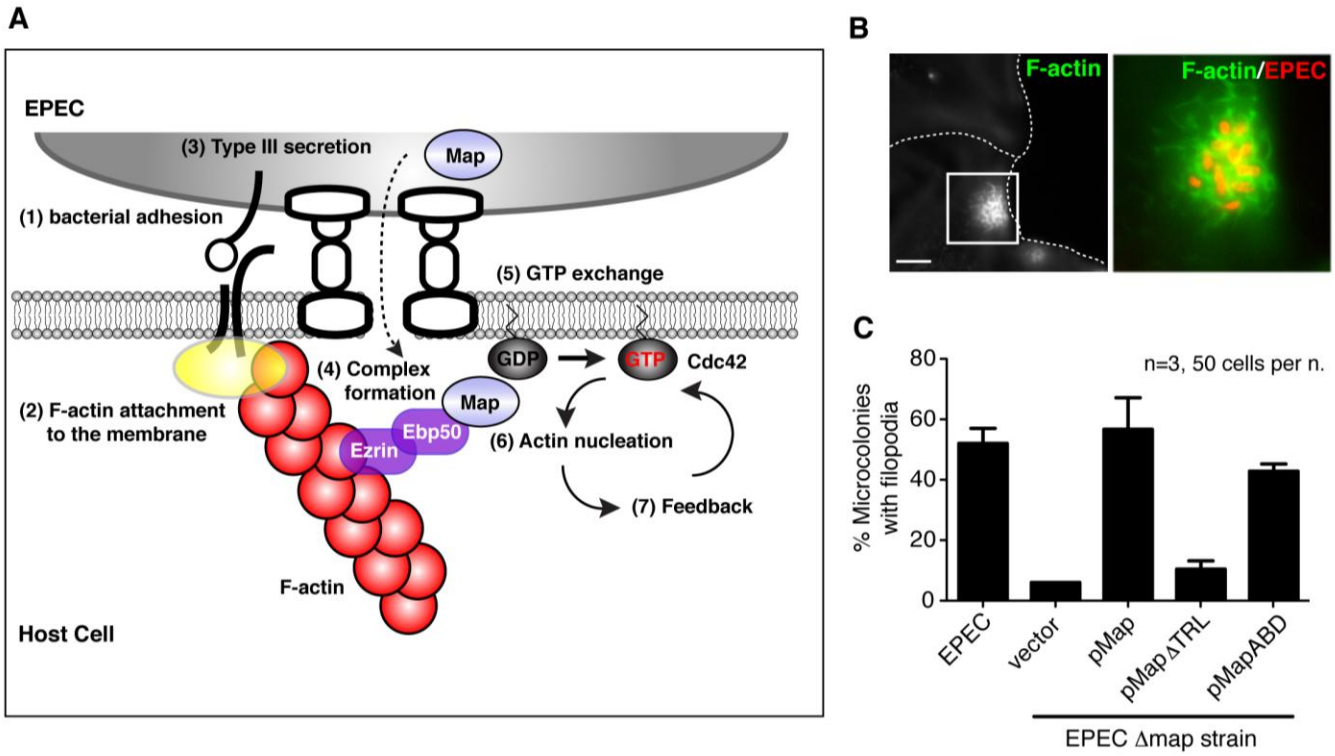

Figure 23. Validation of the Map signaling circuit during bacterial infection. (A) Model of the EPEC induced Cdc42 polarity circuit. EPEC establishes an extracellular landmark by initiating a small outside-in signaling event that generates actin attachments to the membrane (points 1-2). This site is recognized by Type 3 secreted Map protein through the Ebp50-Ezrin-actin complex (points 3-4). Once this signal is initiated, the bacterial GEF controls GTPase activity patterns on the cell surface by engineering an actin-based feedback loop that precisely tunes the location and dynamics of the host cellular response (points 5-7). **(B-C)** Representative example of EPEC infected HeLa cells showing F-actin cytoskeleton **(B)**. Scale bar represents 10 µm. Quantification of localized filopodia in HeLa cells infected with EPEC or EPECΔ*map* strain **(C)**. EPECΔ*map* carrying the indicated plasmids for complementation are shown. At least 50 EPEC infection sites were scored for the formation of filopodia in three independent experiments. Data are presented as mean ±SEM.

Discussion

By asking the simple question: how does an extracellular bacterial pathogen regulate intracellular host actin dynamics, we have uncovered a fundamentally new molecular circuit involved in mammalian cell polarity and bacterial infection. These findings have far-reaching implications on the regulatory mechanisms that control both pathogenic and natural eukaryotic cell behavior.

Our data establish the molecular circuitry that transmits spatial information from extracellular EPEC to the intracellular signaling environment of the host cell. EPEC has evolved Map to interact with the actin-cytoskeleton through the Ebp50/Ezrin scaffolding complex. In the context of bacterial infection, this interaction network functions as a molecular "homing device," allowing EPEC to first mark its position on the extracellular surface via initial actin polymerization and then use the type III secreted effector Map to home in on this intracellular positional landmark (Figure 23A). Once the bacterial position is recognized, Map assembles an actin-based positive feedback loop that spatially amplifies Cdc42 signaling on the membrane. This conclusion is strongly supported by the Fn-bead binding studies (Figure 21 and 22) that recapitulate EPEC infection in an intact, bacterial-free, cellular system. We have previously shown that Map belongs to an extended family of structurally and functionally related bacterial GEF proteins that are required for *Shigella*, *Salmonella,* and *Burkholderia* invasion (Alto et al., 2006; Buchwald et al., 2002; Huang et al., 2009; Upadhyay et al., 2008). Like *E. coli* Map, these GEFs polarize GTPase signaling at the sites of bacterial infection. It is therefore likely that most bacterial GEFs possess targeting sequences that directly or indirectly interact with F-actin or assemble new host polarity circuits that are currently unknown. In a larger context, the ability of

bacteria to engineer signaling circuits from the host cellular machinery provides a mechanism for pathogens to gain "systems level" control over complex host cellular behaviors.

The experimental and theoretical analysis presented here indicates that actin filament dynamics controls the location and magnitude of Cdc42 activity on the plasma membrane. In the circuit described here, actin filament association with the membrane initiates symmetry breaking of Cdc42 by positioning Map in a location competent for GTPase-activation. Once this signaling system has been initiated, actin filament nucleation and branching controls the magnitude of Cdc42 activity by recruiting Map molecules to the tips of actin filaments. Consistent with this model, the actin-depolymerizing agent Latrunculin B rapidly depolarized Cdc42 in cells, indicating that the assembly of actin filaments amplifies GTPase activity on the plasma membrane. These findings are further supported by the observation that Map is recruited to the site of β-integrin stimulation just prior to the excitation of actin polymerization at these sites (see Figure 21). Taken together, these data reveal a previously unrecognized network design that converts actin filament nucleation into GTPase signal amplifier that responds locally and robustly to extracellular spatial cues.

It is notable that Map activates membrane-bound Cdc42 while associated with the tips of actin filaments yet paradoxically, moves away from the plasma membrane at a rate similar to actin retrograde flow (Figure 18D). It is currently unknown how actin subunit treadmilling may influence the interaction between Map and Cdc42 but it is logical to assume that it dampens the signaling system by displacing Map from the membrane. For example, a membrane/N-WASP/F-actin complex (Co et al., 2007) would stabilize actin-bound Map molecules near the cell surface

to activate Cdc42. Release of this complex and subsequent actin retrograde flow would cause the displacement of Map away from Cdc42, thus equilibrating the system. We also suspect that additional actin-binding proteins such as capping proteins or membrane tethering factors (Pollard and Cooper, 2009) will substantially influence GTPase activity in response to actin-bound GEF. It is therefore likely that the relationship between GTPase-activation and F-actin dynamics may be more complex than we have so far described. Nevertheless, our study provides a theoretical and experimental platform to further dissect the various processes and molecular mechanisms that connect actin cytoskeleton dynamics to the polarization GTPase signal transduction cascades in space and time.

Beyond the relatively simple bacterial infection system investigated here, it is intriguing to speculate on how the infection paradigm relates to signaling in higher eukaryotic systems (e.g. cell migration, cell division, and immune function). In those systems, GTPase polarity is precisely controlled through extensive protein-protein and protein-lipid interaction networks. However, they all share a common need for the intrinsically asymmetric distribution of actin polymers and the organization of the cytoskeleton into higher-order structures. It is attractive to hypothesize that the actin-based signaling circuit hijacked by EPEC will also be found in natural Rho GTPase signaling pathways. Both a literature survey and bioinformatic analyses indicates that mammalian Dbl-family GEFs have domains capable of associating directly or indirectly with the actin cytoskeleton (Figure 17). In addition, F-actin has been implicated in the positive feedback regulation of GTPase signaling at the leading edge of chemotactic cells (Xu et al., 2003). Other studies have identified Rac1-specific GEFs that co-localize with F-actin in the

establishment of cell polarity (Park et al., 2004). Despite the close relationship between actin architecture and GTPase activity, the role of actin filament dynamics in the feedback regulation of GTPase signal transduction is still poorly understood. Because bacterial pathogens are unlikely to invent completely new operating principles, we propose that *E. coli* has usurped a conserved circuit topology used to establish direct communication link between the force generating structures of F-actin and the signal transduction systems that control cell polarity.

Most models of cell polarity emphasize the upstream signaling pathways that control downstream F-actin architectures. Conversely, we now propose a fundamentally different view of cell polarity that emphasizes actin filaments as the organizational center of spatially and quantitatively regulated signal transductions pathways. In fact, our findings add significantly to a small, but growing body of literature indicating that F-actin dynamics are the central hub in physiologically relevant signaling processes. For example, Weiner *et al.* recently reported that waves of actin polymerization control the location and activity of the Scar/WAVE signaling complex at the leading edge of migrating neutrophils (Weiner et al., 2007). Likewise, it has been proposed that myosin light chain kinase (MLCK) is transported retrograde with actin filaments, spatially regulating the assembly of focal contacts during directional cell migration (Giannone et al., 2004). It therefore appears that actin-based circuits are not limited to GTPase polarity as described in our study, but are found in a diverse array of signaling systems. Together, these data extend the known functions of the actin cytoskeleton such as force generation, vesicle trafficking, adhesion, and membrane protein dynamics to include the spatial and temporal regulation of signaling transduction. Thus, elucidating the molecular relationships between actin

cytoskeleton dynamics and enzyme regulation promises to be a rewarding area of research in many complex biological systems.

Materials and Methods

Plasmids and Bacterial-Eukaryotic Chimeras

For C-terminal GEF chimeras, Map residues 1-200 was cloned into pEGFP-C1 without a stop codon to allow in frame fusion to the downstream gene fragments including Ebp50 PDZ1 (amino acids 10-110; accession number O14745), Ebp50 PDZ2 (amino acids 129-229), and the actin-binding domain (ABD) of Ezrin (amino acids 541-586; accession number NM_001111077). ^{2xPalm}Map was generated by PCR cloning the dual palmitoylation sequence of Neuromodulin (amino acids 1-20; accession number NP_002036) upstream of eGFP-MapΔTRL in a modified pcDNA 3.1 vector. mCherry-tagged proteins were generated by subcloning constructs into mCherry-tagged pcDNA 3.1. Cdc42 and the CRIB Domain of N-WASP (amino acids 180-267) were cloned into a modified pCDNA3.1 EGFP vector. For protein expression constructs, N-terminal truncations of the Map protein were required to generate soluble protein. Therefore, Map (37-203) and MapGEF (37-200) were cloned into a 6xHis-Maltose Binding Protein (MalE) fusion vector with a pET28 backbone. Site-directed mutagenesis was carried out using the QuickChange Site-Directed Mutagenesis kit (Stratagene). All constructs were verified by DNA sequencing.

Cell Culture and Microscopy

HEK293A and HeLa cells were maintained in DMEM containing 10% (v/v) FBS, 2mM glutamine, and 100 µg/ml penicillin/streptomycin (Thermo Scientific) at 37°C in a 5% CO_2 incubator. Cells were seeded onto coverslips in a 6 well dish and after overnight incubation were transfected using FuGene6 (Roche) and incubated for 16-18 hours. Cells were then fixed and prepared for immunocytochemistry. Fixed cell imaging was performed on a LSM 510 PASCAL scanning confocal microscope (Zeiss, Thornwood, NY). Live cell imaging was performed on an Applied Precision (Seattle, WA) Deltavision RT deconvolution microscope. For fluorescent speckle microscopy, low expressing cells were imaged every 5s on a LSM 510 META scanning confocal microscope (Zeiss, Thornwood, NY). Data was analyzed and quantified using the kymograph plugin for Image J. This plugin captures a narrow region from individual frames of a time-series and stacks them into a single image. Stationary objects appear as a line parallel to the time axis. Object movement is observed as a diagonal streak with the slope being proportional to the velocity. The velocity of retrograde flow was calculated from the distance (µm) over time (seconds) of speckle movement over successive frames.

Fibronectin Bead assays

5 µm polystyrene divinyl-benzene beads (Duke Scientific Corporation, Palo Alto, CA) were diluted in PBS to $2*10^{10}$ beads/mL and incubated with fibronectin (20µg/mL) at 4°C overnight with gentle rocking. Beads were washed once with 5mLs of PBS and resuspended in 1mL of PBS by gentle sonication. 10 µL of the bead slurry were incubated with cells for 20

minutes and subsequently washed with PBS, fixed, and prepared for immunocytochemistry. For live cell imaging, beads were added to cells and immediately monitored using time-lapse microscopy on an Applied Precision (Seattle, WA) Deltavision RT deconvolution microscope.

Protein Purification and GEF Assays

6xHis-MBP-tagged Map or mutant Map protein purification, GST-Cdc42 glutathione pulldown assays, and guanine-nucleotide exchange assays were performed as previously described (Huang et al., 2009).

EPEC infection

EPEC∆*map* strain (Kenny et al., 2002) was complemented with the plasmid pBBRMCS1 encoding wild-type *map* gene, the *map* gene missing the PDZ-ligand ($Map^{\Delta TRL}$, amino acids 1-200), or a chimeric fusion between Map amino acids 1-200 fused to human ezrin residues 541-586 (Map^{ABD}). HeLa cells were infected for 20 minutes with pre-activated EPEC as described previously (Kenny et al., 2002). Briefly, overnight static cultures of EPEC grown at 37°C in LB plus appropriate antibiotics were diluted 1:10 in low glucose DMEM. Bacterial cultures were grown statically at 37°C for two hours and used to infect HeLa cells at an MOI of 100. Plates were centrifuged for 2 minutes at 1,000 *g*. Infection proceeded for 20 minutes and infected cells were fixed and processed for immunofluorescence as described above.

CHAPTER FOUR
A GTPase-phospholipid circuit is required for *Shigella* survival within host cells

Introduction

Current efforts to understand the contribution of bacterial effector proteins to infectious disease outcomes has focused on the cell inhibitory mechanisms of these virulence factors (Cui et al., 2010; Li et al., 2007; Mukherjee et al., 2006; Ribet and Cossart, 2010; Yarbrough et al., 2009). However, a small but growing body of literature indicates that bacterial effector proteins can orchestrate complex cellular phenotypes through the assembly of pathogenic signaling circuits from pre-existing regulatory modules (Patel et al., 2009; Selyunin et al., 2011). Indeed, we have recently demonstrated that the *E. coli* effector protein Map undergoes a positive feedback loop to locally amplify and spatially restrict host GTPase signaling cascades (Orchard et al., 2012). Whether the assembly of "higher order" pathogenic signaling networks by bacterial effector proteins is a global mechanism for hijacking host cellular behaviors is an outstanding question in the field. Additionally, the molecular components enabling the establishment of pathogenic circuits are largely unknown.

A universal mechanism to organize signaling circuits within cells is the local enrichment of pathway components to specific membrane compartments. Identification of the proper membrane microdomain is mediated by the ability of proteins to discriminate the lipid composition of different membranes. Thus, it is not surprising that many enzymes are directly linked to lipid-binding domains to ensure proper subcellular localization. One of the best characterized phospholipid-binding domains is the pleckstrin homology domain (PH domain)

(Balla et al., 2000). The PH domain is one of the most common domains found in the human genome, emphasizing the importance of membrane targeting (Lander et al., 2001). PH domains bind to phosphoinositides with varying affinities, and historically have been utilized as probes for monitoring lipid dynamics in cells (Balla et al., 2000). For example, the PH domain of phospholipase C-delta (PLC-delta), binds specifically to $PI(4,5)P_2$, and is now the standard reagent to observe changes in $PI(4,5)P_2$ localization (Lemmon et al., 1995). In addition to the PH domain, there are other domains that mediate protein-lipid interactions (e.g. BAR, C1, C2, FYVE, PX) (Lemmon, 2008). Despite reports of membrane localization by bacterial effector proteins, currently no effector protein has been identified that possesses any sequence or structural homology to the canonical eukaryotic membrane binding domains (Brombacher et al., 2009; Jank et al., 2012; Patel et al., 2009; Schoebel et al., 2010). Thus, the molecular mechanisms that target effector proteins to eukaryotic membranes and their pathogenic implications are largely unknown. Furthermore, we hypothesize that membrane binding is an important regulatory module that enables effector proteins to assemble pathogenic signaling circuits.

To explore these questions, we sought to identify and characterize novel membrane binding motifs within the WxxxE/SopE family of bacterial GEFs. We chose to focus on this family of effector proteins for several reasons. First, this family encompasses a broad array of pathogenic lifestyles (i.e., extracellular, cytoplasmic, vacuolar). This affords us the ability to compare the diversity of effector-membrane interactions across distinct pathogenic niches. Additionally, most of the bacterial GEFs are associated with host cellular phenotypes providing a

direct means of assaying the pathogenic implications of membrane binding (Orchard and Alto, 2012). Also, several structures of WxxxE/SopE GEFs are available to aid in mapping newly discovered lipid-binding motifs (Buchwald et al., 2002; Huang et al., 2009; Klink et al., 2010; Ohlson et al., 2008; Upadhyay et al., 2004; Williams et al., 2004). Lastly, this family has already been implicated in generating molecular polarity that is predicted to stem from the induction of sophisticated signaling circuits (Orchard et al., 2012). Taken together, we aim to uncover the relationship between effector-membrane interactions and bacterial pathogenesis using the WxxxE/SopE family as a model system.

Here, we utilize a simple yeast genetic screen to identify IpgB1 and SopE2 as novel membrane-interacting proteins. For both proteins we mapped an N-terminal region that is both necessary and sufficient for membrane binding in yeast. We further characterize the molecular mechanisms underlying the direct interaction between IpgB1 and acidic phospholipids. Surprisingly, IpgB1's membrane interactions are dispensable for its known role in cellular invasion, but are necessary for bacterial survival post-internalization. By monitoring the changes in the distribution of host phospholipids, we discover a positive feedback loop that is responsible for maintaining the identity of the transient *Shigella*-containing vacuole. We now propose a model in which membrane remodeling by bacterial pathogens rewires the host-cell signaling landscape to promote bacterial replication.

Results

A yeast genetic screen identifies novel membrane-interacting effector proteins

We assayed bacterial GEFs for membrane localization using an unambiguous yeast life or death screen that was originally designed to identify phosphoinositide-binding proteins in the yeast genome (Isakoff et al., 1998). This screen takes advantage of the *cdc25*^{ts} strain of *Saccharomyces cerevisiae* that grows normally at the non-restrictive temperature of 25°C, but fails to grow at 37°C (Figure 24A). The loss of growth at the selective temperature is due to the inactivation of the Ras cell proliferation pathway that is dependent upon the guanine-nucleotide exchange activity of Cdc25 (Isakoff et al., 1998). Growth at 37°C can be rescued through the introduction of a constitutively active mutant of Ras (G12V) that is localized to any yeast membrane (Yu et al., 2004). Thus, by fusing bacterial GEFs to a mutant of Ras that is constitutively active but on its own, unable to drive membrane localization, we can assay for novel protein-membrane interactions (Figure 24A).

We screened a panel of bacterial GEFs from *Salmonella, Shigella, E. coli* and *Providencia spp* using the "Ras rescue" screen (Figure 24B). Importantly, we introduced mutations in our bacterial GEFs to inhibit catalytic activity, which is known to be toxic to yeast (Alto et al., 2006). Additionally, this mutation blocks effector-GTPase interactions which theoretically could promote Ras signaling and yeast proliferation at 37°C. All chimeras expressed as full-length fusion proteins as determined by western blot analysis (Data not shown). Of the 10 proteins screened, we find 3 proteins (SifA, SopE2, and IpgB1) that are able to reconstitute Ras GTPase signaling in a *cdc25*^{ts} genetic background at 37°C (Figure 24B).

Consistent with previous findings, the screen correctly identified SifA as a membrane-interacting protein (Boucrot et al., 2003; Reinicke et al., 2005). SifA harbors a CaaX box that becomes lipidated and is necessary for SifA's function in maintaining the integrity of the *Salmonella*-containing vacuole (Boucrot et al., 2003).

Previously, IpgB1 has been identified to localize to eukaryotic membranes, but the underlying molecular mechanism governing this localization is currently unknown (Handa et al., 2007). This is the first report that the *Salmonella* GEF SopE2 interacts with cellular membranes. Because both SopE2 and IpgB1 proteins promote the phagocytsosis of *Salmonella* and *Shigella*, respectively, into non-phagocytic cells, it is intriguing to speculate that membrane binding is a necessary feature to orchestrate phagocytic cup formation. To validate IpgB1 and SopE2 as membrane-interacting proteins, we fused these proteins to GFP and monitored their localization in yeast. IpgB1 localizes to the plasma membrane and to intracellular vesicles (Figure 24C). SopE2 is found exclusively on the plasma membrane, but in a more patchy pattern compared to IpgB1 (Figure 24C). These data confirm that IpgB1 and SopE2 interact with eukaryotic cell membranes. We next wanted to characterize the mechanisms that mediate IpgB1's and SopE2's membrane localization.

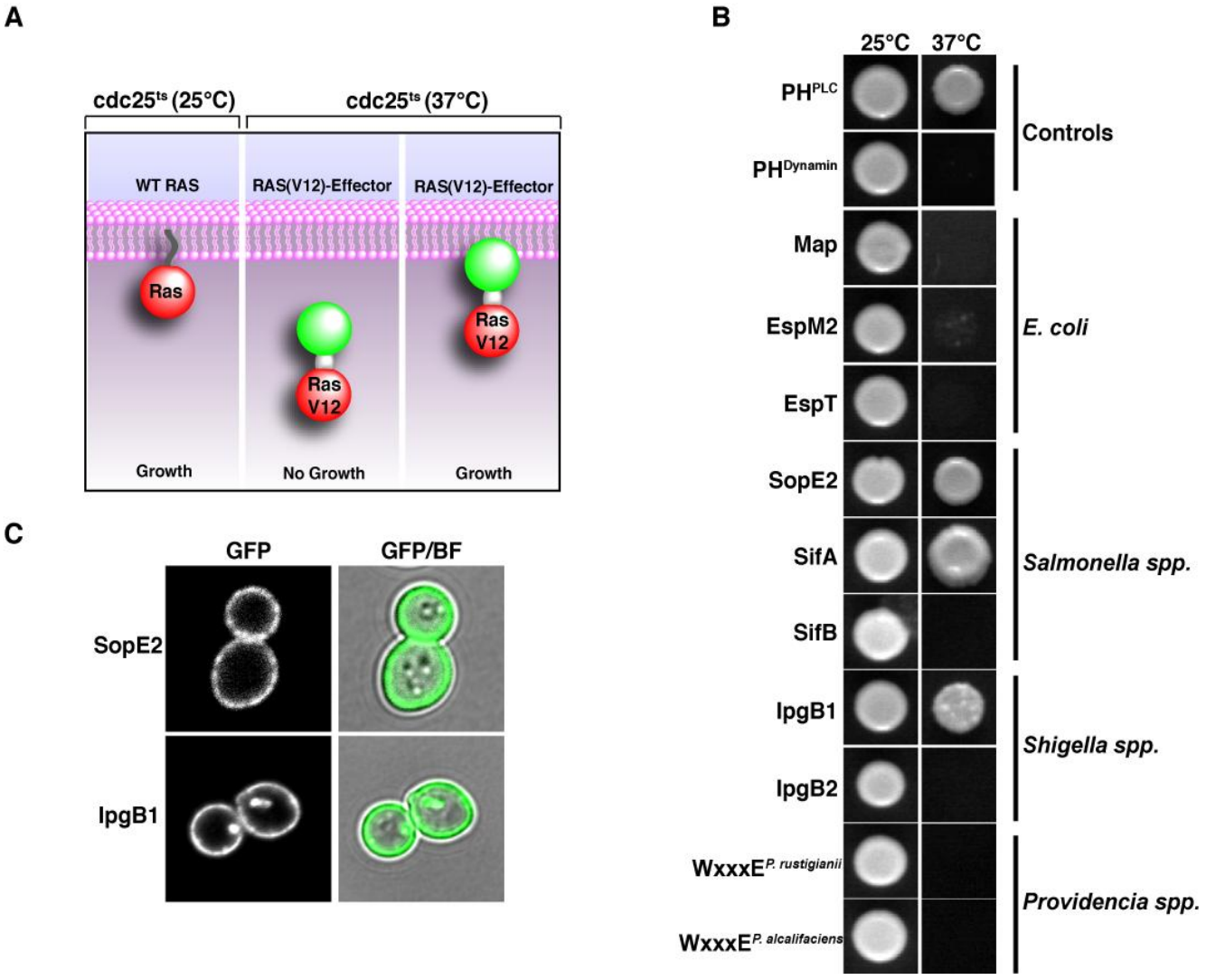

Figure 24. A yeast genetic screen identifies SifA, SopE2, and IpgB1 as membrane-interacting proteins. **(A)** Cartoon diagram of the Ras-rescue screen. Cdc25^{ts} yeast grow normally at 25°C (left panel) but not at 37°C (middle panel). This defect can be overcome by expressing a constitutively active Ras (RasG12V) fused to a membrane targeting sequence (right panel). **(B)** Cdc25^{ts} yeast expressing the listed proteins fused to RasV12 were grown at either the permissive (25°C) or selective temperature (37°C). Each bacterial GEF construct has a single point mutation to block catalytic activity and prevent toxicity (see Materials and Methods). The respective pathogen for each effector protein is listed. *Providencia rustigiannia* and *Providencia alacalifaciens* each have a currently unnamed protein with strong homology towards the WxxxE family of effectors. The PH domains of Phospholipase C (PLC-delta) and Dynamin are used as positive and negative controls respectively. **(C)** Fluorescence microscopy of yeast expressing GFP-tagged SopE2 and IpgB1. GFP fluorescence and brightfield (BF) microscopy shown.

Perturbations of phosphoinositide biosynthetic pathways alter IpgB1 but not SopE2 localization

Our group has recently identified a diverse variety of membrane-interaction mechanisms that are detected by the Ras rescue screen, including lipidation, protein-lipid interactions, protein:protein interactions, and integrated transmembrane proteins (unpublished observations of B.A. Weigele and N.M. Alto). Because the Ras rescue screen was originally designed to identify phosphatidylinositol phosphate (PIP) binding proteins, we sought to determine if IpgB1 and SopE2 localization are dependent upon interactions with PIPs (Isakoff et al., 1998). Importantly, PIPs are essential signaling molecules that control organelle identity, membrane trafficking, cytoskeletal organization, and signal transduction pathways (De Matteis and Godi, 2004; Hansen et al., 2011; Prehoda et al., 2000; Zoncu et al., 2009).

To determine if IpgB1 and SopE2 are spatially regulated by changes in PIP metabolism, we depleted the expression of yeast PI-kinases, the enzyme responsible for site-specific phosphorylation of the myoinositol ring. PI-kinase ablation was accomplished by either isogenic knockout of non-essential genes (VPS34, FAB1, and LSB6) or by doxycycline-mediated repression of TetO7-promoter alleles of the essential PI-kinase genes (PIK1, STT4, and MSS4) (Figure 25A) (Cutler et al., 1997; Desrivieres et al., 1998; Flanagan et al., 1993; Gary et al., 1998; Han et al., 2002; Mnaimneh et al., 2004; Schu et al., 1993; Shelton et al., 2003). We transformed GFP-tagged IgpB1 and SopE2 expression constructs into these six yeast strains and monitored their localization. SopE2 remains plasma-membrane localized despite alterations in PIP availability (Figure 25B). However, we occasionally did observe a large accumulation of GFP-SopE2 fluorescence in Stt4 knockdown (K.D.) cells (Figure 25B). Additionally, the plasma

membrane patches of SopE2 are more pronounced in this strain (Figure 24B). However, the difference in SopE2 localization between the Stt4 knockdown cells and wild-type yeast was not significant enough across a population for a blinded observer to accurately predict genotype from phenotype (Data not shown). Taken together these data suggest that specific phosphoinositides are not required to localize SopE2 to the plasma membrane in yeast.

In contrast to SopE2, the localization of IpgB1 is sensitive to alterations in PIPs (Figure 25B). Surprisingly, in none of the PI-kinase mutant strains did IpgB1 yield cyotplasmic localization. Instead, IpgB1 localization is redistributed from the plasma membrane to vesicles in yeast depleted of Vps34, Pik1, Stt4, and Mss4 kinases (Figure 25B). It is interesting to note that in Pik1 K.D. cells, IpgB1 localization was slightly retained on the plasma membrane compared to Stt4 (Figure 25B). These data are consistent with proposed role of Pik1 in generating nuclear PI4P while Stt4 primarily supplies PI4P to the plasma membrane (Audhya and Emr, 2002; Audhya et al., 2000; Garcia-Bustos et al., 1994). In total these data indicate that the localization of IpgB1 is dependent upon PIPs and IpgB1 can interact with different membrane compartments when higher affinity sites are absent.

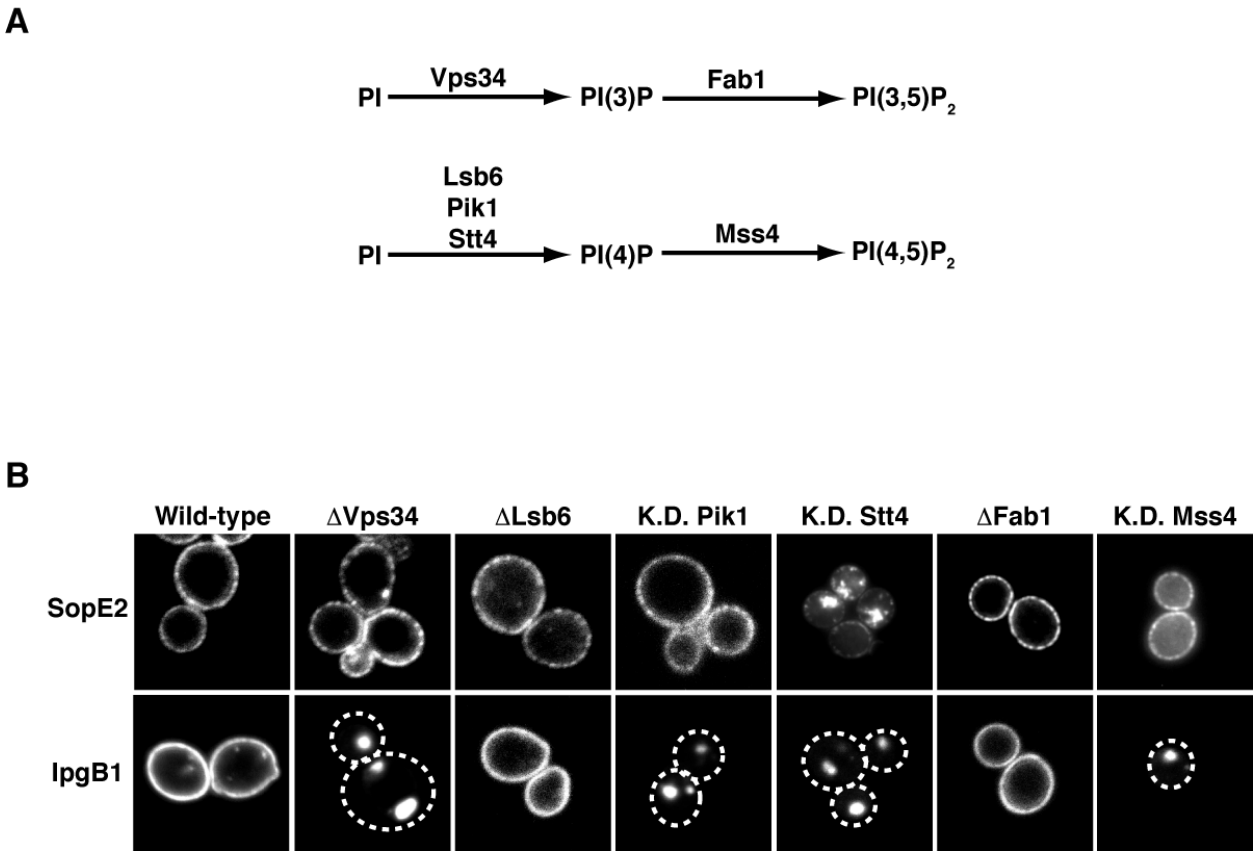

Figure 25. SopE2 and IpgB1 localization in yeast strains depleted for specific phosphoinositide kinases. (A) A schematic of the phosphoinositide biosynthetic pathway in yeast. **(B)** Fluorescence microscopy of EGFP-SopE2 and EGFP-IpgB1 in either wild-type yeast or PI-kinase mutant yeast. Yeast deletion strains are denoted with a Δ (e.g. ΔVps34). Essential genes were knockdown (K.D.) using yeast strains with an integrated Tet-titratable promoter (See Materials and Methods). Yeast cells without fluorescence on the plasma membrane are outlined with dotted lines.

SopE2 utilizes a predicted ALPS motif to interact with cellular membranes

Utilizing the Ras rescue screen, we mapped the membrane localization motif of SopE2 to a linear stretch of 51 amino acids at the N-terminus of the protein (SopE2 residues 26-77; Figure 26A). In this region, we find an abundance of serine and threonine side chains interspersed with hydrophobic amino acids. This feature is reminiscent to the recently described Arf-GAP Lipid Packing Sensor (ALPS) motif (Bigay et al., 2005). ALPS motifs are characterized by the presence of amphipathic alpha helices that contain an abundance of ser/thr residues and a dearth of charged amino acids (Drin et al., 2007). This topology enables the domain to sense the curvature of membranes through the recognition of loosely packed lipids. Interestingly, the predicted ALPS motif of SopE2 is conserved in the *Salmonella* homologue SopE, but not BopE nor CopE from *Burkholderia mallei* and *Chromobacterium violaceum*, respectively. It is intriguing to speculate that the unique lifestyle of *Salmonella* requires the coupling of GEF activity to curved membranes.

A helical wheel projection of the minimal membrane binding region of SopE2 (residues 26-77) reveals an amphipathic helix with proper spatial distribution of serine, threonine, and hydrophobic residues (Figure 26B). Indeed, mutations that either disrupt the stability of the alpha helix (prolines residues) or interfere with the predicted hydrophobic interactions are able to block the ability of SopE2 to restore yeast proliferation in the Ras rescue screen (Figure 26B). Additionally, these mutant proteins do not retain the plasma membrane localization of SopE2, but either display a diffuse localization pattern or are redistributed to vesicular structures (Figure

26C). Therefore, the association of SopE2 to membranes appears to function through an ALPS-like motif in yeast.

Despite being clearly enriched on the plasma membrane in yeast, GFP-SopE2 displayed featureless and cytoplasmic localization in HeLa cells (Figure 26D). Additionally, truncations of SopE2 that contain the predicted ALPS motif also do not yield any specific pattern of localization (Figure 26D). Typically, ALPS motifs are localized to small, highly curved membranes *in vivo* (Antonny, 2011). Due to the absence of membrane localization in mammalian cells, and the uncertainty of SopE2's molecular mechanism, we focused the remainder of our efforts on characterizing the membrane binding mechanism of IpgB1 and its pathogenic consequences.

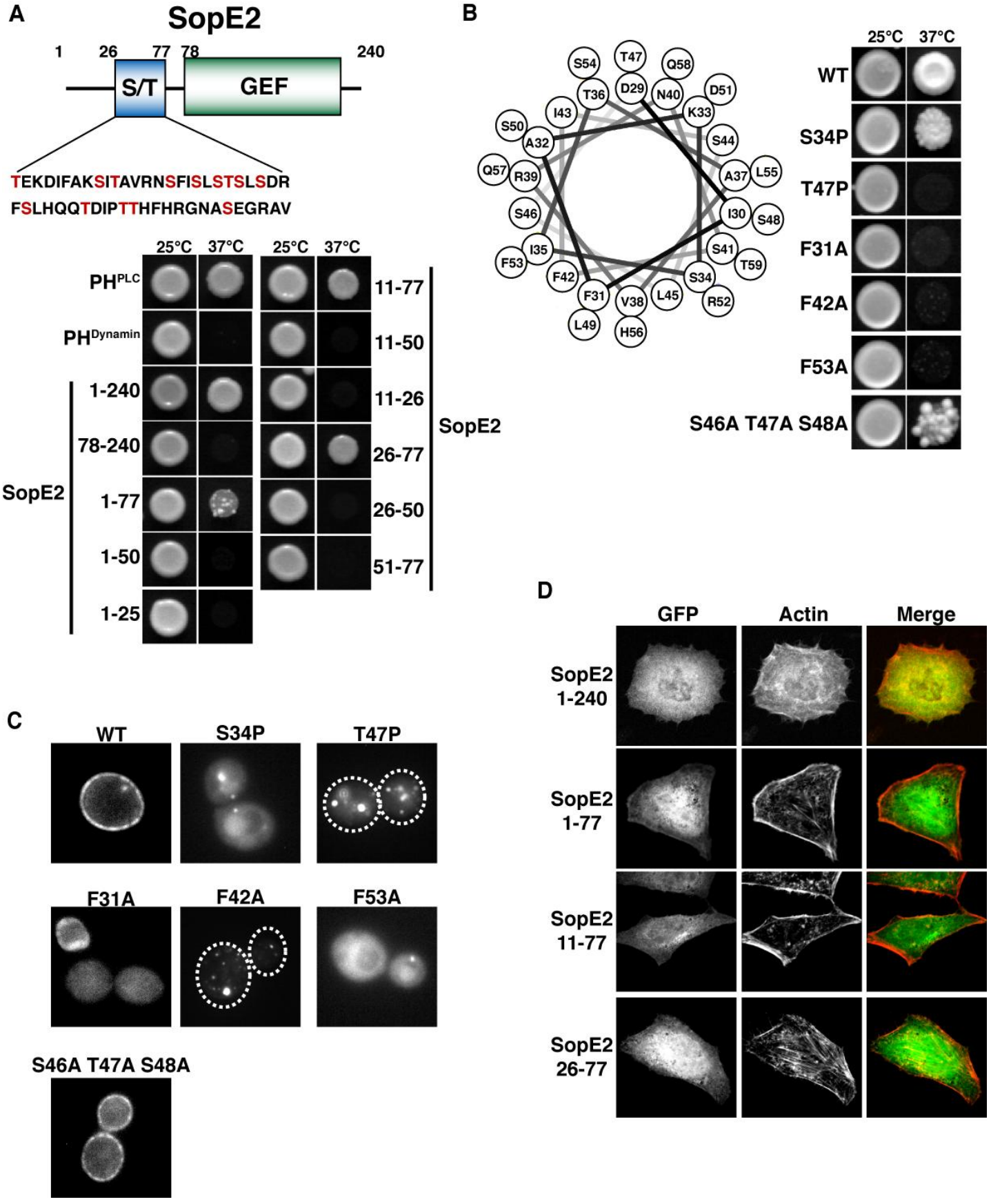
A
SopE2
1
26
77
78
240
S/T
GEF
TEKDIFAKSITAVRNSFISLSTSLSDR
FSLHQQTDIPTTHFHRGNASEGRAV
25°C
37°C
25°C
37°C
PHPLC
PHDynamin
1-240
78-240
1-77
1-50
1-25
SopE2
11-77
11-50
11-26
26-77
26-50
51-77
SopE2
B
S54
T47
Q58
T36
D29
N40
D51
I43
K33
S50
A32
S44
Q57
R39
A37
L55
S46
I30
S48
I35
S41
F53
T59
F42
S34
F31
V38
L45
R52
L49
H56
25°C
37°C
WT
S34P
T47P
F31A
F42A
F53A
S46A T47A S48A
C
WT
S34P
T47P
F31A
F42A
F53A
S46A T47A S48A
D
GFP
Actin
Merge
SopE2
1-240
SopE2
1-77
SopE2
11-77
SopE2
26-77

Figure 26. An N-terminal ALPS like domain mediates SopE2's interactions with eukaryotic membranes. (A) (Top) A cartoon diagram of the SopE2 polypeptide. The amino acid sequence of the Serine/Threonine rich region (residues 51-77) is shown as well. (Bottom) Ras rescue screen as in Figure 24, but utilizing truncations of SopE2 to map the membrane binding region. **(B)** Helical wheel projection illustrating the Ser/Thr amphipathic helix that is similar to the ALPS motif (Drin et al., 2007). On the right is the Ras rescue screen of SopE2 constructs with mutations in the putative ALPS motif. **(C)** Fluorescence microscopy of yeast expressing GFP-SopE2 mutants. **(D)** Fluorescent micrographs of HeLa cells transfected with GFP-SopE2 (green) and GFP-SopE2 truncations. Rhodamine-phalloidin (red) is used to label the actin-cytoskeleton. Alyssa Jimenez kindly provided the data in panels B and C during her rotation in our lab.

A polybasic motif mediates the direct interaction of IpgB1 with acidic phospholipids

Consistent with previous results, we find that the N-terminus of IpgB1 is both necessary and sufficient for membrane localization in mammalian cells (Figure 27A) (Handa et al., 2007). We further refine the minimal sequence to the first 50 amino acids using truncation analysis (Figure 27A). This region is highly basic with an average pI of 10.30. Because IpgB1's localization was redistributed in yeast with altered phosphoinositide metabolism, we hypothesize that this polybasic motif mediates direct interactions with acidic phospholipids. Indeed, using *in vitro* transcribed and translated protein (TNT) we performed lipid overlay assays with full length and truncated versions of mCherry-tagged IpgB1 (Figure 27F). We find that IpgB1 interacts directly with PIPs, but not with other acidic phospholipids such as phosphatidic acid (PA) and phosphatidylserine (PS) (Figure 27F). From these studies, it does not appear that IpgB1 binds to PIPs with any stereospecificity. Importantly, the smallest stable N-terminal fragment produced by TNT, amino acids 1-100, is sufficient for mediating protein-lipid interactions (Figure 27F). These data now show for the first time that IpgB1 is a phosphoinositide-binding protein.

To determine if the polybasic motif is necessary for IpgB1's membrane-interactions, we mutated lysine and arginine residues to alanine and tested their ability to restore Ras signaling in the *Cdc25*^{ts} strain as described above (Figure 27B and 27C). Individual mutations had little effect on membrane binding by IpgB1, but a combinatorial mutation of 5 basic residues (IpgB1^{5xA};R25A, K27A, K30A, K31A, R41A) abolished membrane binding in this assay (Figure 27C). Additional lines of evidence support the finding that IpgB1^{5xA} is a soluble, signaling enzyme. First, GFP- IpgB1^{5xA}, showed a diffuse pattern of localization in yeast compared to the wild-type protein (Figure 27D). Second, while both IpgB1 and IpgB1^{5xA} are able to induce membrane ruffles in mammalian cells, only the wild-type protein is localized to membrane organelles (Figure 27E). Additionally, we performed lipid overlay assays using STREP-affinity tag, full length IpgB1 and IpgB1^{5xA} that were expressed in mammalian cells. In contrast to the TNT production of IpgB1, we are able to purify milligram quantities of protein that are very stable using this purification system (unpublished observations R.C. Orchard, B.A. Weigele, and N.M. Alto). In these assays wild-type IpgB1 robustly interacts with all acidic phospholipids while IpgB1^{5xA} did not interact significantly with any lipid group (Figure 27F). Taken together these data demonstrate that IpgB1^{5xA} is unable to interact with phospholipids *in vitro* or *in vivo* (Figure 27B-F).

We were intrigued to find differences in the lipid-binding profiles of IpgB1 produced by TNT IpgB1 and IpgB1 that was purified from mammalian cells (Figure 27F). By using TNT IpgB1, we originally predicted that this protein interacts exclusively with PIPs. However, our recent data suggest that IpgB1 can interact with other acidic phospholipid groups, most notably,

PA and PS (Figure 27F). The discrepancies in our lipid overlay assays most likely owe to the different quantities of protein utilized, since TNT reactions produce significantly less protein. Therefore, we now hypothesize that IpgB1 utilizes a coincidence detection mechanism with higher affinity for the phosphoinositides and lower affinity for other acidic phospholipid(s). Our hypothesis is consistent with literature reports for other lipid-binding domains. For example, the PH domain of the Ras GEF SOS can binds to both $PI(4,5)P_2$ and PA (Zhao et al., 2007). Additionally, the PX domain of $p47^{phox}$ can simultaneously bind $PI(3,4)P_2$ and PA which increases the proteins affinity for membranes (Karathanassis et al., 2002).

To determine if the localization of IpgB1 is influenced by other acidic phospholipids, we examined the localization of IpgB1 in yeast deficient for phosphatidylserine (ΔCho1) (Hikiji et al., 1988). We chose to examine PS because there are multiple biosynthetic pathways for PA generation in yeast (Carman and Han, 2009). Upon depletion of the Cho1 enzyme, IpgB1 relocalized to several endocytic vescilces, indicating a functional role of PS in promoting the localization of IpgB1 (Figure 27G). With an understanding of the molecular mechanism governing IpgB1-lipid interactions, we can now address the role of these interactions in *Shigella* pathogenesis.

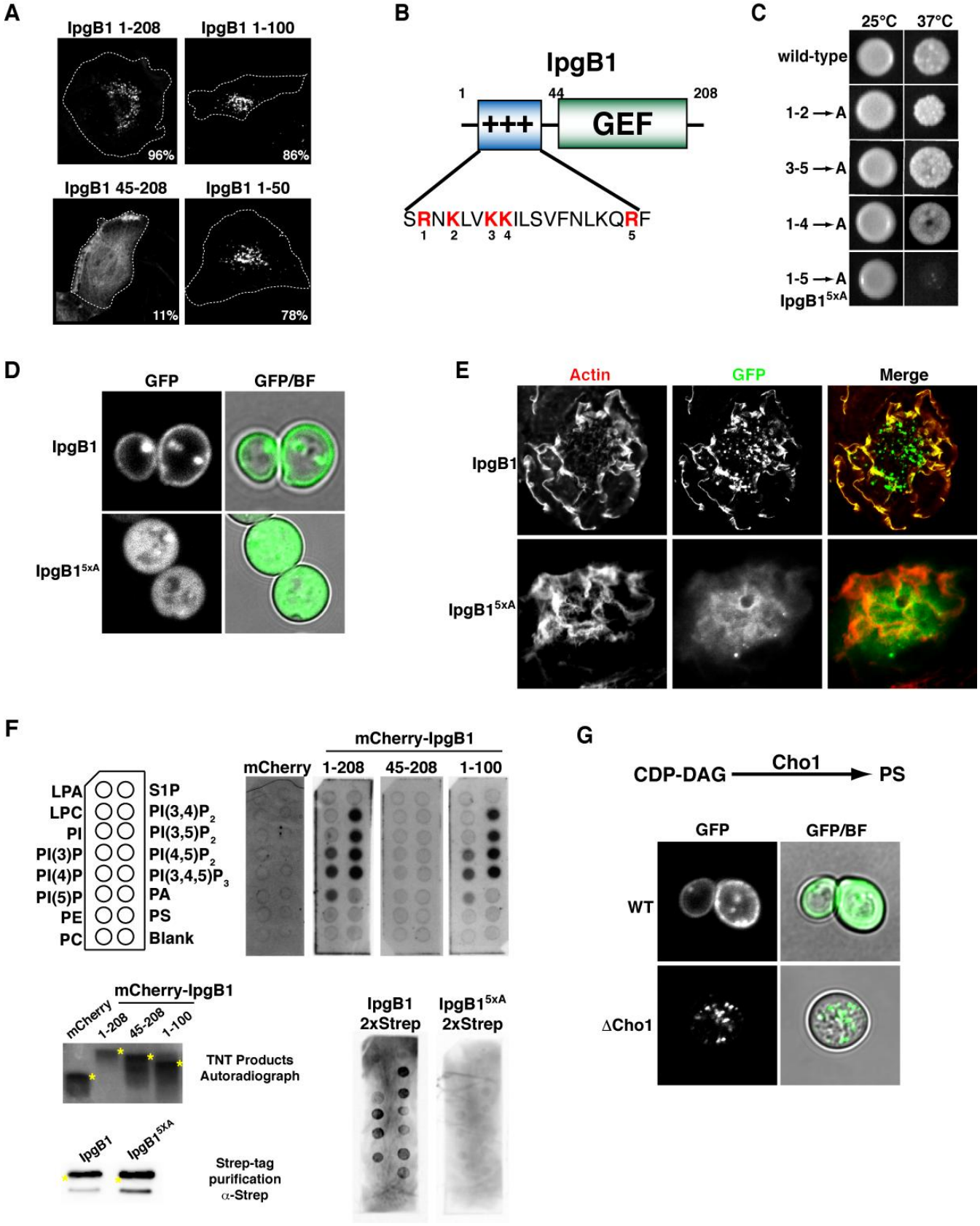
A
IpgB1 1-208
IpgB1 1-100
96%
86%
IpgB1 45-208
IpgB1 1-50
11%
78%
B
IpgB1
1
44
208
+++
GEF
SRNKLVKKILSVFNLKQRF
1 2 3 4 5
C
25°C
37°C
wild-type
1-2 → A
3-5 → A
1-4 → A
1-5 → A
IpgB1 5xA
D
GFP
GFP/BF
IpgB1
IpgB1 5xA
E
Actin
GFP
Merge
IpgB1
IpgB1 5xA
F
LPA
LPC
PI
PI(3)P
PI(4)P
PI(5)P
PE
PC
S1P
PI(3,4)P2
PI(3,5)P2
PI(4,5)P2
PI(3,4,5)P3
PA
PS
Blank
mCherry-IpgB1
mCherry
1-208
45-208
1-100
mCherry-IpgB1
mCherry
1-208
45-208
1-100
TNT Products
Autoradiograph
IpgB1
IpgB1 5xA
Strep-tag
purification
α-Strep
IpgB1
2xStrep
IpgB1 5xA
2xStrep
G
CDP-DAG
Cho1
PS
GFP
GFP/BF
WT
ΔCho1

Figure 27. A polybasic motif mediates the direct interaction of acidic phospholipids with IpgB1. (A) Fluorescent micrographs of HeLa cells expressing mCherry-IpgB1 truncations. The average percentage of cell displaying membrane localization for each construct is shown as well. **(B)** Cartoon diagram of the domain organization of the IpgB1 polypeptide. The sequence of the basic motif is expanded below as well. Five basic resides are shown in red text (1 = R25, 2 = K27, 3 = K30, 4 = K31, 5 = R41). **(C)** Ras rescue screen with either wild-type IpgB1 or constructs with combinatorial mutations in the basic residues. All constructs expressed as full length fusion proteins (data not shown). The numbering is the same as listed in panel B. **(D)** Fluorescence microscopy of yeast expressing either IpgB1 or IpgB1^{5xA}. **(E)** Fluorescent micrographs of HeLa cells expressing GFP-IpgB1 or GFP-IpgB1^{5xA} (green) and stained for the actin cytoskeleton using Rhodamine-phalloidin (Red). **(F)** Lipid overlay assays using *in vitro* transcribed and translated protein or recombinant STREP-tagged IpgB1. Membranes are depicted in the same orientation as the cartoon in the upper right. Bottom left: autoradiograph or western blot showing the IpgB1 proteins at the correct molecular weight (denoted by the yellow asterisk). Bethany Weigele performed the experiments involving STREP-tagged IpgB1 constructs. **(G)** Fluorescence microscopy of GFP-IpgB1 expressed in either wild-type yeast or yeast deficient for the Cho1 enzyme.

Protein-lipid interactions are dispensable for IpgB1-mediated cell invasion

We hypothesize that phospholipid binding is critical for IpgB1's known role in mediating bacterial invasion into non-phagocytic cells. If true, expression of the catalytically active, but membrane binding deficient mutant, IpgB1^{5xA}, will be unable to rescue a ΔIpgB1 strain's defect in phagocytic cup formation and subsequent invasion. However, we find that *Shigella*ΔIpgB1 pIpgB1^{5xA} has no defect in phagocytic cup formation as monitored by fluorescence microscopy (Figure 28A). Additionally, we find no difference in bacterial invasion from *Shigella* expressing IpgB1^{5xA} compared to the wild-type protein (Figure 28B). These data indicate that membrane binding is not required for IpgB1-mediated cellular invasion but may have a functional role beyond facilitating bacterial internalization. Therefore, we focused our efforts on uncovering novel functions of IpgB1 that are dependent upon its interactions with phospholipids.

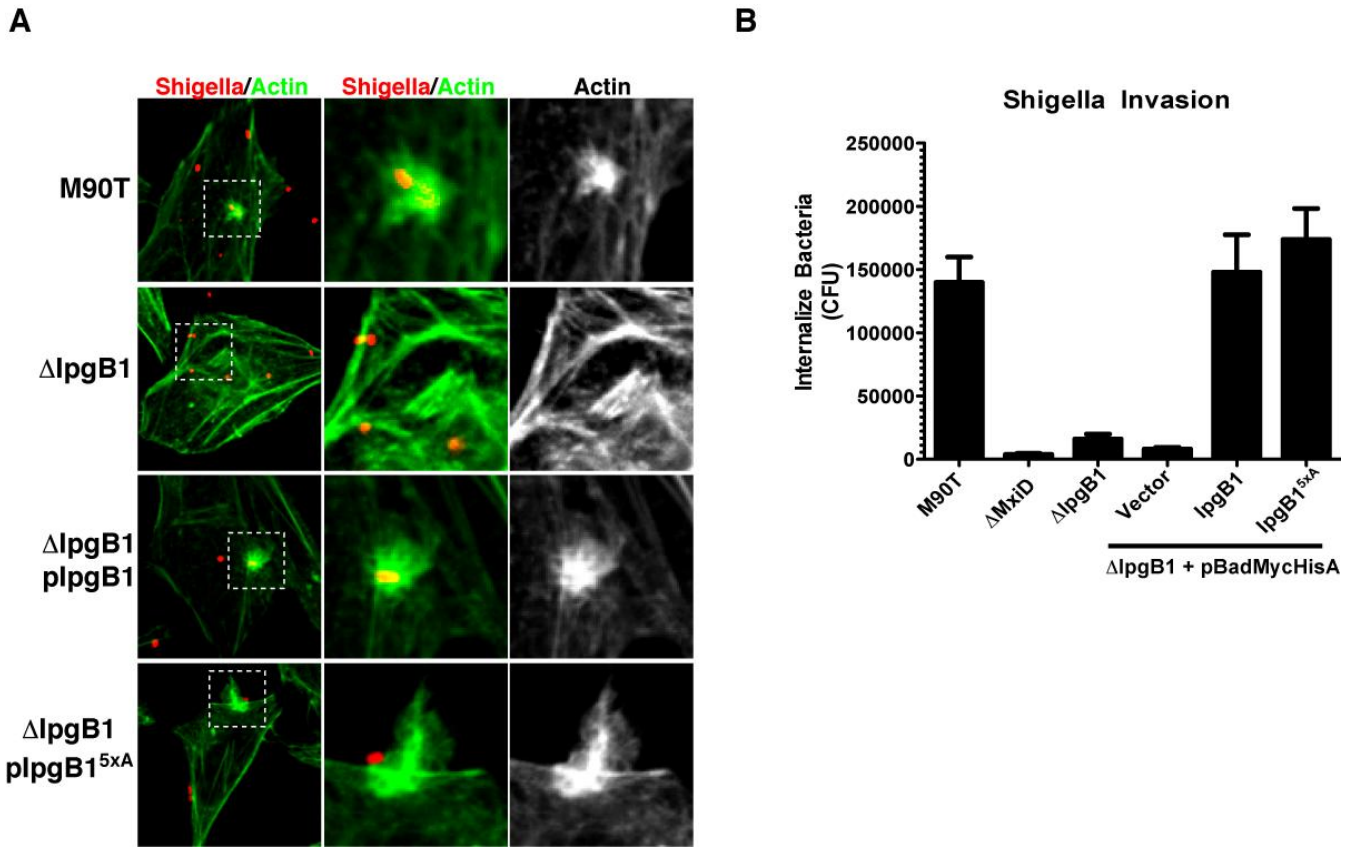

Figure 28. IpgB1-lipid interactions are not required for *Shigella* phagocytic cup formation and bacterial invasion. (A) HeLa cells infected with indicated mCherry expressing *Shigella* strains for 35 minutes were fixed and processed for fluorescent microscopy. The boxed region is magnified to the right to more clearly illustrate the F-actin structures (green). **(B)** HeLa cells were infected with *Shigella* at an MOI of 10. After 90 minutes, cells were washed extensively with gentamicin and colony forming units (CFU) were determined in order to calculate the number of internalized bacteria.

IpgB1's membrane-interactions are required for Shigella survival post-invasion

To explore how IpgB1 binding to phospholipids diversifies effector protein function, we more extensively characterized the localization of IpgB1 in HeLa cells. Consistent with previous results we find IpgB1 enriched on the plasma membrane of Rac-induced membrane protrusions and ruffles (Figure 27E). IpgB1's cell surface localization is consistent with the known role of IpgB1 in inducing phagocytosis (Handa et al., 2007). However, we were intrigued to find IpgB1 on vesicles as well (Figure 27E). We hypothesized that this additional localization may serve as a platform for a diversified function. IpgB1-positive vesicles colocalized with different markers of the endocytic pathway, including APPL1 (endosomes), Dynamin (endocytosis), and LAMP1 (lysosomes) (Figure 29A). Previous reports have shown Rac1 traveling on endocytic vesicles, suggesting a possible role for IpgB1 in mediating membrane-trafficking events (Palamidessi et al., 2008). Therefore, we were curious if IpgB1 vesicles were Rac1 positive. While we did not observe frequent Rac1 vesicles in cells transfected with GFP-Rac1 as had been reported, we do observe that the Rac1 vesicles colocalize with IpgB1 (Figure 29A). These findings suggest that IpgB1 may signal from an endocytic membrane. In support of this notion, overexpression of the constitutively-active mutant of Rab5 (Q79L), which overstimulates endosomal fusion events, caused redistribution of IpgB1 into enlarged endosomes (Figure 29B) (Barbieri et al., 1996; Stenmark et al., 1994). These data indicate that IpgB1's localization is dynamic within the endocytic network and suggest an alternative function involving alterations in endomembrane trafficking.

After inducing its own phagocytosis, *Shigella* rapidly breaks out of its vacuole and replicates to high levels within host cells. Based upon the endocytic localization of IpgB1, we hypothesize that IpgB1 may have a post-invasion function through preventing the *Shigella*-containing vacuole from fusing with lysosomes. To test this hypothesis, we monitored the ability of different *Shigella* strains to persist intracellularly after internalization. Four hours after the addition of gentamicin to kill non-invading bacteria, wild-type *Shigella* replicated to high densities as monitored by fluorescence microscopy and enumerating bacteria loads through colony forming units (Figure 30A and 30B). In contrast, bacteria harboring genetic deletion of an essential component of the T3SS (ΔMxiD) or IpgB1 (ΔIpgB1) are unable to replicate efficiently in this assay, most likely owing to their inability to enter host cells (Figure 30B). Complementing the *Shigella* ΔIpgB1 strain with plasmid encoded IpgB1 restored intracellular replication to wild-type levels (Figure 30A and 30B). However, the catalytically active but membrane binding deficient mutant IpgB1^{5xA} failed to rescue the persistence defect of *Shigella* ΔIpgB1 strain despite equal levels of invasion compared to wild-type *Shigella* (Figure 30A and 30B). Upon closer comparison of the invasion and persistence data (Figure 28B and Figure 30B) we find that the invading IpgB1^{5xA}-expressing bacteria are being killed (174,000 c.f.u. invade vs. 12,880 c.f.u. persist) consistent with our hypothesis that IpgB1 protects the incoming *Shigella*-containing vacuole from fusion with the lysosome. Most importantly, this function is absolutely dependent upon IpgB1's membrane-interactions, highlighting the significance of membrane targeting of effector proteins to bacterial pathogenesis. Our findings also suggest an

evolutionary mechanism to diversify effector protein function through the linkage of membrane targeting motifs to core catalytic domains.

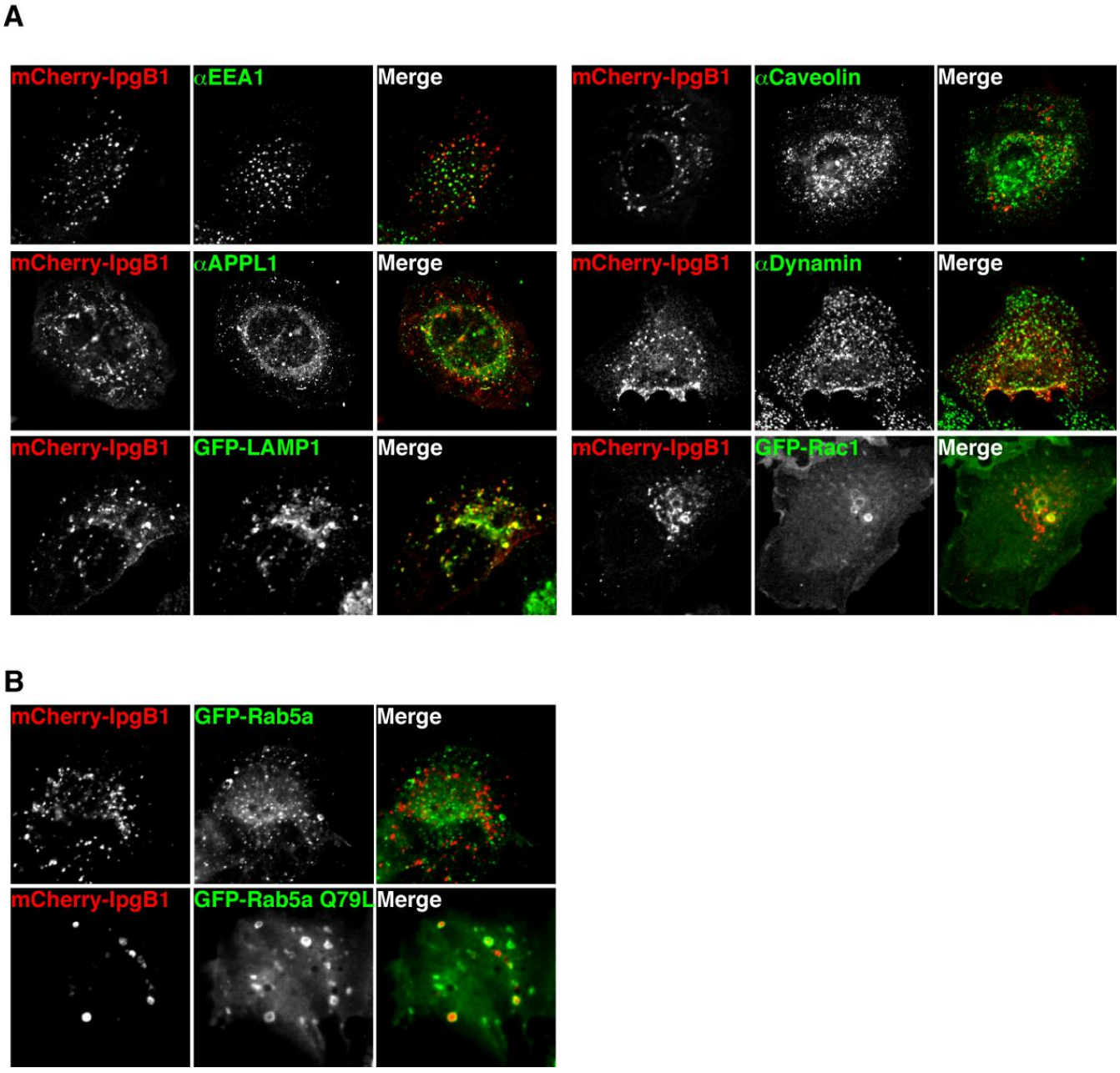

Figure 29. IpgB1 is localized to vesicles in the endocytic pathway. **(A)** The localization of mCherry-tagged IpgB1 in HeLa cells was probed using either specific antibodies or coexpressed GFP-tagged probes. **(B)** HeLa cells were transfected with mCherry-IpgB1 and either wild-type or constitutively active (Q79L) GFP-Rab5a. Rab5a induces enlarged endosomes that are positive for most endocytic markers (Barbieri et al., 1996; Stenmark et al., 1994).

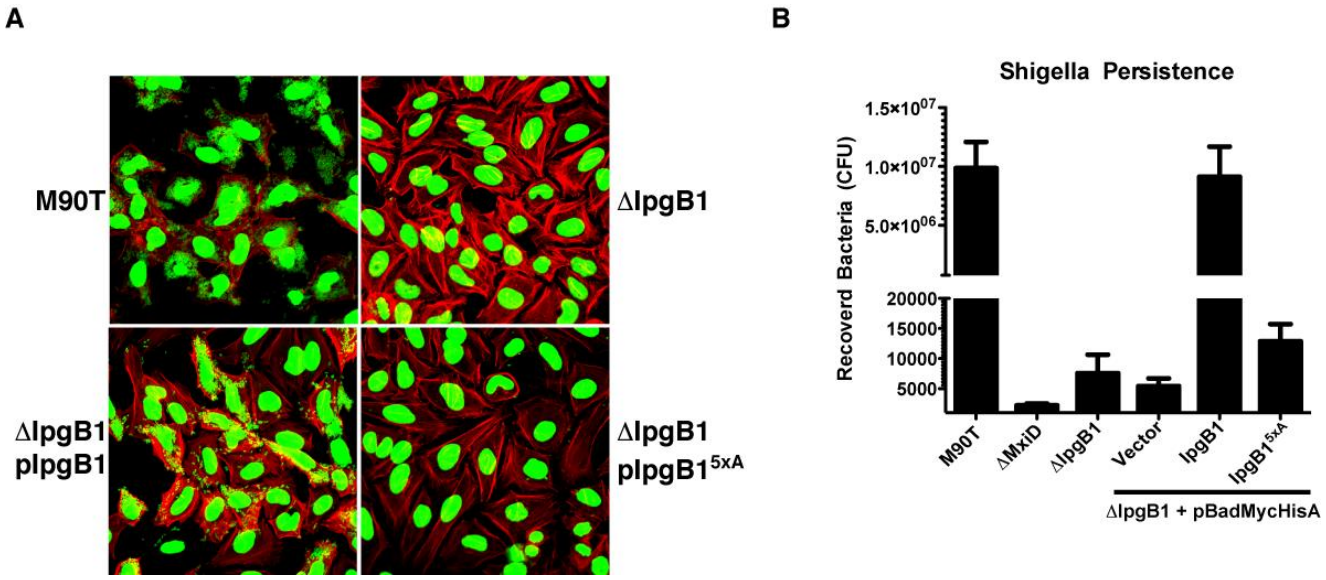

Figure 30. Shigella persistence depends upon IpgB1's membrane localization. (A-B) HeLa cells were infected with indicated strains of *Shigella* for a total of 5.5 hours and either processed for fluorescence microscopy **(A)** or lysed to determine the colony forming units **(B)**. Rhodamine-phalloidin (red) was used to label the actin-cytoskeleton while DAPI (green) marks nucleic acids.

A positive feedback loop remodels the incipient Shigella-containing vacuole to promote bacterial survival

We next wanted to investigate how IpgB1's membrane localization promotes *Shigella* survival post-invasion. While observing the localization of wild-type IpgB1 and its derivatives, we noticed that constructs lacking GEF activity were predominantly localized to vesicles, while wild-type IpgB1 was found on vesicles and the plasma membrane (Figure 27A and 27E). Therefore, we predict that the phospholipid-binding domain of IpgB1 "senses" GEF activity. An underlying tenet of this hypothesis is that Rac signal transduction remodels the lipid composition of the cell, which could itself be a mechanism of promoting *Shigella* survival after internalization. For example, during *Salmonella* infection, the PI-phosphatase SopB is responsible for altering the lipid composition of both the phagocytic cup and the *Salmonella*-containing vacuole (SCV) in order to avoid lysosomal fusion with the SCV (Bakowski et al., 2010). We now propose that an analogous mechanism is exploited by IpgB1 in order to promote *Shigella* persistence within host cells.

Indeed coexpressing a GFP-tagged catalytically inactive IpgB1 construct ($IpgB1^{E80A}$) with a FLAG-tagged IpgB1, recruits the GEF-inactive construct from vesicles onto membrane protrusions (Figure 31A). This relocalization of GFP-$IpgB1^{E80A}$ is dependent upon binding to phospholipids, as mutations that block protein-lipid interactions cause the protein to remain cytoplasmic when coexpressed with FLAG-IpgB1 (Figure 31A). To determine if membrane remodeling occurs with physiological concentrations of IpgB1, we monitored the localization of GFP-$IpgB1^{E80A}$ in transfected HeLa cells during *Shigella* infection. Similar to our

overexpression studies, type III secreted IpgB1 is able to recruit the transfected GFP-IpgB1^{E80A} protein into the phagocytic cup (Figure 31C). Importantly, genetic deletion of IpgB1 from *Shigella*, blocks the redistribution of this fluorescent probe (Figure 31C). These data indicate that IpgB1 induces changes in the phospholipid content in the phagocytic cup. Additionally, the membrane rearrangements are the basis for a positive feedback loop, since the remodeled plasma membrane recruits more IpgB1 molecules which then induces more lipid alterations (Figure 31B). Because the plasma membrane at the site of bacterial internalization will become the membrane encompassing the *Shigella*-containing vacuole, we predict that this transient organelle contains a distinct lipid composition due to the membrane rearrangements triggered by IpgB1. Consistent with this notion, we do observe GFP-IpgB1^{E80A} coating the *Shigella*-containing vacuole (Figure 31D). Taken together, we have discovered a pathogenic signaling circuit linking GTPase signal transduction with the asymmetric distribution of intracellular phospholipids.

We next wanted to identify the lipid groups that are spatially rearranged by IpgB1 in order to gain further insight into the design principles of this pathogenic circuit. First, we characterized a collection of GFP-tagged lipid-binding proteins for localization in the absence of IpgB1 activity (Figure 32). We then tested whether transfection of IpgB1 altered the normal localization of these probes. Transfection of IpgB1 induced the recruitment of PI4P, PI4,5P_2, PS, and PA to membrane protrusions (Figure 33). The most dramatic of these phenotypes observed is the redistribution of phosphatidic acid. Under normal conditions GFP-Spo20p^{PABD} is highly enriched in the nucleus with only minimal localization to the plasma membrane (Figure 32). However, upon expression of IpgB1, this probe becomes more concentrated on the plasma

membrane, specifically outlining the Rac-induced membrane ruffles (Figure 33). In control cells, PI4P, PI4,5P_2, and PS are all found on the plasma membrane (Figure 32). Coexpression of IpgB1 with these lipid-binding probes, leads to an increase of membrane labeling at membrane protrusions (Figure 33). These data indicate that IpgB1 is sufficient for altering the spatial distribution of specific classes of eukaryotic phospholipids.

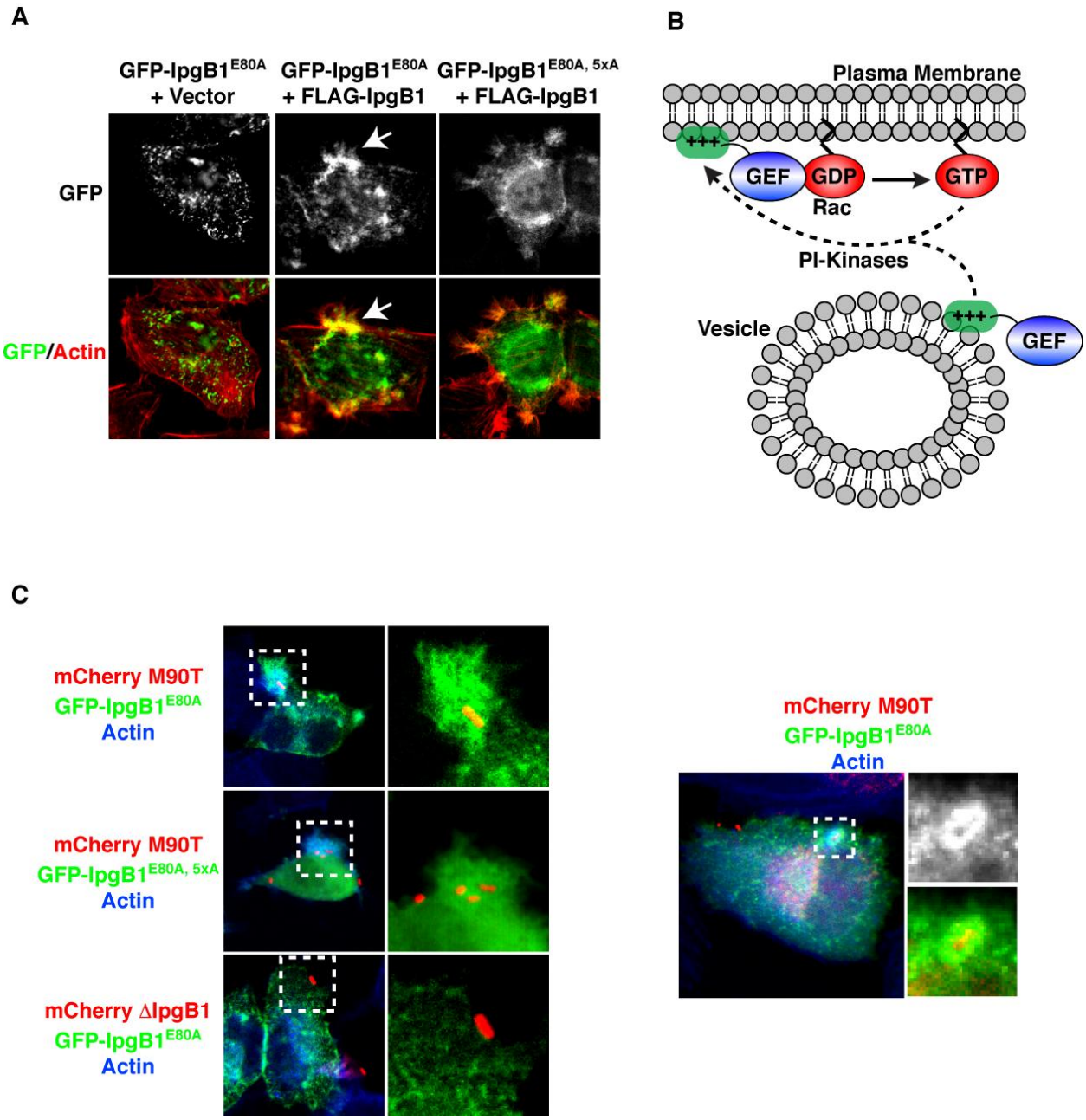
A
GFP-IpgB1E80A + Vector
GFP-IpgB1E80A + FLAG-IpgB1
GFP-IpgB1E80A, 5xA + FLAG-IpgB1
GFP
GFP/Actin
B
Plasma Membrane
+++
GEF
GDP
GTP
Rac
PI-Kinases
Vesicle
+++
GEF
C
mCherry M90T
GFP-IpgB1E80A
Actin
mCherry M90T
GFP-IpgB1E80A, 5xA
Actin
mCherry ΔIpgB1
GFP-IpgB1E80A
Actin
mCherry M90T
GFP-IpgB1E80A
Actin

Figure 31. IpgB1 GEF activity induces a positive feedback loop through recruitment of the IpgB1 phospholipid-binding domain. (A) Fluorescent micrographs of HeLa cells cotransfected with indicated combinations of FLAG-tagged IpgB1 (or empty vector) and GFP-IpgB1^{E80A} or GFP-IpgB1^{E80A,5xA}. Rhodamine-phalloidin (Red) was used to label filamentous actin structures. **(B)** Cartoon model of the localization of IpgB1 in response to Rac signal transduction. Rac1 may activate specific PI-kinases or other lipid modifying enzymes to recruit IpgB1 to the plasma membrane (Chatah and Abrams, 2001; Gomez-Cambronero, 2011). **(C)** HeLa cells transfected with indicated GFP constructs were infected with mCherry expressing *Shigella* strains for 35 minutes to induce phagocytic cup formation. Cells were subsequently fixed and stain with Alexa Fluor 350 Phalloidin (blue). The boxed region is magnified to the right with only the GFP and mCherry channels to illustrate the specific recruitment of IpgB1^{E80A} to the phagocytic cup. **(D)** Experiment same as C, except the *Shigella* is residing within a vacuole. The boxed region is magnified to the right to illustrate GFP-IpgB1^{E80A} localization (top; gray scale) and the residing bacteria within a vacuole (bottom; GFP and mCherry fluorescence shown).

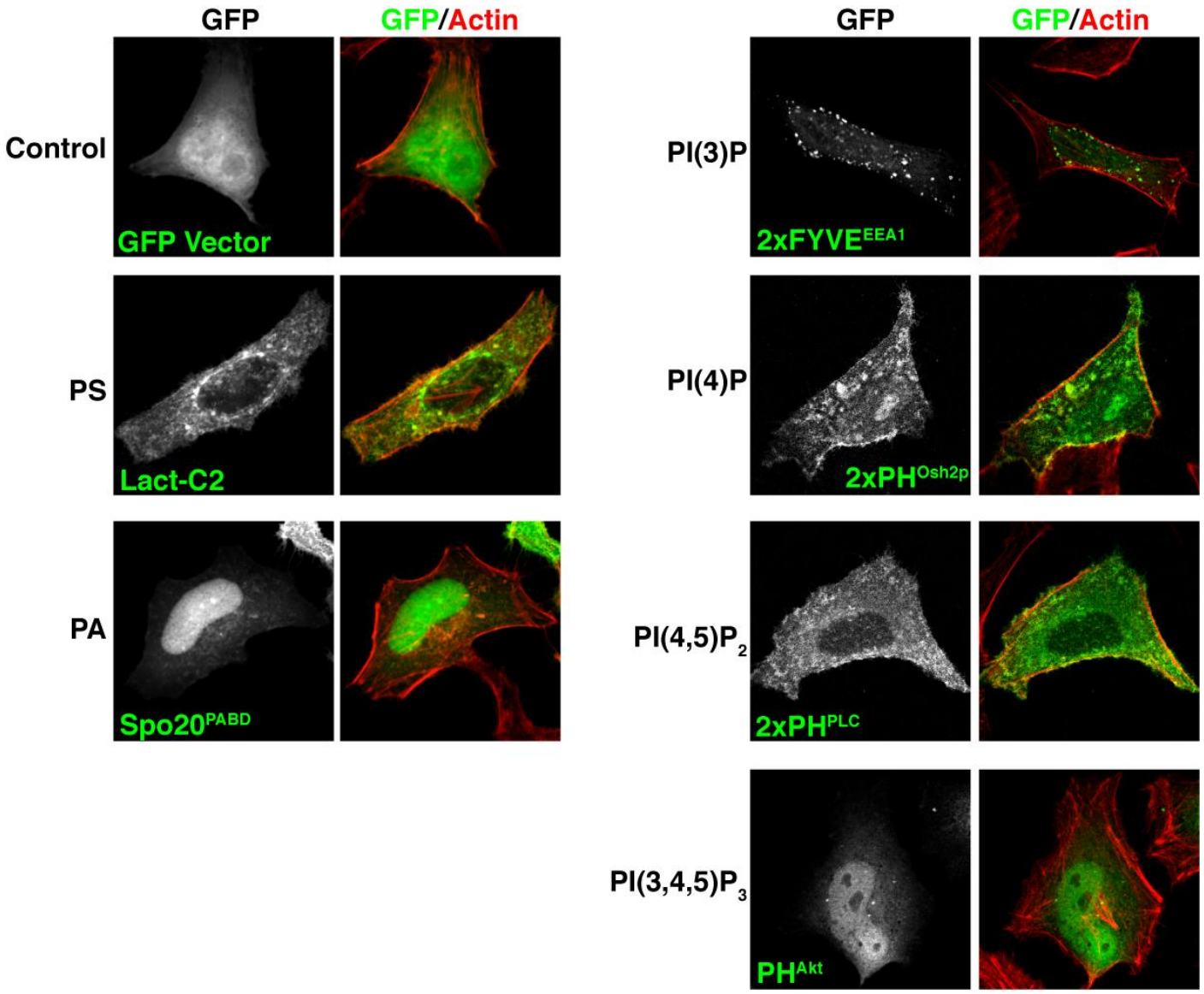

Figure 32. Expression of GFP-tagged lipid-binding domains in HeLa cells. Fluorescent microscopy images of cells expressing indicated GFP-tagged lipid-binding domains. To the left is a description of the lipid that each fluorescent construct is probing.

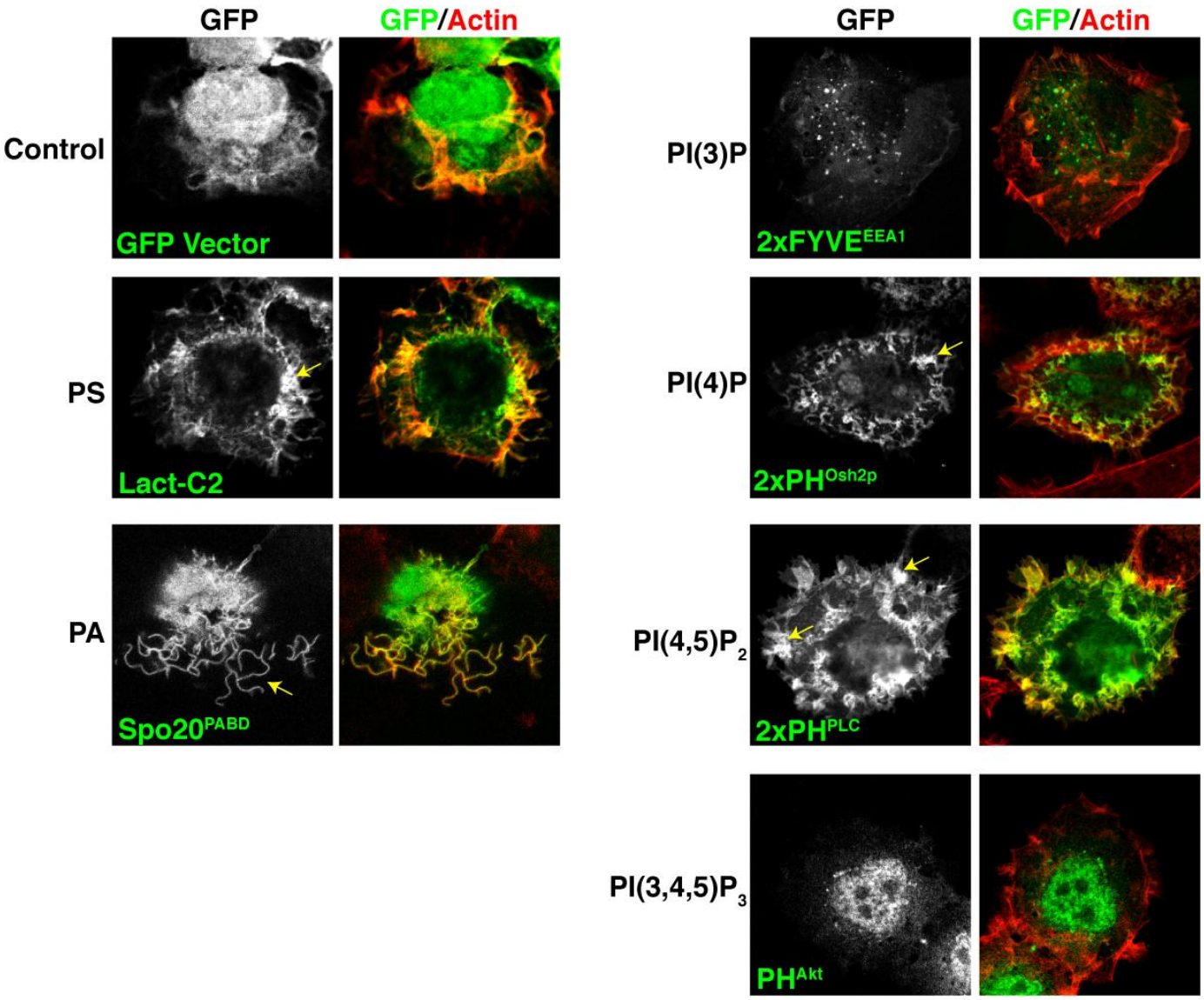

Figure 33. IpgB1 is sufficient to redistribute the subcellular distribution of phospholipids. Fluorescent microscopy of HeLa cells coexpressing FLAG-tagged IpgB1 and the indicated GFP-tagged lipid-binding domains (green). The actin cytoskeleton (Red) is visualized via Rhodamine-phalloidin staining. Arrows mark examples of membrane protrusions enriched for the lipid-binding domain. Images are representative of three independent experiments.

To determine if these lipid rearrangements are a general phenomenon of actin-membrane protrusions, or if they are specific to the IpgB1 signaling cascade, we examined the distribution of the panel of lipid-binding probes in cells expressing the *Salmonella* GEF SopE2. Comparing IpgB1 to SopE2 is intriguing for several reasons. First, both proteins function as GEFs for Rho family GTPases, albeit with differing isoform specificity (i.e. Rac1 for IpgB1 and Cdc42 for SopE2). Also, both effector molecules interact with eukaryotic membranes, but accomplish these interactions using different molecular mechanisms (Figure 26 and 27). Both *Shigella* and *Salmonella* invade host cells and ensure that their respective phagosomes avoid fusion with acidic vesicles containing antimicrobial agents (Ashida et al., 2011; Brumell and Grinstein, 2004). Because these pathogens occupy different niche (i.e. vacuolar for *Salmonella* and cytoplasmic for *Shigella*), their respective virulence proteins have evolved to accommodate the different pathogenic demands. In summation, we predict that the while IpgB1 and SopE2 both activate GTPases to initiate phagocytic cup formation, the specific redistribution of phospholipids by IpgB1 will be distinct from any lipid changes occurring in SopE2-expressing cells. Indeed, we do not observe any detectable change in the spatial distribution of our lipid-binding probes when coexpressed with SopE2 (Figure 34). Therefore, these data demonstrate that IpgB1 potently and specifically induces membrane-remodeling events. Also, these observations suggest that the catalytic activity and membrane binding mechanisms of IpgB1 and SopE2 have been precisely tailored to establish the replicative niche of their respective pathogen.

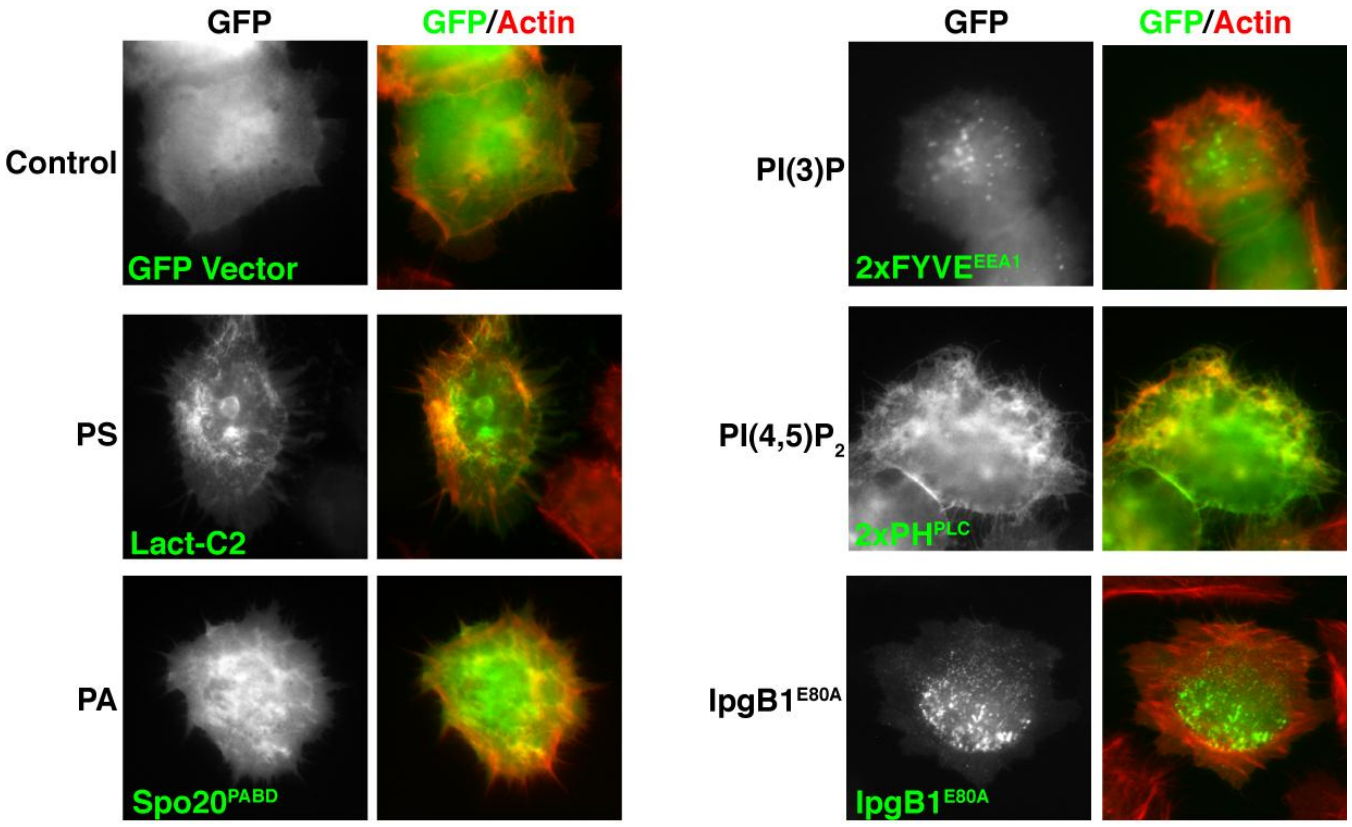

Figure 34. SopE2 does not alter the subcellular localization of acidic phospholipids. Fluorescent microscopy of HeLa cells coexpressing mCherry-SopE2 (not shown) and GFP-tagged lipid-binding domains (green). Alexa Fluor 350 Phalloidin (Red) staining was used to label the actin cytoskeleton.

To determine how these changes in host phospholipid distribution are incorporated into a signaling circuit during infection, we monitored the localization of GFP-tagged lipid-binding domains during *Shigella* invasion. In general, we observe a similar pattern of localization for these probes during infection as with IpgB1 transfection (Figure 33 and 35). For example, we observe robust enrichment of PI4P, PA, and PS into the *Shigella* phagocytic cup (Figure 35). These findings confirm our observations with ectopically-expressed IpgB1 and validate our model of IpgB1-induced lipid rearrangements (Figure 31 and 33). However, there are two lipid groups that differ in subcellular localization when IpgB1 is overexpressed compared to *Shigella* infection (Figure 35). Based upon reports in the literature, these differences can be attributed to the activity of another bacterial effector protein, IpgD. IpgD is a PI-phosphatase that converts $PI(4,5)P_2$ to PI5P (Niebuhr et al., 2002). In this way, the absence of $PI(4,5)P_2$ enrichment at the phagocytic cup can be accounted for by the generation of PI(5)P by IpgD (Figure 35 and 36). Additionally, IpgD is both necessary and sufficient to recruit $PI(3,4,5)P_3$ to the phagocytic cup, through the activation of PI-3 kinases (Figure 35) (Pendaries et al., 2006). Currently we do not have any data to support or refute a role of $PI(3,4,5)P_3$ in the IpgB1 circuit, but we do know that IpgB1 is not sufficient to alter this phospholipid's cellular distribution (Figure 33). Taken together, we have uncovered a complex pathogenic regulatory network that is founded upon the establishment of a unique membrane composition at the site of bacterial invasion.

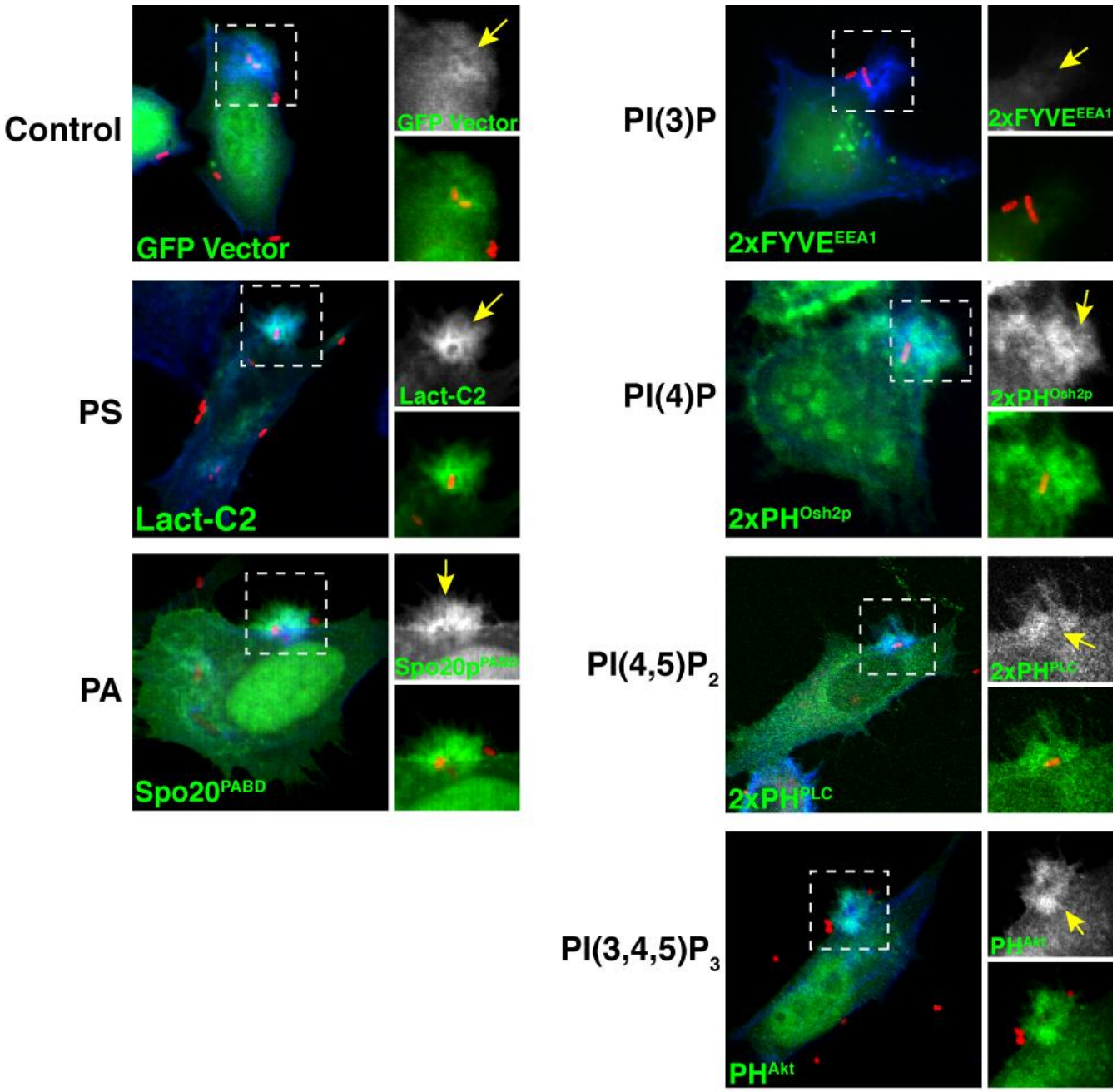

Figure 35. Robust lipid rearrangements define the Shigella phagocytic cup. Fluorescent micrographs of HeLa cells transiently transfected with indicated GFP-tagged lipid-binding probes (Green) and infected with mCherry expressing *Shigella* (Red) for 35 minutes. Cells were stained with Alexa Fluor 350 phallolidin to observe F-actin structures (Blue). The boxed region is magnified to the right to depict the fluorescence intensity of the lipid-binding probe at the phagocytic cup.

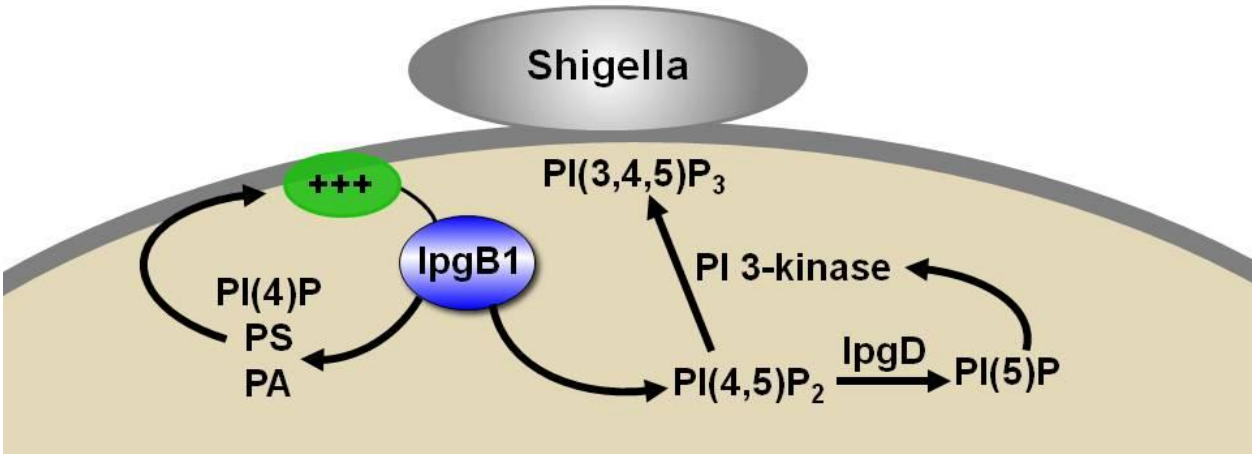

Figure 36. Model of lipid rearrangements during Shigella invasion. IpgB1 is sufficient to recruit PI(4)P, PI(4,5)P_2, PS, and PA to Rac-induced protrusions. PI(4,5)P_2 is absent from the phagocytic cup, suggestion that it is shuttled to PI(5)P and PI(4,5)P_3 in an IpgD dependent manner, as has been described previously (Pendaries et al., 2006). Additionally, IpgB1 is able to recruit its own membrane binding domain, most likely through interactions with PI(4)P, PS and/or PA.

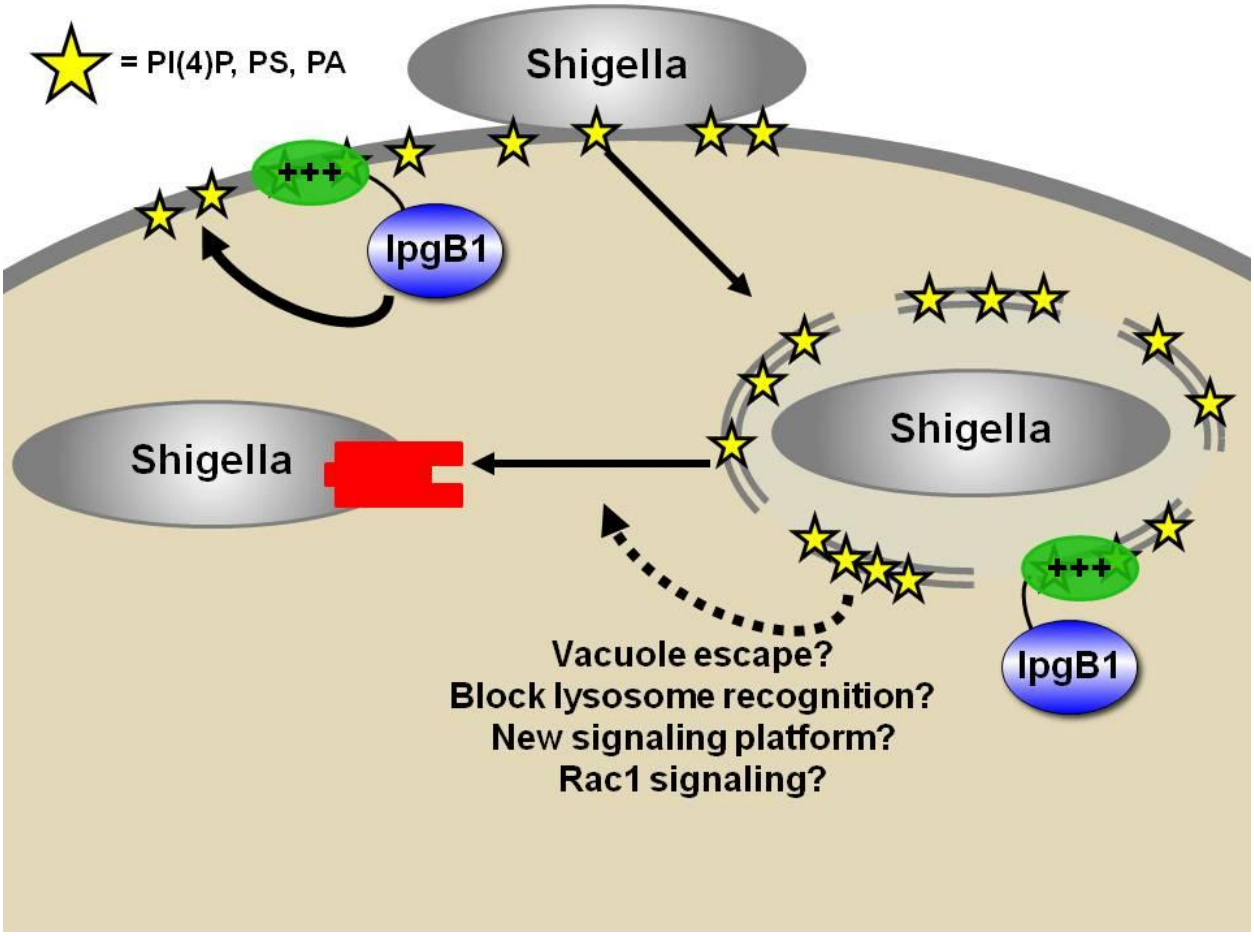

Figure 37. A GTPase-phospholipid circuit promotes *Shigella* survival post-internalization. Cartoon diagram depicting the signaling events that occur to promote *Shigella* survival. A positive feedback loop remodels the phagocytic cup to become enriched with PI(4)P, PS, and PA. After bacterial internalization these lipids constitute the *Shigella*-containing vacuole. This design enables *Shigella* to break out of its vacuole, replicate efficiently, and spread from cell to cell via actin comet tails. Proposed function of membrane remodeling are listed and expanded upon in the text of the discussion.

Discussion

In this study, we provide new insight into the pathogenic function of the *Shigella* GEF IpgB1. Specifically, we identify a phosphoinositide-binding motif that when linked to GEF activity, provides a positive feedback loop that is essential for *Shigella* survival post-internalization. We have characterized the lipid components of the IpgB1 induced feedback loop and now provide a model to describe the dependency of IpgB1-membrane interactions in promoting *Shigella* survival and persistence (Figure 36 and 37).

Ectopic expression of IpgB1 recruits PI(4)P, PI(4,5)P_2, PA, and PS to plasma membrane protrusions (Figure 33). All of these lipids, except PI(4,5)P_2 are enriched at the site of *Shigella* invasion (Figure 35). As stated previously, we attribute this apparent discrepancy to the phosphatase activity of IpgD. Why then does IpgB1 signaling promote PI(4,5)P_2 formation? One can interpret that the recruitment of PI(4,5)P_2 is an artifact of overexpression IpgB1, or is simply not important for *Shigella* pathogenesis. However, we argue that *Shigella* requires the increase in PI(4,5)P_2 in order to fuel the production of PI(5)P and PI(3,4,5)P_3. During infection, both of these lipids are synthesized from PI(4,5)P_2. PI(5)P is the direct product of IpgD hydrolysis of PI(4,5)P_2. PI(5)P activates PI-3 kinases that convert PI(4,5)P_2 to PI(3,4,5)P_3 (Pendaries et al., 2006). Logically, neither of these biosynthetic pathways can operate exclusively and still provide the phenotypes observed during *Shigella* invasion. Therefore, we speculate that IpgB1 replenishes the PI(4,5)P_2 pool in order to increase the metabolic flux of these two pathways. We find this model intriguing because to our knowledge there is only one other pathogenic signaling circuit that accounts for multiple effector proteins (i.e. SopE and

SptP; see Chapter 1). The bacterial pathogenesis field has long held the belief that effector proteins work in concert, but evidence in support of this idea is wanting. Therefore, future endeavors exploring the relationship between IpgD and IpgB1 will emphasize the emergence of specific bacterial effector protein arsenals.

We observe robust enrichment of specific lipid-binding domains to the site of IpgB1 activity. We now suggest that the phagocytic cup becomes a distinct membrane domain that is characterized by a unique phospholipid composition. The mechanism underlying these lipid changes most likely stems from Rac-dependent induction of PI-kinase activity. For example, Rac1 activates PI4P 5-kinases to increase the local $PI(4,5)P_2$ levels (Chatah and Abrams, 2001). An analogous mechanism is predicted for the recruitment of phosphatidic acid to IpgB1 induced protrusions. PA is generated through the hydrolysis of phosphatidylcholine by phospholipase D (PLD). PLD activity has been linked to Rac GTPase signal transduction (Gomez-Cambronero, 2011). Unlike the phosphoinositides or PA, the mechanism enabling phosphatidylserine recruitment to the *Shigella* phagocytic cup is unclear. One possibility is that PS-rich vesicles fuse to the nascent phagocytic cup. Alternatively, the enrichment of Lact-C2 at the site of bacterial internalization may be a result of changes in the local environment that increase the Lact-C2 affinity for membrane even though PS concentrations remain constant. Future studies exploring the enzymes responsible for creating the unique lipid environment of the phagocytic cup will help better define the properties of the pathogenic signaling circuit.

How does establishing the phagocytic cup as a new membrane compartment enable *Shigella* to persist intracellularly? Surprisingly, very little is known about the molecular events

that occur post-internalization but before *Shigella* enters into the host cytoplasm. With this in mind, our data are consistent with four different mechanisms that theoretically could promote intracellular *Shigella* replication. First, extensive remodeling of the *Shigella*-containing vacuole may induce vacuolar lysis (Figure 37). In this scenario the membrane rearrangements recruit host lipases that could destabilize the vacuole and allow *Shigella* to enter into the cytoplasm. Interestingly, despite extensive research into *Shigella* pathogenesis, no bacterial protein has been identified to induce vacuolar lysis, which is consistent with our suggestion of a primarily host-mediated process.

An alternative scenario for promoting *Shigella* survival by membrane bound IpgB1, is the increase in membrane surface charge, directly preventing lysosome fusion with the incoming *Shigella*-containing vacuole (Figure 37). In this model, host proteins that normally target the vacuole towards the lysosome are unable to recognize this membrane organelle. This mechanism will enable *Shigella* enter the host cytoplasm and rapidly replicate. Also, the unique membrane composition of the *Shigella*-containing vacuole may serve as a signaling platform to establish additional pathogenic circuits. In this scenario, the IpgB1 circuit is designed to function upstream of other effector proteins, and thus would be the master regulator of the early secreted effectors.

Lastly, the establishment of a new membrane compartment may be necessary to enhance Rac1 activity on the vacuole. Reports in the literature indicate that actin polymerization around phagosomes alters the normal endomembrane trafficking events of *Mycobacteria* (Anes et al., 2003). In this scenario of our model, we propose that IpgB1 activates Rac1 to produce a

protective actin cage that blocks lysosome fusion and promotes vacuole escape (Figure 37). Indeed, we do observe GFP-IpgB1^{E80A} on the incoming, vacuole, but the impact on Rac1 signaling and membrane dynamics is not known (Figure 31D).

Regardless of the precise mechanism of survival, all of these scenarios depend upon the direct interaction of IpgB1 with acidic phospholipids. Without the positive feedback loop, we predict that *Shigella* remains trapped in the phagosome and becomes degraded when this compartment fuses with the lysosome. In line with this prediction, we have not observed ΔIpgB1 pIpgB1^{5xA} bacteria entering into the host cytoplasm (R.C. Orchard unpublished observations). Therefore, the rapid signal transduction events that occur within minutes of *Shigella* entry determine the fate of the invading bacterium.

The linkage of Rac signal transduction with phosphoinositide metabolism is not unique to *Shigella* pathogenesis, but is a fundamental component of directional cell migration. PI(3,4,5)P_3 synthesis and GTPase signal transduction are coupled in a feedback loop at the leading edge of migrating cells (Weiner et al., 2002). However, a mechanistic understanding of how GEFs contribute to this circuit architecture is unclear. Therefore, IpgB1 may serve as a useful model for elucidating the underlying molecular principles governing GTPase-phospholipid feedback loops.

Our study also sheds light on the evolutionary design principles of bacterial effector proteins. We now propose that distinct bacterial GEFs emerge from the coupling of GTPase signaling with a regulatory motif that senses the desired pathogenic signaling output and modulates GEF activity. The feedback mechanism of IpgB1 and Map clearly illustrate this

point. The isolated GEF domain of Map is insufficient to induce Cdc42 signaling cascades *in vivo* (Orchard et al., 2012). To establish the polarization of Cdc42 signal transduction, *E. coli* has linked Map GEF activity to an actin-binding domain. This design places actin dynamics as the central hub in the pathogenic polarity circuit. In contrast to Map activation of Cdc42, the isolated GEF domain of IpgB1 is still competent for inducing Rac-mediated actin-membrane protrusions (Figure 27). While a soluble GEF promotes *Shigella* invasion, this construct is not capable of sustaining intracellular replication (Figure 28 and 30). Rather than responding to the induction of actin polymerization, IpgB1 has evolved to sense specific lipid rearrangements that promote *Shigella* survival post-internalization (Figure 31 and Figure 37). What other GTPase signaling activities could be incorporated into a bacterial GEF regulatory network? We suggest that alterations in microtubule and endomembrane trafficking by Rho-family GTPases are hijacked to establish pathogenic signaling circuits. For example, the WxxxE protein SifA interacts with SKIP, a kinesin interacting protein (Boucrot et al., 2005). Kinesins are motor proteins that move on microtubules (Drummond, 2011). Because SifA is responsible for mediating microtubule dependent membrane trafficking events, it is intriguing to speculate that GTPase-mediated changes in microtubule dynamics control SifA activity. Additionally, we now report that SopE2 interacts with eukaryotic membranes through an ALPS-like motif (Figure 26). We predict that this ALPS-like motif senses the curved membrane structures of the phagocytic cup to help localize robust GTPase signaling upon internalization. Exploring the relationship between catalytic activity and regulatory factors for other bacterial GEFs promises to be an exciting field of research that expands our understanding of effector protein biology.

Materials and Methods

Plasmids

The Ras rescue plasmid p3S0BL2 was a kind gift of Mark Lemmon (University of Pennsylvania) (Isakoff et al., 1998). To facilitate the rapid transfer of bacterial effector genes into this plasmid, we inserted a gateway expression cassette (Invitrogen) in between Ras and the HA tag. The resulting plasmid is named pRRD for plasmid Ras Rescue DEST. For yeast expression, the bacterial GEFs had the following point mutations to block catalytic function: Map^{E78A}, $EspT^{E67A}$, $EspM2^{E70A}$, $SifB^{E199A}$, $SopE2^{G168V}$, $IpgB1^{E80A}$, $IpgB2^{E66A}$, and $PROVALCAL\_00500^{E81A}$ (accession number: ZP_03317587). The bacterial GEFs SifA, and the currently unnamed WxxxE protein from *Providencia rustigianiia* (accession number: ZP_05971856) are non-toxic to yeast and thusly the wild-type proteins were used in our study. To monitor the subcellular localization of bacterial GEFs in yeast, the p413Gal vector was modified to contain the open reading fame of EGFP with a gateway expression cassette at its 3' end. pENTR plasmids were moved into pRRD or p413Gal GFP DEST using LR Clonase II (Invitrogen) following manufacturer's instructions.

For mammalian expression constructs, SopE2, IpgB1, and their derivatives were subcloned into pcDNA 3.1 epitope tagged vectors (GFP/mCherry/FLAG) vectors. The lipid-binding domains of Spo20p, Osh2p(2 tandem copies of the PH domain; cDNA kindly provided by Dr. Scott Emr), Akt (one PH domain; cDNA kindly provided by Dr. Michael White), were subcloned into pcDNA 3.1-GFP as has been described previously (Franke et al., 1997; Nakanishi et al., 2004; Stefan et al., 2011). Full length Rac1, Rab5a, and $Rab5a^{Q79L}$ was subcloned into

pcDNA 3.1-GFP. pEGFP 2xFYVE^{EEA1} and pEGFP 2xPH$^{PLC\text{-}delta}$ plasmids have been previously described (Gillooly et al., 2000; Stauffer et al., 1998). pEGFP Lact-C2 (Addgene plasmid 22852) and pEGFP-LAMP1 were kindly provided by Dr. Sergio Grinstein (University of Toronto) and Dr. Paul Luzio (University of Cambridge), respectively. Site-directed mutagenesis was carried out using the QuickChange Site-Directed Mutagenesis kit (Stratagene). All constructs were verified by DNA sequencing.

Ras rescue screen and yeast PI-kinase screen

pRRD plasmids were transformed into the *Cdc25^{ts}* yeast strain (a kind gift of Mark Lemmon) using a modified lithium acetate (LiAc) protocol, as described previously (Isakoff et al., 1998). Briefly, an overnight culture of *Cdc25^{ts}* yeast grown at 25°C was diluted 1:50 in YPAD. After 4 hours of growth at 25°C, yeast were washed once with 50 ml of TE and resuspended in 2 ml of 0.1 M LiAc. The yeast suspension was incubated for 10 minutes at room temperature prior to aliquoting 50 µl into tubes containing 500 ng of the pRRD plasmid and 5 µg of freshly denatured salmon sperm DNA as a carrier. 350 µl of 100 mM LiAc, 40% PEG 3350 in 1xTE was added to tubes, mixed well, and placed in a 25°C incubator for 30 minutes. After incubation, 44 µl of DMSO was added and the yeast mixture was heat shocked at 42°C for 15 minutes. Cells were washed once with TE and subsequently plated on synthetic defined (SD) minimal media (leucine dropout). After 3-4 days of growth at 25°C, yeast were replicated onto plates and placed at either 25°C or 37°C and grown for one week. Viability was scored either at the end of one week or immediately after completion of full colony formation.

To examine the localization of fluorescently tagged proteins in yeast, p413 Gal GFP Dest SopE2^{G168V}, p413 Gal GFP Dest IpgB1^{E80A}, and p413 Gal GFP Dest IpgB1$^{5xA,\ E80A}$ were transformed into *InvSc1* using standard LiAc protocol and plated on SD minimal media (histidine dropout). Protein expression was induced by growing a colony of transformed yeast in SD minimal media with galactose/raffinose as the sole carbon source. Yeast were mounted onto slides and subsequently imaged.

For the PI-Kinase screen, constructs were transformed into ΔVPS34 (BY4742 strain; MATalpha his3Δ1 leu2Δ0 lys2Δ0 ura3Δ0), ΔFAB1 (BY4742), ΔLSB6 (BY4742), Stt4 Tet-off (pSTT4::kanR-tet07-TATA URA3::CMV-tTA MATa his3-1 leu2-0 met15-0; Open Biosystems), Pik1 Tet-off (pPIK1::kanR-tet07-TATA URA3::CMV-tTA MATa his3-1 leu2-0 met15-0; Open Biosystems), Mss4 Tet-off (pMSS4::kanR-tet07-TATA URA3::CMV-tTA MATa his3-1 leu2-0 met15-0; Open Biosystems), and Cho1 Tet-off (pCHO1::kanR-tet07-TATA URA3::CMV-tTA MATa his3-1 leu2-0 met15-0) using standard LiAc protocol. Yeast strains ΔVPS34, ΔFAB1, ΔLSB6 are kind gifts of Dr. Joel Goodman. Expression of proteins in yeast strains ΔVPS34, ΔFAB1, ΔLSB6 was identical to that described above. To induce GFP-tagged protein expression in PI-Kinase knockdown yeast, colonies of yeast were initially grown in SD glucose minimal media (histidine dropout) supplemented with 50 µg/ml doxycycline (Sigma) or for Mss4 Tet-off 300 µg/ml doxycycline. After overnight growth, yeast cultures were washed in TE and diluted 1:10 in SD galactose/raffinose minimal media (histidine dropout) supplemented with the same concentration of doxycycline. After a second overnight growth, effector protein localization was assayed using fluorescence microscopy.

Cell culture, antibodies and microscopy

HeLa and HEK293T cells were maintained in DMEM containing 10% (v/v) FBS, 2mM glutamine, and 100 µg/ml penicillin/streptomycin (Thermo Scientific) at 37°C in a 5% CO_2 incubator. Cells were seeded onto coverslips in a 6 well dish and after overnight incubation were transfected using FuGene6 (Roche) and incubated for 16-18 hours. Cells were then fixed and prepared for immunocytochemistry. Detection of endocytic membrane microdomains was accomplished using antibodies for Caveolin (BD Biosciences; 1:500 dilution), APPL1 (Cell Signaling; 1:100 dilution), EEA1 (BD Biosciences, 1:500 dilution), and Dynamin (provided by Dr. Sandra Schmid; 1:500 dilution). Imaging was performed on a LSM 510 PASCAL scanning confocal microscope (Zeiss, Thornwood, NY).

Isolation of recombinant IpgB1 and lipid overlay assays

Production of recombinant IpgB1 was achieved through either *in vitro* transcribed and translation (TNT) or STREP purification of proteins from mammalian cells. The TNT T7 quick coupled transcription/translation system (Promega) was used to generate radiolabeled (S^{35}) mCherry-IpgB1 proteins by following the manufacturer's instructions. To determine the purity and stability of TNT produced protein 5% of the total reaction was analyzed using autoradiography. Full length proteins were immediately used in lipid overlay assays.

To purify larger quantities of protein, IpgB1 and $IpgB1^{5xA}$ were subcloned into a modified pcDNA3.1-GFP vector containing a dual STREP-tag in frame at the C-terminus of the protein. HEK293T cells grown in 10 cm plates were transfected with 10 ug of plasmid DNA.

After 24 to 48 hours of expression, cells were broken in lysis buffer (20mM Tris pH 7.5, 4 mM $MgCl_2$, 20 mM EDTA, and 0.5% Triton X-100). After 10 minutes of lysis with intermittent vortexing, the whole cell lysates were cleared via centrifugation and incubated with Strep-Tactin agarose beads (Millipore) for 1.5 hours with gentle rocking at 4°C. Beads were subsequently washed three times with lysis buffer and eluted using Strep-Tactin Elution Buffer (Millipore). Purified samples were analyzed by western blot to confirm expression of the full length fusion protein.

PIP strips (Invitrogen) were incubated with blocking buffer (3% fatty acid free BSA in TBS-T) for 1 hour prior to incubation with recombinant protein. TNT reactions or STREP purified proteins were diluted to a final volume of 1 mL in blocking buffer and incubated with pre-blocked PIP strips for either 1 hour (STREP purified proteins) or 3 hours (TNT reactions). Membranes were washed 5 times with blocking buffer and protein-lipid interactions were determined by either western blot or autoradiography.

Shigella strains and infections

The *ipgB1* and *mxiD* genes were individually disrupted using the λ red recombinase mediated recombination system (Datsenko and Wanner, 2000). Briefly, the PCR primers IpgB1 5’ (TGAACTAACATATAGGGGGTATCATGCAAATTCTAAACAAAATACTTCCACAGG TGTAGGCTGGAGCTGCTTC) and IpgB1 3’ (AAGATTTAATATAAAAGATTTAATTTG TATTGCTTTGACGGTATACAGCCATATGAATATCCTCCTTAG for *ipgB1* and MxiD 5’ (ATGAAAAAATTTAATATTAAATCTTTGACTCTCTTGATTGTATTGTTACCCAGCCAT

ATGAATATCCTCCTTAG) and MxiD 3' (GAAGCAGCTCCAGCCTACACCTACTTTGCT GGAAGACGAAAAATCATTGGTTTCATACTTAAATTACTAA) for *mxiD* were used to amplify the Kanamycin resistance marker from the plasmid pKD4. PCR products were electroporated into *Shigella flexeneri* strain M90T carrying the red recombinase plasmid pKD46. Transformants were selected by growth on LB agar plates containing kanamycin (50 µg/ml) and simultaneously cured of pKD46 by growth at 42ºC overnight. The kanamycin resistance gene was eliminated through the introduction of the pCP20 helper plasmid which contains the FLP recombinase. Subsequent curing of pCP20 was carried out by growing strains at 42ºC for 5 hours. Disruption of the *ipgB1* and m*xiD* genes was confirmed through DNA sequencing of the respective genetic loci. Plasmid complementation of ΔIpgB1 strains was achieved by subcloning *ipgB1* into the multiple cloning site of pBadMycHisA (Invitrogen)

For infection of HeLa cells, overnight cultures of *Shigella* grown in brain heart infusion (BHI) broth at 30ºC were diluted 1:50 in BHI and incubated for 2.5 hours at 37ºC. 500 µl of bacterial culture was collected, washed, and resuspended in 1 ml of 0.003 % congo red (Sigma) diluted in PBS. After a 15 minute static incubation at 37ºC, *Shigella* at an MOI of 10 were added to HeLa cells. Infection was initiated by centrifugation at 1,000 *g* for 10 minutes at room temperature. For imaging the phagocytic cup, cells are fixed and processed for fluorescence microscopy at 35 minutes post infection. To enumerate bacterial invasion, 90 minutes post infection cells are extensively washed in PBS supplemented with gentamicin (100 µg/ml) and lysed in PBS plus 0.5% Triton X-100. Cellular lysates were diluted to determine colony forming units (c.f.u.). For *Shigella* persistence assays, cells are initially infected for 90 minutes and

washed in a PBS solution containing gentamicin to kill all extracellular bacteria. Fresh media is then added and the infection proceeds for an additional 4 hours to allow bacterial replication. Cells are then lysed to determine bacterial burden (c.f.u.) or fixed and stained for fluorescence microscopy.

CHAPTER FIVE
Conclusions and Future Directions

Conclusions

A versatile structural design

Despite not sharing any sequence or structural homology with endogenous GEFs, we now show that the WxxxE family of bacterial GEFs chemically mimics the GTPase-activation and specificity mechanisms of the Dbl family of eukaryotic GEFs. Because only a handful of amino acids are strictly required for mediating the nucleotide-exchange reaction, the majority of the polypeptide has a large functional sequence space to roam, which explains the low primary sequence homology between bacterial GEFs. The α4 and α6 helices of the bacterial GEFs account for a significant amount of sequence variability (Figure 11A and 11B). This hypervariable region generates pathogenic diversity because the amino acid composition of the α4- α6 helices dictates GTPase-isoform specificity (Figure 11). These findings suggest that the unique architecture of the bacterial GEFs facilitates the evolution of novel virulence factors.

The compact V-shaped fold of bacterial GEFs does limit the number and type of regulatory interactions plausible compared to their eukaryotic counterparts (Figure 5). Importantly, our findings suggest that GEF activity alone is not sufficient for the observed pathogenic phenotypes (Figure 23 and Figure 30). How do bacterial GEFs reconcile the conflict between the necessity of regulatory modules and maintaining a compact structure? For both Map and IpgB1, we observe relatively small motifs just outside the GEF domain that have a

profound impact on the spatial and temporal signaling dynamics of their respective molecules. Importantly, the properties that emerge from these regulator motifs could not have been predicted *a priori*, but required detailed analysis of the signaling networks. We suggest that the coupling of the bacterial GEF fold with a relatively short regulatory sequence allows pathogens the ability to fine tune eukaryotic signaling events while still fulfilling the thermodynamic folding requirements of the type III secretion system. Because relatively few effector proteins have structural insight at this level of detail, the WxxxE/SopE family of bacterial GEFs is an excellent model system to study the emergence of novel virulence factors.

Befriending the enemy to learn more about ourselves

Pathogens exploit critical eukaryotic signaling processes to promote their own survival. Historically, studying pathogenesis has revealed important insights into the underlying, native biological system. For example, deciphering the nature of the genetic code was accomplished using the bacteriophage T4 (Crick et al., 1961). Also, the identification of the Ras-oncogene was discovered by investigating the Rat sarcoma virus's ability to induce tumorgenesis (Chien et al., 1979; Der et al., 1982; Santos et al., 1982). With this in mind, we now propose that the bacterial GEFs serve as excellent tools to probe mechanisms underlying GTPase mediated cellular behaviors. Importantly, these proteins are compact, amenable to synthetic manipulations, potent activators of GTPase signal transduction, and have robust cellular phenotypes. Already, we have taken advantage of the *E. coli* GEF Map's ability to induce cell polarity to uncover an actin-based feedback loop. This feedback loop senses actin dynamics to spatially regulate GTPase

signal transduction. Importantly, it has been well established that GTPase activity cycles correspond to changes in cytoskeletal dynamics, through an unknown mechanism (Machacek et al., 2009). We now propose that GEFs and other signaling molecules traveling on the actin cytoskeleton provide a direct means of coupling actin dynamics with GTPase signaling.

Further exploration of the actin-based feedback loop is necessary to more fully understand the emergent properties of this signaling circuit. Actin dynamics is a broad term that encompasses several different features including actin polymerization, depolymerization, filament capping, filament branching, and retrograde flux. Deciphering how individual processes contribute to the actin-based feedback loop is not trivial, since most of these events are interconnected. For example, increasing the rate of actin polymerization also increases the rate of retrograde flow. The best means to decipher this interconnected network is to reconstitute this signaling network in a cell-free environment. In an analogous system, reconstituting actin-based motility by the *Listeria* protein ActA has significantly progressed our understanding of how the actin polymerization machinery provides the protrusive force for cellular motility (Bear et al., 2001; Loisel et al., 1999). In an effort to bridge the gap between a cell free system and the native signaling network, we reconstituted cue dependent cellular polarity in a bacterial-free system by using fibronectin beads as discrete spatial cues (Figure 21). The future ideal system would combine this bead assay with the formation of filopodia protrusions on lipid bilayers that has been recently reported by Marc Kirschner and colleagues (Lee et al., 2010). While the path to this reconstitution is not in the immediate future, the analysis that this system is capable of

producing will greatly enhance our understanding of how the complex dynamics of the actin cytoskeleton contribute to GTPase signal polarity.

In addition, we have begun laying the foundation for using IpgB1 as a model system to explore the interconnection between GTPase signal transduction and phospholipid metabolism. Because migrating cells form a similar GTPase-phosphoinositide circuit, a theoretical understanding of the IpgB1 signaling network will be broadly applicable. While we are still characterizing the molecular features of this signaling circuit, we predict in the future that rewiring this pathogenic circuit to respond to different lipid classes will provide keen insight into the design principles of pathogenic and endogenous signaling events.

Lastly, there are several other bacterial GEFs including IpgB2 and SifB in which we know very little about the pathogenic phenotypes and regulatory mechanisms underlying their signaling. Exploring these "orphan" GEFs will not only shed light onto new pathways hijacked by bacterial pathogens, but also add to the tool box of probes to dissect the complex environment of eukaryotic signal transduction.

The construction of pathogenic membrane compartments within host cells

It has been well established that intracellular pathogens residing within vacuoles, like *Salmonella* and *Legionella*, establish a novel membrane organelle (Ge and Shao, 2011; Schroeder et al., 2011). However, our data involving the lipid rearrangements induced by IpgB1, suggest that the establishment of pathogenic membrane compartments within host cells is not restricted to these pathogens. The modulation of phospholipid metabolism determines the fate of

invading *Shigellae* (Figure 30 and 31). In addition to *Shigella*, a recent report suggests that the extracellular pathogen, EPEC also remodels host membranes in order to promote its pathogenesis (Smith et al., 2010). We predict that these newly constructed membrane compartments are necessary for the rewiring of host circuits by bacterial pathogens.

The molecular mechanisms governing membrane remodeling by bacterial pathogens is still emerging. While it is known that *Shigella*, *Salmonella*, and *Legionella* all utilize PI-phosphatases to alter host phospholipid metabolism, it is largely unknown how these changes effect host and bacterial protein localization and circuitry (Hsu et al., 2012; Niebuhr et al., 2002; Norris et al., 1998). Additionally, other effector protein signaling events directly alter phospholipid dynamics (Smith et al., 2010) (Figure 32). Therefore, a more systems level analysis is necessary to fully comprehend how pathogenic membrane compartments are established and their pathogenic implications. Because membrane microdomains serve as essential signaling platforms for all forms of life, we expect new and more sophisticated mechanisms of membrane remodeling to emerge in the future.

The assembly of pathogenic circuits by bacterial effector proteins

Recent reports in the literature have suggested that pathogens assemble signaling circuits (Alto et al., 2006; Kubori and Galan, 2003; Patel et al., 2009; Selyunin et al., 2011). However, a thorough understanding of the circuit architecture and design principles of these systems is lacking. Here, we have identified and characterized two novel pathogenic signaling circuits. We find that the *E. coli* Cdc42-specific GEF Map induces a polarity circuit that is dependent upon F-

actin as the dynamic signaling hub (Orchard et al., 2012). In this study, we provide the first mathematical model that describes interkingdom signaling events at the molecular level. Importantly, this computational model of the Map polarity circuit provides a means to illustrate complex signaling events in simple terms and also to develop novel hypotheses. We believe that future studies investigating effector protein biology can benefit from similar theoretical analyses. In addition to the Map polarity circuit, we uncover a GTPase-phospholipid circuit that controls *Shigella* survival post internalization (Figure 37). Future work will be necessary to more fully define the molecular components involved in this circuit. We predict that pathogenic signaling circuits are a common virulence strategy and that future studies will identify additional effector proteins that assemble circuits.

What do pathogenic signaling circuits tell us about bacterial pathogenesis? Historically, research has focused on effectors globally inhibiting eukaryotic signal transduction. Indeed, these mechanisms are common and important for pathogenesis (Cui et al., 2010; Li et al., 2007; Mukherjee et al., 2006; Ribet and Cossart, 2010; Yarbrough et al., 2009). However, to hijack host cellular behaviors, pathogens must contend with the complex signaling environment of eukaryotic cells. Assembling circuits enables bacteria to promote pathogenic signaling networks while at the same time repressing undesired signaling events. Additionally, many signaling circuits provide emergent behaviors like excitatory dynamics, oscillations, and bistable switches (Brandman and Meyer, 2008). As shown with the Map polarity circuit, these emergent properties can have important implications for bacterial pathogenesis (Orchard et al., 2012). Therefore, we speculate that the assembly of pathogenic signaling circuits enables a systems

level control over eukaryotic signal transduction that would not otherwise occur through simple overactivation of a single pathway.

In conclusion, bacterial pathogens assemble pathogenic signaling circuits within eukaryotic cells to hijack host cellular behaviors. The sophisticated mechanisms linking proteins of prokaryotic and eukaryotic origin together highlight the intimate evolutionary relationship between host and pathogen. Exploration of these circuits and their emergent properties is an exciting avenue of research that promises to expand our understanding of the architecture of cellular signaling networks in a wide array of biological settings.

Future Directions

Re-engineering WxxxE effector proteins to alter GTPase-isoform specificity

We have proposed a bacterial GEF-GTPase pairing mechanism in which the hyper variable region of the bacterial GEFs (α4-α6 helices) interact with the β2-3 interswitch region of GTPases (Figure 11). Supporting our model, converting the amino acids in the Rac β2-3 interswitch region to mimic those found in Cdc42 permitted the Cdc42-specific GEF Map to recognize this mutant of Rac (Figure 10C). However, we have not yet targeted the α4-α6 helices for switch of function studies. One hurdle has been the lack of structural information for other WxxxE proteins to compare the three dimensional structure of the α4-α6 helices. Recently, the IpgB2 structure in complex with RhoA has been elucidated (Klink et al., 2010). Comparing the interactions of the α4-α6 helices of Map with IpgB2 will gain insight into the critical amino acids to target for mutagenesis. We predict that converting the amino acids in the Map α4-α6 helices

to resemble IpgB2 will broaden the substrate specificity of the Map to now include RhoA. Conversely, analogous mutations in IpgB2 should inhibit its interactions with RhoA and promote Cdc42 specificity. It is unlikely that individual mutations will appreciably change substrate specificity, and therefore grouping mutations, or even fully converting the α4-α6 helical residues will be a more productive endeavor. A similar strategy can be undertaken for Rac1 specificity when IpgB1 or EspT structures become available. In addition to confirming our GTPase pairing mechanism, these switch of function mutants may be useful in the future for generating synthetic bacterial GEF constructs.

Investigating the spatial and temporal dynamics of endogenous actin binding GEFs

A key finding of our study is the identification of F-actin as a critical regulator of GTPase signal transduction. Specifically, we discovered that actin polymerization locally amplifies and spatially retricts Cdc42 signaling induced by Map. We hypothesize that eukaryotic GEFs can also be regulated by F-actin dynamics. In support of this notion, a literature search illustrates a number of eukaryotic GEFs that interact with the actin cytoskeleton either directly or indirectly (Figure 17). Additionally, we have clear anecdotal evidence to support the existence of actin-based circuit architectures within natural signaling systems. For example, Park *et al*. have identified a Rac1-specific GEF (RacGEF1) that colocalizes with F-actin in the establishment of GTPase polarity in chemotactic cells (Park et al., 2004). This polarity is actin-dependent but the molecular mechanism is still unknown. Additionally, Umikawa *et al*. report that microspike induction by the eukaryotic GEF Frabin strictly requires its upstream actin-binding domain

(Umikawa et al., 1999). To determine if these GEFs utilize an actin-based feedback loop to regulate their signaling dynamics, we propose perturbing actin dynamics through addition of LatB in cells expressing RacGEF1 or Frabrin. The subcellular localization of GFP-Cdc42 and GFP-CRIB$^{N\text{-}WASP}$ can be monitored to assay GEF activity *in vivo*. By blocking actin polymerization, we predict that these GEFs are unable to generate molecular polarity of Cdc42.

Our computation model predicts, that a molecule with an actin-based positive feedback loop can be polarized to extracellular bound fibronectin beads (Fn-beads; Figure 19). Therefore, we predict that similar to Map, RacGEF1 and Frabin will induce Cdc42 polarity in response to Fn-bead stimulation. These studies will begin to address the universality of our discovered feedback loop. Negative results in these experiments may stem from the integration of multiple signals beyond actin dynamics by these GEFs. If this occurs, we propose generating a more simplified molecule that only contains the GEF and actin-binding domains. Using the same assays described above, we can test the ability of these engineered GEFs to generate Cdc42 polarity. Taken together, these studies will begin to look at the universality of actin-based feedback loops.

Testing the ability of SopE2 to interact directly with highly curved membranes

We identified an ALPS-like motif in SopE2 that is both necessary and sufficient for interacting with eukaryotic membranes *in vivo* (Figure 26). ALPS motifs are able to sense loosely-packed lipids in order to bind strongly to highly-curved membranes and weakly to relatively flat membranes (Bigay et al., 2005). A variation in liposome size also changes the

packing of lipids. For example, smaller liposomes have more loosely packed lipids and interact strongly with ALPS motifs compared to the more tightly packed larger liposomes. Therefore, testing the ability of SopE2 to bind directly to liposomes in a size-dependent manner will determine the functionality of the putative ALPS motif. If the ALPS motif is validated, future studies exploring the relationship between GEF activity, membrane curvature, and *Salmonella* pathogenesis should be performed.

Determining how the IpgB1 lipid feedback loop promotes Shigella survival post-internalization

We now show that *Shigella* survival post-invasion depends upon the lipid-binding domain of IpgB1 (Figure 30) Also, we demonstrate that IpgB1 induces membrane remodeling at the site of bacterial entry, but how these processes promote *Shigella* survival are not well understood. Determining the binding affinity of IpgB1 with specific lipids will be important for understanding the implications of membrane remodeling *in vivo.* Currently, studies are ongoing to reconstitute IpgB1-lipid interactions onto liposomes with defined lipid composition. Based on our lipid overlay assays, we predict that IpgB1 will bind to several lipid groups with appreciable affinities and possibility in a synergistic fashion. Once these studies are complete, targeting the biosynthetic pathway(s) using RNAi or pharmacological inhibitors during infection will confirm the role specific lipid(s) play in IpgB1 localization dynamics.

A more challenging prospect, is determining the sequence of events that happen post-internalization that promote *Shigella* survival. *Shigella* rapidly breaks out of its vacuole within minutes of invasion (Ehsani et al., 2012). Because of the time scale, the membrane trafficking,

Rac activity, and lipid rearrangements that occur between internalization and vacuolar escape are unknown. Live cell imaging of invading *Shigella* strains using a spinning disk confocal microscope will greatly aid in these efforts. Combining pharmacological inhibitors with these single cell analyses will also assist in deciphering between the plausible scenarios proposed (Figure 37). While difficult, these proposed studies will significantly enhance our understanding of *Shigella* pathogenesis and provide insight into bacteria access the host cytoplasm.

APPENDIX A
Mathematically Modeling the Map Signaling Network

Introduction

Because of the central role our mathematical model has in describing the Map signaling system, I have included a detailed description of the model written primarily by Mark Kittisopikul under the guidance of Dr Gürol Süel, Dr. Lani Wu, and Dr. Steven Altschuler, Dr. Neal Alto, and myself. This Appendix will greatly complement the information provided in Chapter 3 of this thesis.

Overview

We seek to understand how a core set of molecular interactions between Map, actin, and Cdc42 are sufficient to explain the development of localized areas of filopodia on the membrane of eukaryotic cells expressing Map. Notably, the foci of filopodia appear to form both spontaneously and in response to a cue.

We model the association and dissociation of Actin and Map to and from a membrane associated area as well as the spatial distribution of a membrane diffusible species, Cdc42. This model is meant to focus on the synthetic Map-ABD that is transfected into the cell and that qualitatively recapitulates the phenotype of the wild-type Map expression. The naturally occurring system involves additional scaffolding proteins, Ezrin binding phosphoprotein 50 (Ebp50) and Ezrin, that link wild-type Map to actin. This scaffolding complex is not directly considered here. However, as the Actin-Binding Domain (ABD) is from Ezrin, we do

incorporate some physical measurements from the natural system. This model applies to the wild-type system to the degree that the scaffolding proteins serve to couple Map with actin and is less applicable to the natural system if these scaffolding proteins serve other functions such as maintaining high local membrane concentrations.

Actin is represented in the model by discrete actin filaments. These are actin polymers which can associate and dissociate from the membrane. Association occurs spontaneously but is also enhanced by Cdc42 signaling due to increased actin polymerization.

Map is a discrete guanine-nucleotide exchange factor for Cdc42 in the model. It activates Cdc42 by exchanging GDP for GTP. Map is positioned close to the membrane by binding to actin filaments through an actin-binding domain (ABD) from Ezrin. Map is removed from the membrane through two mechanisms. One is simply unbinding from an actin filament. Unbinding represents any event by which Map is no longer able to function as a GEF for Cdc42. This may include the removal of Map to the cytosol. Another is detachment of an actin filament from the membrane to which Map molecules are bound. When an actin filament detaches, a proportional amount of Map is removed in the relevant compartment.

Activated Cdc42 is modeled as a continuous concentration that can diffuse along the membrane. Cdc42 is activated by Map. It is inactivated via hydrolysis by GAPs that are not explicitly simulated. Cdc42 is able to diffuse laterally within the membrane and in this way provides for lateral communication of molecular signaling along the membrane. Activated Cdc42 signals to a number of downstream effectors which leads to actin polymerization and thus encourages further actin filament association to the membrane.

For the purposes of simulation, we divide the cell into many small compartments along the inner surface of the plasma membrane and a cytosolic region that is functionally away from the membrane. Each membrane surface compartment represents a small volume along the membrane of a cell that contains a discrete number of actin molecules, a discrete number of Map molecules, and a concentration of Cdc42. Actin and Map move between the membrane surface compartments and further into the cytosolic region of the cell, but are only active along the membrane. In contrast, Cdc42 is the only species that directly moves from one membrane surface compartment to another through diffusion.

Assumptions

1. Map binds to actin filaments that associate with the cellular membrane.
2. Map acts as guanine-nucleotide exchange factor for Cdc42.
3. Activation of Cdc42 by Map increases the likelihood of actin filament attachment by encouraging actin polymerization.
4. Polymerization of actin provides more binding partners for Map.
5. Unactivated Cdc42, bound to GDP, is assumed to be in excess such that the rate of Cdc42 activation by Map does not inversely depend on the active Cdc42 concentration.
6. Cdc42 diffuses laterally along the membrane.
7. Cdc42 signaling zones induced by ectopically expressed Map occur spontaneously.

8. Cdc42 signaling zones can be induced by seeding Map (as when injected by a Type 3 secretion system) or by seeding Actin (through contract with a Fibronectin bead).
9. The number of binding sites for Map on an actin filament is not limiting.
10. Actin associated Map molecules are removed from the membrane when an actin filament detaches from the membrane.
11. The total amount of Map and actin filaments are considered to be constant over the course of the simulation.

Variables

Please see Table 2 for a listing of the variables used in this study. Time is simulated in discrete and constant timesteps such that events are relatively rare for each timestep. A spatial aspect along the membrane is introduced by dividing the membrane into many compartments identified by *x*. $a_x(t), m_x(t), and\ c_x(t)$ describe the amount of actin, Map, and Cdc42 functionally associated with each membrane surface compartment at position *x*, respectively. *A(t)* and *M(t)* describe the amount of actin and Map not functionally associated with the membrane.

Parameters

Please see Table 3 for a listing of the parameters used in this study.

1. k_{on} and k_{off} represent the spontaneous association and dissociation of actin filaments to the membrane, independent of Cdc42.
2. k_{bind} and k_{unbind} define the binding and unbinding rates of Map to an actin filament.

3. k_{gef} and k_{hydro} describe the activation of Cdc42 by Map and the deactivation of Cdc42 by GAPs, respectively.
4. D describes the diffusion of Cdc42 laterally along the membrane
5. k_{fb} represents active recruitment of actin filaments in a Cdc42 dependent fashion.

Physical basis for parameters

Dimensions of the cell and compartments

We estimated the 2D circumference of the cell as 60 μm. Approximating the cell as a disc gives a radius of 9.55 μm (which is within 10.5 ± 2.2 μm) (Milo et al., 2010; Zhao et al., 2008). This corresponds to a volume of 3648 μm^3 or 3.6 x 10^{-12} L. The depth of the volume near the membrane by which Map can signal to Cdc42 is approximated as 60 Angstroms or 6 nm as estimated from structural information (Figure 18A).

Since the membrane is divided up into 1000 compartments, each compartment spans 60 nm. The volume of each compartment, $V_{compartment}$, is therefore 60 nm x 60 nm x 6 nm = 2.16 nm^3. The membrane surface area is $(60\ nm)^2$ or 3600 nm^2

Since one nm^3 = 10^{-24} L, each compartment thus has a volume of 2.16 x 10^{-20} L. Therefore a molar concentration in a compartment represents a density of 1 mol/L x 6.022 x 10^{23} molecules/mol x 2.16 x 10^{-20} L = 1.30 x 10^4 molecules per compartment. Thus, a 1 mM concentration in a compartment corresponds to about 13 molecules in that compartment. For the purposes of the stochastic description and simulation, we will describe actin and Map in terms of quantized units of molecules per compartment which corresponds to increments of 77 μM.

1 mM can also be converted into an area density in that 1 mM corresponds to about 13 molecules per 3600 nm^2 of membrane or 1 molecule per 277 nm^2 on average. Thus we can estimate that half of the average distance is the radius of a circle with area 277 nm^2. From πr^2 = 277 nm^2, r = 9.39 nm or a mean intermolecular distance of 18.8 nm. The distance scales with the square root of the molecular concentration.

Diffusion constant of Cdc42

The most directly relatable physical constant to the dimensions of the cell is the diffusion constant of Cdc42. This has been measured to be 0.036 μm^2/sec in *S. cervisiae* and estimated be about ten times faster in *H. sapiens* due to prenylation: 0.36 μm^2 / sec (Marco et al., 2007; Wedlich-Soldner et al., 2003). This corresponds to a simulation unit of 100 compartments^2/sec.

Association and dissociation rate of actin filaments

To calibrate the association rate of actin filaments, we use the binding kinetics of Arp2/3 to WASP. The K_D has been measured to be 0.25 µM while the k_{off} has been measured to be 0.6 sec^{-1} (Marchand et al., 2001). This yields a calculated k_{on} rate of 2.4 μM^{-1} sec^{-1}. For the simulation the rate is converted in terms of molecules per compartment and a fixed local membrane concentration of 79 nM WASP. We use an effective association rate of 0.19 sec^{-1} or 1.9 x 10^{-4} sec^{-1} per compartment for 1000 compartments. The rate used dictates that 24% of the available actin filaments in the simulation will be associated to the membrane in the absence of feedback at steady-state conditions.

Binding of Map to actin

The binding rates of Map to Actin are derived from K_D of 500 nM for the Ezrin Actin-Binding Domain (ABD) and Actin. In the natural system, Map is associated with Ezrin and its ABD through scaffolding proteins. In the constructed system, Map is tethered directly to an ABD derived from Ezrin. k_{bind} is set to 1 filament^{-1} sec^{-1} for each of the 1000 compartments and k_{unbind} to 6.5 sec^{-1} in a single compartment (Roy et al., 1997).

Activation and hydrolysis of Cdc42

The estimated k_{cat} of Map is 5-19 sec^{-1} and the estimated K_M is 6-14 μM (Friebel et al., 2001; Huang et al., 2009). We thus estimate the k_{cat} to be 10 sec^{-1} and the K_M to be 10 μM. The effective simulation constant for k_{gef} is 77 μM molecule^{-1} sec^{-1} incorporating both the k_{cat} and K_M values since we do not simulate inactive Cdc42. The catalyzed hydrolysis rate has a k_{cat} of 2103.9 min^{-1} or about 35 sec^{-1} (Zhang et al., 1997). Assuming 0.1 μM GAP present, this leads to a simulated rate of 3.5 sec^{-1}.

Feedback term: Cdc42 to actin polymerization

The feedback term, k_{fb} is a difficult term to relate as its physical basis depends on a number of species that signal between Cdc42 and the actin polymerization machinery that are not modeled here. This term was determined on an empirical basis based upon the mean number of filopodia foci observed in parameter variation studies (Figure 20). The rate is 0.012 μM^{-1} sec^{-1}.

Number of foci and width of foci

The number and width of Cdc42 signaling zones that form foci of filopodia are measured in this work. The number is dependent on how many positive feedback loops can be initiated spontaneously before the available supply of Map and actin filaments is depleted. The number is

thus dependent on the k_{on} and k_{fb} rates. High k_{on} rates increase the spontaneous association of actin filaments to the membrane and thus increases the number of foci. High k_{fb} rates increases the rate at which such an association recruits more actin filaments in competition with other spatially distinct sites. Thus high k_{fb} will eventually decrease the number of foci since foci that form earlier will attract more molecules. This is examined in a parameter variation study as shown in the Figure 20D and 20E and discussed below.

Another consideration for the number of foci is the ability to spatially distinguish them, which is a function of foci width. The width of the foci is determined by how far an activated Cdc42 molecule can diffuse before hydrolysis inactivates it. Hydrolysis subjects active Cdc42 to exponential decay with a temporal half-life of $ln(2)/k_{hydro}$. Diffusion distributes active Cdc42 in space with a standard deviation of $\sqrt{2Dt}$.

In order to analyze foci, a low threshold (2 μM) is first used to determine when the Cdc42 concentration exceeds a certain value indicating the beginning and end of a focus. The number of compartments for which the concentration exceeds this value is considered the width of the focus. A higher threshold, 100 μM, is then used to further screen the maxima of potential foci for areas where Cdc42 is intensely concentrated. In summary, foci of filopodia are first distinguished by a low threshold and then only counted if their maxima exceed a high threshold.

Number of molecules of Map and actin filaments

Because the experimental results from this study demonstrated non-deterministic behavior in that discrete foci formed spontaneously, the number molecules involved should be small such that foci initiation is a rare event. In the simulation, the number of possible events per

time step scales with the number compartments. This suggests that we select a discrete number of molecules less than the number of compartments such that it is not possible for all membrane compartments to be simultaneously occupied. This also means that we must select enough discrete compartments such that the number of molecules is physically reasonable. Since the total amount of Map and actin are fixed in the simulation, we chose the totals to be 40% of the number of compartments or 400 molecules within the cell for both Map and actin filaments. This corresponds to 400 molecules or filaments per 3.6 x 10^{-12} L in a cell or 182 pM on average and 1000 compartments.

Conservation of Map and Actin

$$M_T = M + \sum_x m_x \tag{1}$$

$$A_T = A + \sum_x a_x \tag{2}$$

$$M = M_T - \sum_x m_x \tag{3}$$

$$A = A_T - \sum_x a_x \tag{4}$$

For the purposes of the simulation, the total amount of Actin and Map available in the cell are considered to be fixed. Essentially, we assume that production and degradation of Actin and Map remain constant and that the cell is at or near steady state conditions for these two species. The total number of Actin and Map is thus the sum of the amount that is in equivalent compartments along the inner surface of the membrane and the amount of molecules not functionally associated with the membrane.

Partial differential equations

The following is a deterministic approximation of the model. Actin and Map are simulated stochastically as discrete molecules. Cdc42 is actually modeled as a continuous variable that represents the concentration of Cdc42 near the membrane.

$$\frac{\partial a_x}{\partial t} = (k_{on} + k_{fb} c_x) A - k_{off} a_x \quad (5)$$

$$\frac{\partial m_x}{\partial t} = k_{bind} M\, a_x - (k_{unbind} + k_{off}) m_x \quad (6)$$

$$\frac{\partial c_x}{\partial x} = k_{gef} m_x - k_{hydro} c_x + D\nabla^2 c \quad (7)$$

Actin is added in an intrinsic (k_{on} term) and Cdc42 dependent manner (k_{fb} term) based upon the number of actin filaments not associated with the membrane. Actin is removed by an intrinsic, linear rate dependent on the amount of actin in each membrane surface compartment (k_{off} term).

Map binds to actin in each membrane surface compartment in such a way that binding sites are not consumed significantly (k_{bind} term). Map can also unbind from actin in a manner proportional to the amount of Map on the membrane (k_{unbind} term). Molecules of Map can also leave the membrane through the loss of an actin filament described by the k_{off} term for actin. A proportional amount of Map is thus removed from the membrane: $k_{off}\, a_x * m_x / a_x = k_{off}\, m_x$.

Cdc42 is activated by Map (k_{gef} term) and hydrolyzed at a linear rate that is assumed to be catalyzed by GAPs (k_{hydro} term). Cdc42 is also able to diffuse along the membrane and thus accounts for communication between the different membrane surface compartments.

Stochastic description

Actin and Map are actually simulated as discrete molecules upon which stochastic Poisson processes act. First we define the following expressions:

- $p_{am(t)} = \Pr[a_x(t) = a, m_{x(t)} = m]$, Probability of having *a* Actin and *m* Map at time *t*
- $W_{am(t)}$, Transition propensity to *a* Actin and *m* Map at time *t*
- $\dot{p}_{am} \equiv \frac{dp_{am(t)}}{dt}$, Time derivative of the probability

We can then express the stochastic simulation as follows:

$$W_{am} = k_{off}(a+1)p_{a+1,m} - (k_{on} + k_{fb}c_x)p_{am} + (k_{unbind} + k_{off})(m+1)p_{a,m+1} - k_{bind}a\,p_{am} \quad (8)$$

$$\dot{p}_{am} = W_{am} - W_{a,m-1} - W_{a-1,m} - W_{a-1,m-1} \quad (9)$$

c(x,t) is governed by Equation(7) . Equation(9) is the master equation that describes the stochastic evolution of Map and Actin.

Simulation

The simulation implements the above by simulating Map and Actin events as Poisson random processes and Cdc42 deterministically according the PDE, Eqn. (7), in a specific order:

1. Remove actin as per the k_{off} term.
    a. Remove Map proportionally with actin k_{off} events.
2. Remove Map due to unbinding from actin, k_{unbind} term.
3. Add Map due to binding with actin, k_{bind} term.
4. Hydrolyze Cdc42 according to exponential decay, k_{hydro} term.
5. Activate Cdc42 deterministically with respect to Map, k_{gef} term.
6. Diffuse Cdc42 along the membrane, D diffusion term.
7. Add actin by nucleation on the membrane, k_{on} and k_{fb} term.

Time progresses according to constant, discrete time steps chosen to minimize the number of events per iteration of the simulation.

Implementation

We implemented a fixed time increment simulation in MATLAB that simulates actin filaments and Map stochastically while treating Cdc42 deterministically. The stochastic events are determined by using a Poisson pseudo-random number with a mean propensity according to the corresponding rate law and time increment.

With this scheme it is possible for more actin or Map to be removed from a compartment than present. This is minimized by using small time increments. In case of such a rare situation, we explicitly cap the amount of a species that can be removed from a membrane surface compartment to the amount present. Similarly, for events where more of a species is moved to a membrane surface compartment from the cytosolic compartment we randomly cancel the excess number of moves. This error correction code is rarely used and does produce warnings when run.

The deterministic terms affecting Cdc42 are integrated per term in a fixed sequence. Hydrolysis is evaluated as an exponential decay. Cdc42 activation occurs deterministically based upon the presence of Map in a compartment. Cdc42 diffusion is calculated based on convolution with a Gaussian kernel as described below.

Note on diffusion of Cdc42

Cdc42 is able to diffuse laterally between nearby membrane surface compartments. This is simulated by convolution with a Gaussian kernel. The Gaussian kernel is the Green's function of the 1D diffusion equation (Strauss, 1992). The 1D diffusion equation is represented here:

$$\frac{\partial c_x}{\partial t} = D\nabla^2 \mathrm{c} \qquad (10)$$

Where D represents the diffusion constant expressed in μm^2 / sec . The Gaussian kernel has standard deviation $\sigma = \sqrt{2Ddt}$. *dt* is the small time interval used for each iteration of the simulation. Thus, the kernel is expressed as

$$G(x, dt) = \frac{1}{\sqrt{4\pi Ddt}} \exp\left(-\frac{x^2}{4Ddt}\right) \tag{11}$$

The solution to the diffusion equation, Eqn. (10), is the convolution of the Cdc42 with this kernel:

$$c(x, t - t_0) = \int_{-\infty}^{+\infty} G(x - y, t - t_0) c(y, t_0) dy \tag{12}$$

However, we note that Eqn. (10) is not the solution to the full Cdc42 equation, Eqn. (7). Use of the convolution for diffusion in this case is thus an approximation which is only valid for small time steps.

Depending on *dt* the standard deviation, σ, may become less than the physical span of one compartment. Thus the simulation provides a facility by which Cdc42 may be monitored at higher spatial resolution than for Map or actin. For interaction with Map or actin the high spatial resolution Cdc42 distribution is converted to a distribution with the lower resolution of the original compartments.

Parameter variation

Non-dimensional steady-state equation

We used a parameter variation study to examine how the parameters k_{on} and k_{fb} affected the number of foci that formed. More specifically, we nondimensionalized the parameters by considering the ratios of the k_{on} and k_{fb} parameters relative to k_{off} parameter. This is justified by dividing Eqn. (5) through by k_{off} and A_T and calculating the steady state proportion of actin on the membrane:

$$\frac{1}{k_{off}A_T}\frac{\partial a_x}{\partial t} = \left(\frac{k_{on}}{k_{off}} + \frac{k_{fb}}{k_{off}}c_x\right)\left(\frac{A}{A_T}\right) - \frac{a_x}{A_T} \tag{13}$$

$$\alpha(t) \equiv \frac{\sum_x a_{x(t)}}{A_T} \tag{14}$$

$$\frac{1}{k_{off}}\frac{d\alpha}{dt} = N\left(\frac{k_{on}}{k_{off}} + \frac{k_{fb}}{k_{off}}C\right)(1-\alpha) - \alpha \tag{15}$$

$$\frac{1}{k_{off}}\frac{d\alpha_{ss}}{dt} = N\left(\frac{k_{on}}{k_{off}} + \frac{k_{fb}}{k_{off}}\frac{k_{gef}}{k_{hydro}}\frac{\alpha_{ss}}{\frac{K}{A_T}+\alpha_{ss}}M_T\right)(1-\alpha_{ss}) - \alpha_{ss} \tag{16}$$

$$= 0 \tag{17}$$

Where N is the number of compartments, C is the Cdc42 concentration averaged over the compartments on the membrane (the steady state formula for this is derived below) and K is the effective dissociation constant for Map-actin binding:

$$C(t) \equiv \frac{1}{N}\sum_{x} c_{x(t)} \tag{18}$$

$$K \equiv \frac{k_{unbind} + k_{off}}{k_{bind}} \tag{19}$$

The effective feedback scaling factor, γ, is thus:

$$\gamma = \frac{k_{fb}}{k_{off}}\frac{k_{gef}}{k_{hydro}}M_T \tag{20}$$

$$\frac{1}{k_{off}}\frac{d\alpha_{ss}}{dt} = N\left(\frac{k_{on}}{k_{off}} + \gamma\frac{\alpha_{ss}}{\frac{K}{A_T} + \alpha_{ss}}\right)(1-\alpha_{ss}) - \alpha_{ss} = 0 \tag{21}$$

The actual steady state amount of actin on the membrane still depends on *K*. However, we can estimate the amount of actin on the membrane assuming total binding, $k_{bind} \gg k_{unbind} + k_{off}$ such that $K \approx 0$:

$$0 \approx N\left(\frac{k_{on}}{k_{off}} + \gamma\right)(1-\alpha_{ss}) - \alpha_{ss} \tag{22}$$

$$0 \approx N\left(\frac{k_{on}}{k_{off}} + \gamma\right) - \alpha_{ss}N\left(\frac{k_{on}}{k_{off}} + \gamma + \frac{1}{N}\right) \tag{23}$$

(24)

$$\alpha_{ss}\left(\frac{k_{on}}{k_{off}}+\gamma+\frac{1}{N}\right)\approx\left(\frac{k_{on}}{k_{off}}+\gamma\right)$$

$$\alpha_{ss}\approx\frac{\frac{k_{on}}{k_{off}}+\gamma}{\frac{k_{on}}{k_{off}}+\gamma+\frac{1}{N}} \quad (25)$$

The main difference between the k_{on} parameter and γ is that k_{on} applies equally to all membrane associated compartments, while γ is modulated by on the state of each compartment. k_{on} affects the initialization of polarity at a compartment. γ describes the strength at which a focus develops once initiated. The rate constants here are scaled for each compartment which is why the *1/N* term is present (e.g. k_{on} is the spontaneous binding rate for a single compartment whereas Nk_{on} is the spontaneous binding rate for the entire membrane). We directed our parameter variation efforts on understanding how k_{on} and γ affect the number of prominent foci.

Derivation of total steady state active Cdc42

Equation (16) is derived at steady state at conditions by first evaluating Map at steady state:

$$\frac{dM}{dt}=-k_{bind}M(A_T-A)+\left(k_{unbind}+k_{off}\right)(M_T-M) \quad (26)$$

$$\frac{1}{k_{unbind}+k_{off}}\frac{dM}{dt}=-\frac{k_{bind}}{k_{unbind}+k_{off}}M(A_T-A)+(M_T-M) \quad (27)$$

(28)

$$= -\frac{1}{K}M(A_T - A) + (M_T - M) \tag{29}$$

$$= M_T - \left(1 + \frac{1}{K}(A_T - A)\right)M = 0 \tag{30}$$

$$\frac{M_{ss}}{M_T} = \frac{1}{1 + \frac{A_T - A}{K}} \tag{31}$$

$$\frac{M_{ss}}{M_T} = \frac{K}{K + (A_T - A)} \tag{32}$$

$$\frac{M_{memb}}{M_T} = \frac{M_T - M_{ss}}{M_T} = \frac{A_T - A}{K + (A_T - A)} = \frac{\alpha_{ss}}{\frac{K}{A_T} + \alpha_{ss}}$$

Once we have the steady state amount of Map on the membrane, we then also derive the average steady state concentration of Cdc42 on the membrane:

$$\frac{dC}{dt} = k_{gef}(M_T - M) - k_{hydro}C \tag{33}$$

$$= 0 \tag{34}$$

$$C = \frac{k_{gef}}{k_{hydro}}(M_T - M_{ss}) \tag{35}$$

$$= \frac{k_{gef}}{k_{hydro}} \frac{\alpha_{ss}}{\frac{K}{A_T} + \alpha_{ss}} M_T \tag{36}$$

Parameter variation results

We varied the k_{on} / k_{off} ratio and γ, effective feedback, as explained above with Equation (16). The results of the effects on number of polarity sites, foci, and foci width are shown in Supplemental Figure 20D. γ was varied by changing the k_{fb} term. Ten simulations were run for each pair of parameters using a timestep of 10^{-4} seconds for 10^4 timesteps. This equates to a simulation time of one second. As expected, the number of actin filaments associated with the membrane increased directly with either k_{on} / k_{off} or γ. We also then counted the number of foci formed as discussed above. Distinct and prominent foci formed at low levels of k_{on} and increased in number with γ. In this parameter regime, few foci are initiated but those that do form are able to become prominent.

At high levels of k_{on} relative to k_{off} prominent foci failed to form since many foci are initiated but they fail to become prominent or distinct. At very high levels of γ not shown in the parameter variation, the number of foci begin to decrease as one or two foci quickly become prominent and out-compete subsequent foci that may be initiated later.

At k_{on} = 0 no foci were initiated and thus no actin filaments associated with the membrane. At k_{on} / k_{off} x 1000 = 1 about half of the actin filaments are associated with the membrane. The factor of 1000 is multiplied since the k_{on} rate is always evaluated for 1000 compartments on the membrane, whereas k_{off} only applies to compartments which have actin associated with them.

Foci width increases with k_{on} and decreases slightly with γ. The increase in widths with k_{on} is mostly due to an increased likelihood of two foci being close together in space. The two

foci are counted as one foci with greater width. The slight decrease in width with increasing γ is due to greater feedback intensity at the center of foci which are more concentrated in the middle. Foci width are mainly dependent on the diffusion constant, D, and the hydrolysis rate, k_{hydro}, as explained above.

Map accumulated on the membrane in significant numbers because of high binding affinity as derived from the literature. The amount of active Cdc42 mainly increases with k_{on}. With higher k_{on} active Cdc42 is more evenly spread out over the membrane. This prevents GAPs from reaching V_{max} and thus decreases hydrolysis in total, allowing for more Cdc42 overall.

Overall, the parameter variation shows that distinct foci of filopodia form with a low to intermediate spontaneous association rate, k_{on} ,and a high effective feedback rate, γ, dependent on k_{fb} and Cdc42 dynamics relative to the spontaneous dissociation rate, k_{off}.

Ten minute simulation

The ten minute simulation shown in Figure 10C was done by running the simulation at a timestep of 6×10^{-4} for 10^6 timesteps yielding a total simulation time of 600 seconds or 10 minutes. Three foci spontaneously form at the beginning of the simulation. The foci are shown to be dynamic over this timespan, but are relatively stable.

Distribution of number of foci

To determine the distribution of the number and width of foci as shown in Figure 20A and 20B, 1000 simulations were run with the parameters detailed above with a timestep of 10^{-4} seconds.

BIBLIOGRAPHY

Aktories, K. (2011). Bacterial protein toxins that modify host regulatory GTPases. Nature Reviews Microbiology *9*, 487-498.

Algrain, M., Turunen, O., Vaheri, A., Louvard, D., and Arpin, M. (1993). Ezrin contains cytoskeleton and membrane binding domains accounting for its proposed role as a membrane-cytoskeletal linker. The Journal of Cell Biology *120*, 129-139.

Alto, N.M., Shao, F., Lazar, C.S., Brost, R.L., Chua, G., Mattoo, S., McMahon, S.A., Ghosh, P., Hughes, T.R., Boone, C., *et al.* (2006). Identification of a bacterial type III effector family with G protein mimicry functions. Cell *124*, 133-145.

Anes, E., Kuhnel, M.P., Bos, E., Moniz-Pereira, J., Habermann, A., and Griffiths, G. (2003). Selected lipids activate phagosome actin assembly and maturation resulting in killing of pathogenic mycobacteria. Nature Cell Biology *5*, 793-802.

Antonny, B. (2011). Mechanisms of membrane curvature sensing. Annual Review of Biochemistry *80*, 101-123.

Arbeloa, A., Blanco, M., Moreira, F.C., Bulgin, R., Lopez, C., Dahbi, G., Blanco, J.E., Mora, A., Alonso, M.P., Mamani, R.C., *et al.* (2009). Distribution of EspM and EspT Among Enteropathogenic and Enterohaemorrhagic Escherichia coli. J Med Microbiol *58*, 988-995.

Arbeloa, A., Bulgin, R.R., MacKenzie, G., Shaw, R.K., Pallen, M.J., Crepin, V.F., Berger, C.N., and Frankel, G. (2008). Subversion of actin dynamics by EspM effectors of attaching and effacing bacterial pathogens. Cell Microbiol *10*, 1429-1441.

Arbeloa, A., Garnett, J., Lillington, J., Bulgin, R.R., Berger, C.N., Lea, S.M., Matthews, S., and Frankel, G. (2010). EspM2 is a RhoA guanine nucleotide exchange factor. Cell Microbiol *12*, 654-664.

Ashida, H., Ogawa, M., Mimuro, H., Kobayashi, T., Sanada, T., and Sasakawa, C. (2011). Shigella are versatile mucosal pathogens that circumvent the host innate immune system. Current Opinion in Immunology *23*, 448-455.

Audhya, A., and Emr, S.D. (2002). Stt4 PI 4-kinase localizes to the plasma membrane and functions in the Pkc1-mediated MAP kinase cascade. Dev Cell *2*, 593-605.

Audhya, A., Foti, M., and Emr, S.D. (2000). Distinct roles for the yeast phosphatidylinositol 4-kinases, Stt4p and Pik1p, in secretion, cell growth, and organelle membrane dynamics. Molecular Biology of the Cell *11*, 2673-2689.

Bakowski, M.A., Braun, V., Lam, G.Y., Yeung, T., Heo, W.D., Meyer, T., Finlay, B.B., Grinstein, S., and Brumell, J.H. (2010). The phosphoinositide phosphatase SopB manipulates membrane surface charge and trafficking of the Salmonella-containing vacuole. Cell Host Microbe *7*, 453-462.

Bakshi, C.S., Singh, V.P., Wood, M.W., Jones, P.W., Wallis, T.S., and Galyov, E.E. (2000). Identification of SopE2, a Salmonella secreted protein which is highly homologous to SopE and involved in bacterial invasion of epithelial cells. J Bacteriol *182*, 2341-2344.

Balla, T., Bondeva, T., and Varnai, P. (2000). How accurately can we image inositol lipids in living cells? Trends in Pharmacological Sciences *21*, 238-241.

Banerjee, J., Fischer, C.C., and Wedegaertner, P.B. (2009). The amino acid motif L/IIxxFE defines a novel actin-binding sequence in PDZ-RhoGEF. Biochemistry *48*, 8032-8043.

Barbieri, M.A., Li, G., Mayorga, L.S., and Stahl, P.D. (1996). Characterization of Rab5:Q79L-stimulated endosome fusion. Arch Biochem Biophys *326*, 64-72.

Bear, J.E., Krause, M., and Gertler, F.B. (2001). Regulating cellular actin assembly. Current Opinion in Cell Biology *13*, 158-166.

Bellanger, J.M., Astier, C., Sardet, C., Ohta, Y., Stossel, T.P., and Debant, A. (2000). The Rac1- and RhoG-specific GEF domain of Trio targets filamin to remodel cytoskeletal actin. Nature Cell Biology *2*, 888-892.

Berger, C.N., Crepin, V.F., Jepson, M.A., Arbeloa, A., and Frankel, G. (2009). The mechanisms used by enteropathogenic Escherichia coli to control filopodia dynamics. Cellular Microbiology *11*, 309-322.

Beuzon, C.R., Meresse, S., Unsworth, K.E., Ruiz-Albert, J., Garvis, S., Waterman, S.R., Ryder, T.A., Boucrot, E., and Holden, D.W. (2000). Salmonella maintains the integrity of its intracellular vacuole through the action of SifA. EMBO J *19*, 3235-3249.

Bi, F., Debreceni, B., Zhu, K., Salani, B., Eva, A., and Zheng, Y. (2001). Autoinhibition mechanism of proto-Dbl. Mol Cell Biol *21*, 1463-1474.

Bigay, J., Casella, J.F., Drin, G., Mesmin, B., and Antonny, B. (2005). ArfGAP1 responds to membrane curvature through the folding of a lipid packing sensor motif. EMBO J *24*, 2244-2253.

Bos, J.L., Rehmann, H., and Wittinghofer, A. (2007). GEFs and GAPs: critical elements in the control of small G proteins. Cell *129*, 865-877.

Boucrot, E., Beuzon, C.R., Holden, D.W., Gorvel, J.P., and Meresse, S. (2003). Salmonella typhimurium SifA effector protein requires its membrane-anchoring C-terminal hexapeptide for its biological function. J Biol Chem *278*, 14196-14202.

Boucrot, E., Henry, T., Borg, J.P., Gorvel, J.P., and Meresse, S. (2005). The intracellular fate of Salmonella depends on the recruitment of kinesin. Science *308*, 1174-1178.

Brandman, O., and Meyer, T. (2008). Feedback loops shape cellular signals in space and time. Science *322*, 390-395.

Bretscher, A., Chambers, D., Nguyen, R., and Reczek, D. (2000). ERM-Merlin and EBP50 protein families in plasma membrane organization and function. Annual Review of Cell and Developmental Biology *16*, 113-143.

Brombacher, E., Urwyler, S., Ragaz, C., Weber, S.S., Kami, K., Overduin, M., and Hilbi, H. (2009). Rab1 guanine nucleotide exchange factor SidM is a major phosphatidylinositol 4-phosphate-binding effector protein of Legionella pneumophila. J Biol Chem *284*, 4846-4856.

Brumell, J.H., and Grinstein, S. (2004). Salmonella redirects phagosomal maturation. Curr Opin Microbiol *7*, 78-84.

Brumell, J.H., Tang, P., Mills, S.D., and Finlay, B.B. (2001). Characterization of Salmonella-induced filaments (Sifs) reveals a delayed interaction between Salmonella-containing vacuoles and late endocytic compartments. Traffic *2*, 643-653.

Brumell, J.H., Tang, P., Zaharik, M.L., and Finlay, B.B. (2002). Disruption of the Salmonella-containing vacuole leads to increased replication of Salmonella enterica serovar typhimurium in the cytosol of epithelial cells. Infect Immun *70*, 3264-3270.

Buchwald, G., Friebel, A., Galan, J.E., Hardt, W.D., Wittinghofer, A., and Scheffzek, K. (2002). Structural basis for the reversible activation of a Rho protein by the bacterial toxin SopE. The EMBO Journal *21*, 3286-3295.

Bulgin, R., Arbeloa, A., Goulding, D., Dougan, G., Crepin, V.F., Raymond, B., and Frankel, G. (2009a). The T3SS effector EspT defines a new category of invasive enteropathogenic E. coli (EPEC) which form intracellular actin pedestals. PLoS Pathogens *5*, e1000683.

Bulgin, R.R., Arbeloa, A., Chung, J.C., and Frankel, G. (2009b). EspT triggers formation of lamellipodia and membrane ruffles through activation of Rac-1 and Cdc42. Cell Microbiol *11*, 217-229.

Burnaevskiy, N., Fox, T., Plymire, D., Weigele, B., Selyunin, A., Patrie, S., Ertelt, J., Way, S., and Alto, N. (2013). Proteolytic Elimination of N-myristoyl Modifications by the Shigella Virulence Factor IpaJ. Nature *In press*.

Carman, G.M., and Han, G.S. (2009). Regulation of phospholipid synthesis in yeast. Journal of Lipid Research *50 Suppl*, S69-73.

Chatah, N.E., and Abrams, C.S. (2001). G-protein-coupled receptor activation induces the membrane translocation and activation of phosphatidylinositol-4-phosphate 5-kinase I alpha by a Rac- and Rho-dependent pathway. J Biol Chem *276*, 34059-34065.

Chien, U.H., Lai, M., Shih, T.Y., Verma, I.M., Scolnick, E.M., Roy-Burman, P., and Davidson, N. (1979). Heteroduplex analysis of the sequence relationships between the genomes of Kirsten and Harvey sarcoma viruses, their respective parental murine leukemia viruses, and the rat endogenous 30S RNA. Journal of virology *31*, 752-760.

Christen, M., Coye, L.H., Hontz, J.S., LaRock, D.L., Pfuetzner, R.A., Megha, and Miller, S.I. (2009). Activation of a bacterial virulence protein by the GTPase RhoA. Sci Signal *2*, ra71.

Co, C., Wong, D.T., Gierke, S., Chang, V., and Taunton, J. (2007). Mechanism of actin network attachment to moving membranes: barbed end capture by N-WASP WH2 domains. Cell *128*, 901-913.

Cornelis, G.R. (2006). The type III secretion injectisome. Nat Rev Microbiol *4*, 811-825.

Crick, F.H., Barnett, L., Brenner, S., and Watts-Tobin, R.J. (1961). General nature of the genetic code for proteins. Nature *192*, 1227-1232.

Cui, J., Yao, Q., Li, S., Ding, X., Lu, Q., Mao, H., Liu, L., Zheng, N., Chen, S., and Shao, F. (2010). Glutamine deamidation and dysfunction of ubiquitin/NEDD8 induced by a bacterial effector family. Science *329*, 1215-1218.

Cutler, N.S., Heitman, J., and Cardenas, M.E. (1997). STT4 is an essential phosphatidylinositol 4-kinase that is a target of wortmannin in Saccharomyces cerevisiae. J Biol Chem *272*, 27671-27677.

Datsenko, K.A., and Wanner, B.L. (2000). One-step inactivation of chromosomal genes in Escherichia coli K-12 using PCR products. Proc Natl Acad Sci U S A *97*, 6640-6645.

De Matteis, M.A., and Godi, A. (2004). PI-loting membrane traffic. Nature Cell Biology *6*, 487-492.

Der, C.J., Krontiris, T.G., and Cooper, G.M. (1982). Transforming genes of human bladder and lung carcinoma cell lines are homologous to the ras genes of Harvey and Kirsten sarcoma viruses. Proc Natl Acad Sci U S A *79*, 3637-3640.

Desrivieres, S., Cooke, F.T., Parker, P.J., and Hall, M.N. (1998). MSS4, a phosphatidylinositol-4-phosphate 5-kinase required for organization of the actin cytoskeleton in Saccharomyces cerevisiae. J Biol Chem *273*, 15787-15793.

Diakowski, W., Grzybek, M., and Sikorski, A.F. (2006). Protein 4.1, a component of the erythrocyte membrane skeleton and its related homologue proteins forming the protein 4.1/FERM superfamily. Folia Histochem Cytobiol *44*, 231-248.

Djinovic-Carugo, K., Gautel, M., Ylanne, J., and Young, P. (2002). The spectrin repeat: a structural platform for cytoskeletal protein assemblies. FEBS Lett *513*, 119-123.

Drin, G., Casella, J.F., Gautier, R., Boehmer, T., Schwartz, T.U., and Antonny, B. (2007). A general amphipathic alpha-helical motif for sensing membrane curvature. Nat Struct Mol Biol *14*, 138-146.

Drubin, D.G., and Nelson, W.J. (1996). Origins of cell polarity. Cell *84*, 335-344.

Drummond, D.R. (2011). Regulation of microtubule dynamics by kinesins. Seminars in Cell & Developmental Biology *22*, 927-934.

Dumont, A., Boucrot, E., Drevensek, S., Daire, V., Gorvel, J.P., Pous, C., Holden, D.W., and Meresse, S. (2010). SKIP, the host target of the Salmonella virulence factor SifA, promotes kinesin-1-dependent vacuolar membrane exchanges. Traffic *11*, 899-911.

Ehsani, S., Santos, J.C., Rodrigues, C.D., Henriques, R., Audry, L., Zimmer, C., Sansonetti, P., Tran Van Nhieu, G., and Enninga, J. (2012). Hierarchies of host factor dynamics at the entry site of Shigella flexneri during host cell invasion. Infect Immun *80*, 2548-2557.

Eichelberg, K., Ginocchio, C.C., and Galan, J.E. (1994). Molecular and functional characterization of the Salmonella typhimurium invasion genes invB and invC: homology of InvC to the F0F1 ATPase family of proteins. J Bacteriol *176*, 4501-4510.

Elliott, S.J., Krejany, E.O., Mellies, J.L., Robins-Browne, R.M., Sasakawa, C., and Kaper, J.B. (2001). EspG, a novel type III system-secreted protein from enteropathogenic Escherichia coli with similarities to VirA of Shigella flexneri. Infect Immun *69*, 4027-4033.

Flanagan, C.A., Schnieders, E.A., Emerick, A.W., Kunisawa, R., Admon, A., and Thorner, J. (1993). Phosphatidylinositol 4-kinase: gene structure and requirement for yeast cell viability. Science *262*, 1444-1448.

Flatau, G., Lemichez, E., Gauthier, M., Chardin, P., Paris, S., Fiorentini, C., and Boquet, P. (1997). Toxin-induced activation of the G protein p21 Rho by deamidation of glutamine. Nature *387*, 729-733.

Franke, T.F., Kaplan, D.R., Cantley, L.C., and Toker, A. (1997). Direct regulation of the Akt proto-oncogene product by phosphatidylinositol-3,4-bisphosphate. Science *275*, 665-668.

Friebel, A., Ilchmann, H., Aepfelbacher, M., Ehrbar, K., Machleidt, W., and Hardt, W.D. (2001). SopE and SopE2 from Salmonella typhimurium activate different sets of RhoGTPases of the host cell. J Biol Chem *276*, 34035-34040.

Fu, Y., and Galan, J.E. (1999). A salmonella protein antagonizes Rac-1 and Cdc42 to mediate host-cell recovery after bacterial invasion. Nature *401*, 293-297.

Garcia-Bustos, J.F., Marini, F., Stevenson, I., Frei, C., and Hall, M.N. (1994). PIK1, an essential phosphatidylinositol 4-kinase associated with the yeast nucleus. EMBO J *13*, 2352-2361.

Gary, J.D., Wurmser, A.E., Bonangelino, C.J., Weisman, L.S., and Emr, S.D. (1998). Fab1p is essential for PtdIns(3)P 5-kinase activity and the maintenance of vacuolar size and membrane homeostasis. J Cell Biol *143*, 65-79.

Ge, J., and Shao, F. (2011). Manipulation of host vesicular trafficking and innate immune defence by Legionella Dot/Icm effectors. Cell Microbiol *13*, 1870-1880.

Giannone, G., Dubin-Thaler, B.J., Dobereiner, H.G., Kieffer, N., Bresnick, A.R., and Sheetz, M.P. (2004). Periodic lamellipodial contractions correlate with rearward actin waves. Cell *116*, 431-443.

Gillooly, D.J., Morrow, I.C., Lindsay, M., Gould, R., Bryant, N.J., Gaullier, J.M., Parton, R.G., and Stenmark, H. (2000). Localization of phosphatidylinositol 3-phosphate in yeast and mammalian cells. EMBO J *19*, 4577-4588.

Gomez-Cambronero, J. (2011). The exquisite regulation of PLD2 by a wealth of interacting proteins: S6K, Grb2, Sos, WASp and Rac2 (and a surprise discovery: PLD2 is a GEF). Cellular signalling *23*, 1885-1895.

Hachani, A., Biskri, L., Rossi, G., Marty, A., Menard, R., Sansonetti, P., Parsot, C., Van Nhieu, G.T., Bernardini, M.L., and Allaoui, A. (2008). IpgB1 and IpgB2, two homologous effectors secreted via the Mxi-Spa type III secretion apparatus, cooperate to mediate polarized cell invasion and inflammatory potential of Shigella flexenri. Microbes Infect *10*, 260-268.

Han, G.S., Audhya, A., Markley, D.J., Emr, S.D., and Carman, G.M. (2002). The Saccharomyces cerevisiae LSB6 gene encodes phosphatidylinositol 4-kinase activity. J Biol Chem *277*, 47709-47718.

Handa, Y., Suzuki, M., Ohya, K., Iwai, H., Ishijima, N., Koleske, A.J., Fukui, Y., and Sasakawa, C. (2007). Shigella IpgB1 promotes bacterial entry through the ELMO-Dock180 machinery. Nature Cell Biology *9*, 121-128.

Hansen, S.B., Tao, X., and MacKinnon, R. (2011). Structural basis of PIP2 activation of the classical inward rectifier K+ channel Kir2.2. Nature *477*, 495-498.

Hardt, W.D., Chen, L.M., Schuebel, K.E., Bustelo, X.R., and Galan, J.E. (1998). S. typhimurium encodes an activator of Rho GTPases that induces membrane ruffling and nuclear responses in host cells. Cell *93*, 815-826.

Harris, B.Z., and Lim, W.A. (2001). Mechanism and role of PDZ domains in signaling complex assembly. J Cell Sci *114*, 3219-3231.

Hikiji, T., Miura, K., Kiyono, K., Shibuya, I., and Ohta, A. (1988). Disruption of the CHO1 gene encoding phosphatidylserine synthase in Saccharomyces cerevisiae. Journal of Biochemistry *104*, 894-900.

Hou, P., Estrada, L., Kinley, A.W., Parsons, J.T., Vojtek, A.B., and Gorski, J.L. (2003). Fgd1, the Cdc42 GEF responsible for Faciogenital Dysplasia, directly interacts with cortactin and mAbp1 to modulate cell shape. Human Molecular Genetics *12*, 1981-1993.

Hsu, F., Zhu, W., Brennan, L., Tao, L., Luo, Z.Q., and Mao, Y. (2012). Structural basis for substrate recognition by a unique Legionella phosphoinositide phosphatase. Proc Natl Acad Sci U S A *109*, 13567-13572.

Huang, Z., Sutton, S.E., Wallenfang, A.J., Orchard, R.C., Wu, X., Feng, Y., Chai, J., and Alto, N.M. (2009). Structural insights into host GTPase isoform selection by a family of bacterial GEF mimics. Nat Struct Mol Biol *16*, 853-860.

Isakoff, S.J., Cardozo, T., Andreev, J., Li, Z., Ferguson, K.M., Abagyan, R., Lemmon, M.A., Aronheim, A., and Skolnik, E.Y. (1998). Identification and analysis of PH domain-containing targets of phosphatidylinositol 3-kinase using a novel in vivo assay in yeast. EMBO J *17*, 5374-5387.

Jackson, L.K., Nawabi, P., Hentea, C., Roark, E.A., and Haldar, K. (2008). The Salmonella virulence protein SifA is a G protein antagonist. Proc Natl Acad Sci U S A *105*, 14141-14146.

Jaffe, A.B., and Hall, A. (2005). Rho GTPases: biochemistry and biology. Annual Review of Cell and Developmental Biology *21*, 247-269.

Jank, T., Bohmer, K.E., Tzivelekidis, T., Schwan, C., Belyi, Y., and Aktories, K. (2012). Domain organization of Legionella effector SetA. Cell Microbiol *14*, 852-868.

Jarvis, K.G., Giron, J.A., Jerse, A.E., McDaniel, T.K., Donnenberg, M.S., and Kaper, J.B. (1995). Enteropathogenic Escherichia coli contains a putative type III secretion system necessary for the export of proteins involved in attaching and effacing lesion formation. Proc Natl Acad Sci U S A *92*, 7996-8000.

Jarvis, K.G., and Kaper, J.B. (1996). Secretion of extracellular proteins by enterohemorrhagic Escherichia coli via a putative type III secretion system. Infect Immun *64*, 4826-4829.

Jepson, M.A., Pellegrin, S., Peto, L., Banbury, D.N., Leard, A.D., Mellor, H., and Kenny, B. (2003). Synergistic roles for the Map and Tir effector molecules in mediating uptake of enteropathogenic Escherichia coli (EPEC) into non-phagocytic cells. Cell Microbiol *5*, 773-783.

Kahn, R.A., Goddard, C., and Newkirk, M. (1988). Chemical and immunological characterization of the 21-kDa ADP-ribosylation factor of adenylate cyclase. J Biol Chem *263*, 8282-8287.

Karathanassis, D., Stahelin, R.V., Bravo, J., Perisic, O., Pacold, C.M., Cho, W., and Williams, R.L. (2002). Binding of the PX domain of p47(phox) to phosphatidylinositol 3,4-

bisphosphate and phosphatidic acid is masked by an intramolecular interaction. EMBO J *21*, 5057-5068.

Kenny, B., Ellis, S., Leard, A.D., Warawa, J., Mellor, H., and Jepson, M.A. (2002). Co-ordinate regulation of distinct host cell signalling pathways by multifunctional enteropathogenic Escherichia coli effector molecules. Mol Microbiol *44*, 1095-1107.

Kenny, B., and Jepson, M. (2000). Targeting of an enteropathogenic Escherichia coli (EPEC) effector protein to host mitochondria. Cell Microbiol *2*, 579-590.

Klink, B.U., Barden, S., Heidler, T.V., Borchers, C., Ladwein, M., Stradal, T.E., Rottner, K., and Heinz, D.W. (2010). Structure of Shigella IpgB2 in complex with human RhoA: implications for the mechanism of bacterial guanine nucleotide exchange factor mimicry. J Biol Chem *285*, 17197-17208.

Kubori, T., and Galan, J.E. (2003). Temporal regulation of salmonella virulence effector function by proteasome-dependent protein degradation. Cell *115*, 333-342.

Lander, E.S., Linton, L.M., Birren, B., Nusbaum, C., Zody, M.C., Baldwin, J., Devon, K., Dewar, K., Doyle, M., FitzHugh, W., *et al.* (2001). Initial sequencing and analysis of the human genome. Nature *409*, 860-921.

Lee, K., Gallop, J.L., Rambani, K., and Kirschner, M.W. (2010). Self-assembly of filopodia-like structures on supported lipid bilayers. Science *329*, 1341-1345.

Lemmon, M.A. (2008). Membrane recognition by phospholipid-binding domains. Nature Reviews Molecular Cell Biology *9*, 99-111.

Lemmon, M.A., Ferguson, K.M., O'Brien, R., Sigler, P.B., and Schlessinger, J. (1995). Specific and high-affinity binding of inositol phosphates to an isolated pleckstrin homology domain. Proc Natl Acad Sci U S A *92*, 10472-10476.

Li, H., Xu, H., Zhou, Y., Zhang, J., Long, C., Li, S., Chen, S., Zhou, J.M., and Shao, F. (2007). The phosphothreonine lyase activity of a bacterial type III effector family. Science *315*, 1000-1003.

Loisel, T.P., Boujemaa, R., Pantaloni, D., and Carlier, M.F. (1999). Reconstitution of actin-based motility of Listeria and Shigella using pure proteins. Nature *401*, 613-616.

Machacek, M., Hodgson, L., Welch, C., Elliott, H., Pertz, O., Nalbant, P., Abell, A., Johnson, G.L., Hahn, K.M., and Danuser, G. (2009). Coordination of Rho GTPase activities during cell protrusion. Nature *461*, 99-103.

Marchand, J.B., Kaiser, D.A., Pollard, T.D., and Higgs, H.N. (2001). Interaction of WASP/Scar proteins with actin and vertebrate Arp2/3 complex. Nature Cell Biology *3*, 76-82.

Marco, E., Wedlich-Soldner, R., Li, R., Altschuler, S.J., and Wu, L.F. (2007). Endocytosis optimizes the dynamic localization of membrane proteins that regulate cortical polarity. Cell *129*, 411-422.

Mejillano, M.R., Kojima, S., Applewhite, D.A., Gertler, F.B., Svitkina, T.M., and Borisy, G.G. (2004). Lamellipodial versus filopodial mode of the actin nanomachinery: pivotal role of the filament barbed end. Cell *118*, 363-373.

Michiels, T., Wattiau, P., Brasseur, R., Ruysschaert, J.M., and Cornelis, G. (1990). Secretion of Yop proteins by Yersiniae. Infect Immun *58*, 2840-2849.

Miki, H., Sasaki, T., Takai, Y., and Takenawa, T. (1998). Induction of filopodium formation by a WASP-related actin-depolymerizing protein N-WASP. Nature *391*, 93-96.

Miki, T., Akiba, K., Iguchi, M., Danbara, H., and Okada, N. (2011). The Chromobacterium violaceum type III effector CopE, a guanine nucleotide exchange factor for Rac1 and Cdc42, is involved in bacterial invasion of epithelial cells and pathogenesis. Mol Microbiol *80*, 1186-1203.

Milo, R., Jorgensen, P., Moran, U., Weber, G., and Springer, M. (2010). BioNumbers--the database of key numbers in molecular and cell biology. Nucleic acids research *38*, D750-753.

Miyamoto, S., Akiyama, S.K., and Yamada, K.M. (1995). Synergistic roles for receptor occupancy and aggregation in integrin transmembrane function. Science (New York, NY *267*, 883-885.

Mnaimneh, S., Davierwala, A.P., Haynes, J., Moffat, J., Peng, W.T., Zhang, W., Yang, X., Pootoolal, J., Chua, G., Lopez, A., *et al.* (2004). Exploration of essential gene functions via titratable promoter alleles. Cell *118*, 31-44.

Mukherjee, S., Keitany, G., Li, Y., Wang, Y., Ball, H.L., Goldsmith, E.J., and Orth, K. (2006). Yersinia YopJ acetylates and inhibits kinase activation by blocking phosphorylation. Science *312*, 1211-1214.

Nakanishi, H., de los Santos, P., and Neiman, A.M. (2004). Positive and negative regulation of a SNARE protein by control of intracellular localization. Molecular biology of the cell *15*, 1802-1815.

Nalbant, P., Hodgson, L., Kraynov, V., Toutchkine, A., and Hahn, K.M. (2004). Activation of endogenous Cdc42 visualized in living cells. Science (New York, NY *305*, 1615-1619.

Niebuhr, K., Giuriato, S., Pedron, T., Philpott, D.J., Gaits, F., Sable, J., Sheetz, M.P., Parsot, C., Sansonetti, P.J., and Payrastre, B. (2002). Conversion of PtdIns(4,5)P(2) into PtdIns(5)P by the S.flexneri effector IpgD reorganizes host cell morphology. EMBO J *21*, 5069-5078.

Norris, F.A., Wilson, M.P., Wallis, T.S., Galyov, E.E., and Majerus, P.W. (1998). SopB, a protein required for virulence of Salmonella dublin, is an inositol phosphate phosphatase. Proc Natl Acad Sci U S A *95*, 14057-14059.

Obaishi, H., Nakanishi, H., Mandai, K., Satoh, K., Satoh, A., Takahashi, K., Miyahara, M., Nishioka, H., Takaishi, K., and Takai, Y. (1998). Frabin, a novel FGD1-related actin filament-binding protein capable of changing cell shape and activating c-Jun N-terminal kinase. J Biol Chem *273*, 18697-18700.

Ohlson, M.B., Fluhr, K., Birmingham, C.L., Brumell, J.H., and Miller, S.I. (2005). SseJ deacylase activity by Salmonella enterica serovar Typhimurium promotes virulence in mice. Infect Immun *73*, 6249-6259.

Ohlson, M.B., Huang, Z., Alto, N.M., Blanc, M.P., Dixon, J.E., Chai, J., and Miller, S.I. (2008). Structure and function of Salmonella SifA indicate that its interactions with SKIP, SseJ, and RhoA family GTPases induce endosomal tubulation. Cell Host Microbe *4*, 434-446.

Ohya, K., Handa, Y., Ogawa, M., Suzuki, M., and Sasakawa, C. (2005). IpgB1 is a novel Shigella effector protein involved in bacterial invasion of host cells. Its activity to promote membrane ruffling via Rac1 and Cdc42 activation. J Biol Chem *280*, 24022-24034.

Olson, M.F., Sterpetti, P., Nagata, K., Toksoz, D., and Hall, A. (1997). Distinct roles for DH and PH domains in the Lbc oncogene. Oncogene *15*, 2827-2831.

Orchard, R.C., and Alto, N.M. (2012). Mimicking GEFs: a common theme for bacterial pathogens. Cell Microbiol *14*, 10-18.

Orchard, R.C., Kittisopikul, M., Altschuler, S.J., Wu, L.F., Suel, G.M., and Alto, N.M. (2012). Identification of F-actin as the dynamic hub in a microbial-induced GTPase polarity circuit. Cell *148*, 803-815.

Palamidessi, A., Frittoli, E., Garre, M., Faretta, M., Mione, M., Testa, I., Diaspro, A., Lanzetti, L., Scita, G., and Di Fiore, P.P. (2008). Endocytic trafficking of Rac is required for the spatial restriction of signaling in cell migration. Cell *134*, 135-147.

Park, K.C., Rivero, F., Meili, R., Lee, S., Apone, F., and Firtel, R.A. (2004). Rac regulation of chemotaxis and morphogenesis in Dictyostelium. EMBO J *23*, 4177-4189.

Parsot, C., Menard, R., Gounon, P., and Sansonetti, P.J. (1995). Enhanced secretion through the Shigella flexneri Mxi-Spa translocon leads to assembly of extracellular proteins into macromolecular structures. Mol Microbiol *16*, 291-300.

Patel, J.C., and Galan, J.E. (2006). Differential activation and function of Rho GTPases during Salmonella-host cell interactions. J Cell Biol *175*, 453-463.

Patel, J.C., Hueffer, K., Lam, T.T., and Galan, J.E. (2009). Diversification of a Salmonella virulence protein function by ubiquitin-dependent differential localization. Cell *137*, 283-294.

Pendaries, C., Tronchere, H., Arbibe, L., Mounier, J., Gozani, O., Cantley, L., Fry, M.J., Gaits-Iacovoni, F., Sansonetti, P.J., and Payrastre, B. (2006). PtdIns5P activates the host cell PI3-kinase/Akt pathway during Shigella flexneri infection. EMBO J *25*, 1024-1034.

Pollard, T.D., and Cooper, J.A. (2009). Actin, a central player in cell shape and movement. Science (New York, NY *326*, 1208-1212.

Prehoda, K.E., Scott, J.A., Mullins, R.D., and Lim, W.A. (2000). Integration of multiple signals through cooperative regulation of the N-WASP-Arp2/3 complex. Science *290*, 801-806.

Preston, G., Huang, H.C., He, S.Y., and Collmer, A. (1995). The HrpZ proteins of Pseudomonas syringae pvs. syringae, glycinea, and tomato are encoded by an operon containing Yersinia ysc homologs and elicit the hypersensitive response in tomato but not soybean. Molecular plant-microbe interactions : MPMI *8*, 717-732.

Reinicke, A.T., Hutchinson, J.L., Magee, A.I., Mastroeni, P., Trowsdale, J., and Kelly, A.P. (2005). A Salmonella typhimurium effector protein SifA is modified by host cell prenylation and S-acylation machinery. J Biol Chem *280*, 14620-14627.

Ribet, D., and Cossart, P. (2010). Pathogen-mediated posttranslational modifications: A re-emerging field. Cell *143*, 694-702.

Riedl, J., Crevenna, A.H., Kessenbrock, K., Yu, J.H., Neukirchen, D., Bista, M., Bradke, F., Jenne, D., Holak, T.A., Werb, Z., *et al.* (2008). Lifeact: a versatile marker to visualize F-actin. Nature Methods *5*, 605-607.

Rottner, K., Behrendt, B., Small, J.V., and Wehland, J. (1999). VASP dynamics during lamellipodia protrusion. Nat Cell Biol *1*, 321-322.

Roy, C., Martin, M., and Mangeat, P. (1997). A dual involvement of the amino-terminal domain of ezrin in F- and G-actin binding. J Biol Chem *272*, 20088-20095.

Ruiz-Albert, J., Yu, X.J., Beuzon, C.R., Blakey, A.N., Galyov, E.E., and Holden, D.W. (2002). Complementary activities of SseJ and SifA regulate dynamics of the Salmonella typhimurium vacuolar membrane. Mol Microbiol *44*, 645-661.

Saleh, H.S., Merkel, U., Geissler, K.J., Sperka, T., Sechi, A., Breithaupt, C., and Morrison, H. (2009). Properties of an ezrin mutant defective in F-actin binding. Journal of Molecular Biology *385*, 1015-1031.

Santos, E., Tronick, S.R., Aaronson, S.A., Pulciani, S., and Barbacid, M. (1982). T24 human bladder carcinoma oncogene is an activated form of the normal human homologue of BALB- and Harvey-MSV transforming genes. Nature *298*, 343-347.

Schoebel, S., Blankenfeldt, W., Goody, R.S., and Itzen, A. (2010). High-affinity binding of phosphatidylinositol 4-phosphate by Legionella pneumophila DrrA. EMBO Reports *11*, 598-604.

Schroeder, N., Mota, L.J., and Meresse, S. (2011). Salmonella-induced tubular networks. Trends Microbiol *19*, 268-277.

Schu, P.V., Takegawa, K., Fry, M.J., Stack, J.H., Waterfield, M.D., and Emr, S.D. (1993). Phosphatidylinositol 3-kinase encoded by yeast VPS34 gene essential for protein sorting. Science *260*, 88-91.

Sekine, A., Fujiwara, M., and Narumiya, S. (1989). Asparagine residue in the rho gene product is the modification site for botulinum ADP-ribosyltransferase. J Biol Chem *264*, 8602-8605.

Selyunin, A.S., Sutton, S.E., Weigele, B.A., Reddick, L.E., Orchard, R.C., Bresson, S.M., Tomchick, D.R., and Alto, N.M. (2011). The assembly of a GTPase-kinase signalling complex by a bacterial catalytic scaffold. Nature *469*, 107-111.

Shao, F., Merritt, P.M., Bao, Z., Innes, R.W., and Dixon, J.E. (2002). A Yersinia effector and a Pseudomonas avirulence protein define a family of cysteine proteases functioning in bacterial pathogenesis. Cell *109*, 575-588.

Shelton, S.N., Barylko, B., Binns, D.D., Horazdovsky, B.F., Albanesi, J.P., and Goodman, J.M. (2003). Saccharomyces cerevisiae contains a Type II phosphoinositide 4-kinase. Biochem J *371*, 533-540.

Simovitch, M., Sason, H., Cohen, S., Zahavi, E.E., Melamed-Book, N., Weiss, A., Aroeti, B., and Rosenshine, I. (2010). EspM inhibits pedestal formation by enterohaemorrhagic Escherichia coli and enteropathogenic E. coli and disrupts the architecture of a polarized epithelial monolayer. Cell Microbiol *12*, 489-505.

Simpson, N., Shaw, R., Crepin, V.F., Mundy, R., FitzGerald, A.J., Cummings, N., Straatman-Iwanowska, A., Connerton, I., Knutton, S., and Frankel, G. (2006). The enteropathogenic Escherichia coli type III secretion system effector Map binds EBP50/NHERF1: implication for cell signalling and diarrhoea. Mol Microbiol *60*, 349-363.

Smith, K., Humphreys, D., Hume, P.J., and Koronakis, V. (2010). Enteropathogenic Escherichia coli recruits the cellular inositol phosphatase SHIP2 to regulate actin-pedestal formation. Cell Host Microbe *7*, 13-24.

Snyder, J.T., Worthylake, D.K., Rossman, K.L., Betts, L., Pruitt, W.M., Siderovski, D.P., Der, C.J., and Sondek, J. (2002). Structural basis for the selective activation of Rho GTPases by Dbl exchange factors. Nature Structural Biology *9*, 468-475.

Stauffer, T.P., Ahn, S., and Meyer, T. (1998). Receptor-induced transient reduction in plasma membrane PtdIns(4,5)P2 concentration monitored in living cells. Current biology : CB *8*, 343-346.

Stefan, C.J., Manford, A.G., Baird, D., Yamada-Hanff, J., Mao, Y., and Emr, S.D. (2011). Osh proteins regulate phosphoinositide metabolism at ER-plasma membrane contact sites. Cell *144*, 389-401.

Stein, M.A., Leung, K.Y., Zwick, M., Garcia-del Portillo, F., and Finlay, B.B. (1996). Identification of a Salmonella virulence gene required for formation of filamentous structures containing lysosomal membrane glycoproteins within epithelial cells. Mol Microbiol *20*, 151-164.

Stender, S., Friebel, A., Linder, S., Rohde, M., Mirold, S., and Hardt, W.D. (2000). Identification of SopE2 from Salmonella typhimurium, a conserved guanine nucleotide exchange factor for Cdc42 of the host cell. Mol Microbiol *36*, 1206-1221.

Stenmark, H., Parton, R.G., Steele-Mortimer, O., Lutcke, A., Gruenberg, J., and Zerial, M. (1994). Inhibition of rab5 GTPase activity stimulates membrane fusion in endocytosis. EMBO J *13*, 1287-1296.

Strauss, W. (1992). Partial Differential Equations: An Introduction (John Wiley & Sons, Inc).

Svitkina, T.M., Bulanova, E.A., Chaga, O.Y., Vignjevic, D.M., Kojima, S., Vasiliev, J.M., and Borisy, G.G. (2003). Mechanism of filopodia initiation by reorganization of a dendritic network. The Journal of Cell Biology *160*, 409-421.

Takai, Y., Sasaki, T., and Matozaki, T. (2001). Small GTP-binding proteins. Physiological Reviews *81*, 153-208.

Theriot, J.A., Mitchison, T.J., Tilney, L.G., and Portnoy, D.A. (1992). The rate of actin-based motility of intracellular Listeria monocytogenes equals the rate of actin polymerization. Nature *357*, 257-260.

Tobe, T., Beatson, S.A., Taniguchi, H., Abe, H., Bailey, C.M., Fivian, A., Younis, R., Matthews, S., Marches, O., Frankel, G., *et al.* (2006). An extensive repertoire of type III secretion effectors in Escherichia coli O157 and the role of lambdoid phages in their dissemination. Proceedings of the National Academy of Sciences of the United States of America *103*, 14941-14946.

Turunen, O., Wahlstrom, T., and Vaheri, A. (1994). Ezrin has a COOH-terminal actin-binding site that is conserved in the ezrin protein family. The Journal of Cell Biology *126*, 1445-1453.

Ulrich, R.L., and DeShazer, D. (2004). Type III secretion: a virulence factor delivery system essential for the pathogenicity of Burkholderia mallei. Infect Immun *72*, 1150-1154.

Umikawa, M., Obaishi, H., Nakanishi, H., Satoh-Horikawa, K., Takahashi, K., Hotta, I., Matsuura, Y., and Takai, Y. (1999). Association of frabin with the actin cytoskeleton is essential for microspike formation through activation of Cdc42 small G protein. J Biol Chem *274*, 25197-25200.

Upadhyay, A., Williams, C., Gill, A.C., Philippe, D.L., Davis, K., Taylor, L.A., Stevens, M.P., Galyov, E.E., and Bagby, S. (2004). Biophysical characterization of the catalytic domain of guanine nucleotide exchange factor BopE from Burkholderia pseudomallei. Biochim Biophys Acta *1698*, 111-119.

Upadhyay, A., Wu, H.L., Williams, C., Field, T., Galyov, E.E., van den Elsen, J.M., and Bagby, S. (2008). The guanine-nucleotide-exchange factor BopE from Burkholderia pseudomallei adopts a compact version of the Salmonella SopE/SopE2 fold and undergoes a closed-to-open conformational change upon interaction with Cdc42. The Biochemical journal *411*, 485-493.

Van Engelenburg, S.B., and Palmer, A.E. (2008). Quantification of real-time Salmonella effector type III secretion kinetics reveals differential secretion rates for SopE2 and SptP. Chem Biol *15*, 619-628.

Van Gijsegem, F., Gough, C., Zischek, C., Niqueux, E., Arlat, M., Genin, S., Barberis, P., German, S., Castello, P., and Boucher, C. (1995). The hrp gene locus of Pseudomonas solanacearum, which controls the production of a type III secretion system, encodes eight proteins related to components of the bacterial flagellar biogenesis complex. Mol Microbiol *15*, 1095-1114.

Vetter, I.R., and Wittinghofer, A. (2001). The guanine nucleotide-binding switch in three dimensions. Science *294*, 1299-1304.

Watanabe, N., and Mitchison, T.J. (2002). Single-molecule speckle analysis of actin filament turnover in lamellipodia. Science (New York, NY *295*, 1083-1086.

Wedlich-Soldner, R., Altschuler, S., Wu, L., and Li, R. (2003). Spontaneous cell polarization through actomyosin-based delivery of the Cdc42 GTPase. Science *299*, 1231-1235.

Wedlich-Soldner, R., and Li, R. (2003). Spontaneous cell polarization: undermining determinism. Nature Cell Biology *5*, 267-270.

Weiner, O.D., Marganski, W.A., Wu, L.F., Altschuler, S.J., and Kirschner, M.W. (2007). An actin-based wave generator organizes cell motility. PLoS Biology *5*, e221.

Weiner, O.D., Neilsen, P.O., Prestwich, G.D., Kirschner, M.W., Cantley, L.C., and Bourne, H.R. (2002). A PtdInsP(3)- and Rho GTPase-mediated positive feedback loop regulates neutrophil polarity. Nature Cell Biology *4*, 509-513.

Williams, C., Galyov, E.E., and Bagby, S. (2004). solution structure, backbone dynamics, and interaction with Cdc42 of Salmonella guanine nucleotide exchange factor SopE2. Biochemistry *43*, 11998-12008.

Xu, J., Wang, F., Van Keymeulen, A., Herzmark, P., Straight, A., Kelly, K., Takuwa, Y., Sugimoto, N., Mitchison, T., and Bourne, H.R. (2003). Divergent signals and cytoskeletal assemblies regulate self-organizing polarity in neutrophils. Cell *114*, 201-214.

Yahr, T.L., Goranson, J., and Frank, D.W. (1996). Exoenzyme S of Pseudomonas aeruginosa is secreted by a type III pathway. Mol Microbiol *22*, 991-1003.

Yarbrough, M.L., Li, Y., Kinch, L.N., Grishin, N.V., Ball, H.L., and Orth, K. (2009). AMPylation of Rho GTPases by Vibrio VopS disrupts effector binding and downstream signaling. Science *323*, 269-272.

Yu, B., Martins, I.R., Li, P., Amarasinghe, G.K., Umetani, J., Fernandez-Zapico, M.E., Billadeau, D.D., Machius, M., Tomchick, D.R., and Rosen, M.K. (2010). Structural and energetic mechanisms of cooperative autoinhibition and activation of Vav1. Cell *140*, 246-256.

Yu, J.W., Mendrola, J.M., Audhya, A., Singh, S., Keleti, D., DeWald, D.B., Murray, D., Emr, S.D., and Lemmon, M.A. (2004). Genome-wide analysis of membrane targeting by S. cerevisiae pleckstrin homology domains. Molecular Cell *13*, 677-688.

Zhang, B., Wang, Z.X., and Zheng, Y. (1997). Characterization of the interactions between the small GTPase Cdc42 and its GTPase-activating proteins and putative effectors. Comparison of kinetic properties of Cdc42 binding to the Cdc42-interactive domains. J Biol Chem *272*, 21999-22007.

Zhang, F.L., and Casey, P.J. (1996). Protein prenylation: molecular mechanisms and functional consequences. Annual Review of Biochemistry *65*, 241-269.

Zhao, C., Du, G., Skowronek, K., Frohman, M.A., and Bar-Sagi, D. (2007). Phospholipase D2-generated phosphatidic acid couples EGFR stimulation to Ras activation by Sos. Nature Cell Biology *9*, 706-712.

Zhao, L., Sukstanskii, A.L., Kroenke, C.D., Song, J., Piwnica-Worms, D., Ackerman, J.J., and Neil, J.J. (2008). Intracellular water specific MR of microbead-adherent cells: HeLa cell intracellular water diffusion. Magn Reson Med *59*, 79-84.

Zheng, Y., Hart, M.J., and Cerione, R.A. (1995). Guanine nucleotide exchange catalyzed by dbl oncogene product. Methods Enzymol *256*, 77-84.

Zoncu, R., Perera, R.M., Balkin, D.M., Pirruccello, M., Toomre, D., and De Camilli, P. (2009). A phosphoinositide switch controls the maturation and signaling properties of APPL endosomes. Cell *136*, 1110-1121.